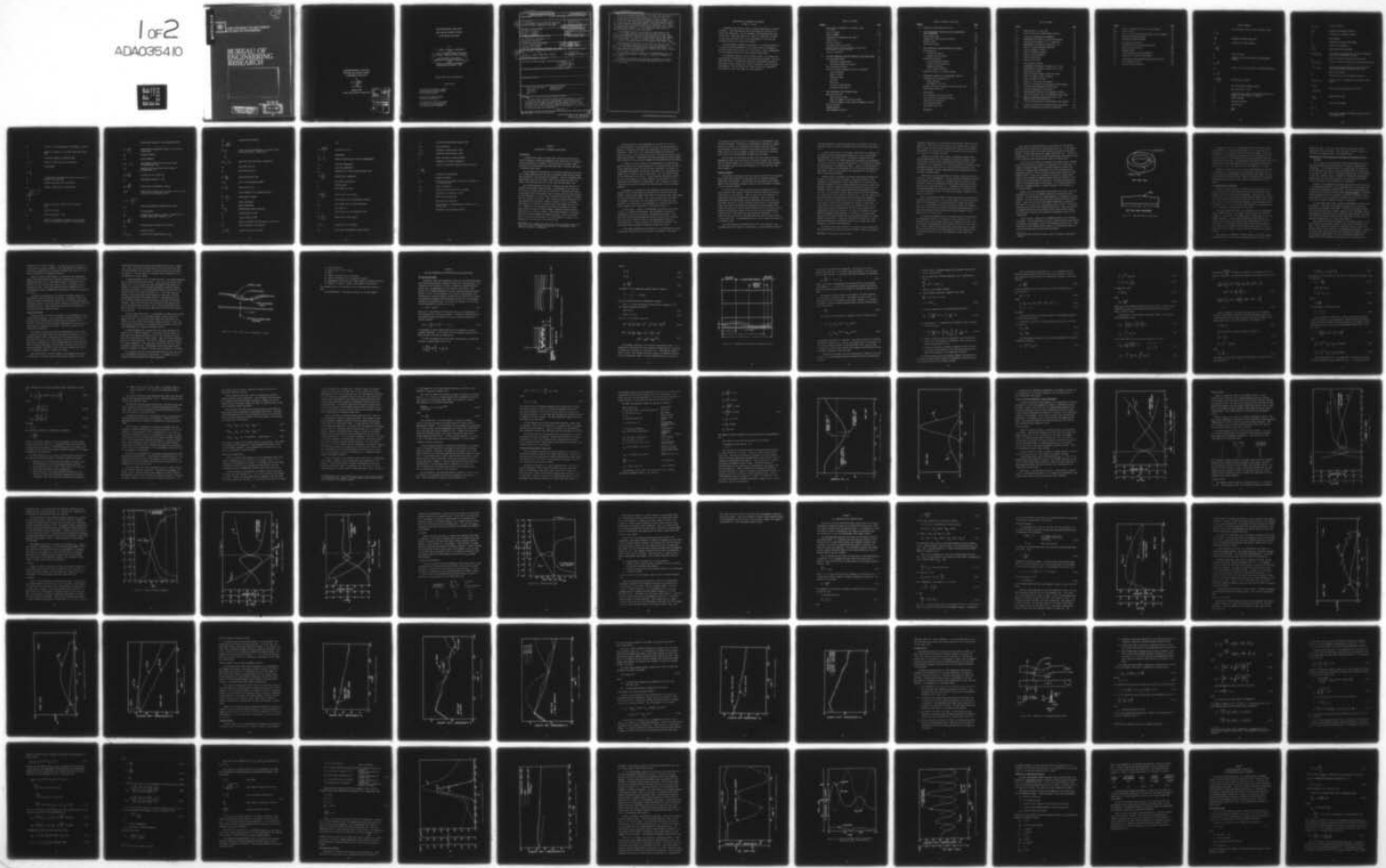
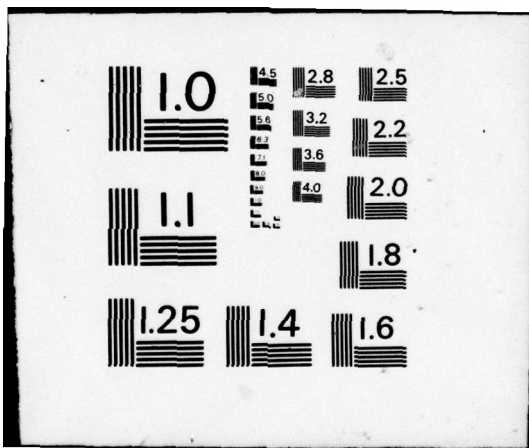


AD-A035 410 NEW MEXICO UNIV ALBUQUERQUE DEPT OF MECHANICAL ENGI--ETC F/G 11/1  
ELASTOHYDRODYNAMIC LUBRICATION WITH WEAR AND ASPERITY CONTACT I--ETC(U)  
JAN 77 A O LEBECK, J L TEALE, R E PIERCE N00014-76-C-0071  
UNCLASSIFIED ME-76(77)ONR-414-1 NL

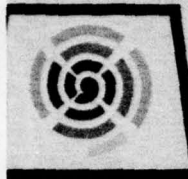
1 of 2  
ADA035410





ADA 035410

(12)  
nw



THE UNIVERSITY OF NEW MEXICO  
COLLEGE OF ENGINEERING

# BUREAU OF ENGINEERING RESEARCH



DISTRIBUTION STATEMENT A  
Approved for public release;  
Distribution Unlimited

DDC  
FEB 7 1977  
REF ID: A6200  
B

ELASTOHYDRODYNAMIC LUBRICATION  
WITH WEAR AND ASPERITY CONTACT  
IN MECHANICAL FACE SEALS

by

A. O. Lebeck

J. L. Teale

and

R. E. Pierce

January 1976

Annual Report ME-76(77)ONR-414-1

ACCESSION NO.	
NSB	White Seal <input checked="" type="checkbox"/>
DSB	Def. Seal <input type="checkbox"/>
UNANNOUCED <input type="checkbox"/>	
JUSTIFICATION	
BY	
DISTRIBUTION/AVAILABILITY CODES	
ORIG.	AVAIL. FOR SPARES
A	

ELASTOHYDRODYNAMIC LUBRICATION  
WITH WEAR AND ASPERITY CONTACT  
IN MECHANICAL FACE SEALS

by

A. O. Lebeck, Principal Investigator  
and  
J. L. Teale, Graduate Research Assistant  
R. E. Pierce, Graduate Research Assistant

The University of New Mexico  
Department of Mechanical Engineering  
and  
Bureau of Engineering Research  
Albuquerque, New Mexico 87131

Annual Report ME-76(77)ONR-414-1

January 1977

Prepared for the Office of Naval  
Research under contract number  
ONR N 00014-76-C-0071.

Approved for public release;  
distribution unlimited.

Reproduction in whole or in part  
is permitted for any purpose of  
the United States Government.

Unrestricted

SECURITY CLASSIFICATION OF THIS PAGE (When Data Entered)

REPORT DOCUMENTATION PAGE		READ INSTRUCTIONS BEFORE COMPLETING FORM
1. REPORT NUMBER	2. GOVT ACCESSION NO.	3. RECIPIENT'S CATALOG NUMBER
4. TITLE (and Subtitle) ELASTOHYDRODYNAMIC LUBRICATION WITH WEAR AND ASPERITY CONTACT IN MECHANICAL FACE SEALS		5. TYPE OF REPORT & PERIOD COVERED Annual Report 12/1/75 - 11/30/76
6. PERFORMING ORG. REPORT NUMBER ME-76(77)ONR-414-1		7. AUTHOR(s) A. O. Lebeck J. L. Teale R. E. Pierce
8. CONTRACT OR GRANT NUMBER(s) ONR N 00014-76-C-0071-new		9. PERFORMING ORGANIZATION NAME AND ADDRESS The University of New Mexico Albuquerque, New Mexico
10. CONTROLLING OFFICE NAME AND ADDRESS Director, Power Program Department of the Navy Office of Naval Research, Arlington, Va. 22217.		11. REPORT DATE January 1977
12. MONITORING AGENCY NAME & ADDRESS (if different from Controlling Office) Annual rept. 1 Dec 75-30 Nov 76		13. NUMBER OF PAGES 140
14. DISTRIBUTION STATEMENT (of this Report) Approved for public release; distribution unlimited		15. SECURITY CLASS. (of this report) Unclassified
16. DISTRIBUTION STATEMENT (of the abstract entered in Block 20, if different from Report)		15. DECLASSIFICATION/DOWNGRADING SCHEDULE <i>(12) 157P</i>
17. SUPPLEMENTARY NOTES		
18. KEY WORDS (Continue on reverse side if necessary and identify by block number) Mechanical Face Seals      Asperity Contact Face Seals      Hydrodynamic Lubrication Wear		
19. ABSTRACT (Continue on reverse side if necessary and identify by block number) In this report lubrication effects caused by waviness in contacting mechanical face seals are investigated. A lubrication model is developed which includes the effects of hydrodynamic lubrication in conjunction with asperity contact, asperity contact pressure, elastic deformation of the seal rings, and wear of the surfaces. Several sources of initial waviness are considered. → over		

~~Unrestricted~~

~~SECURITY CLASSIFICATION OF THIS PAGE(When Data Entered)~~

Based on a one dimensional model, it is shown that some amount of hydrodynamic load support can be expected to occur in a water seal even though there is a considerable fraction of rubbing contact. As the fraction of load supported by hydrodynamic pressure becomes greater, the average wear rate will become smaller. Thus any parameter changes which cause greater hydrodynamic support are desirable. It is shown that there exists an optimum initial waviness and face width to maximize hydrodynamic load support. It is also shown that lower values of surface roughness lead to higher load support.

Time dependent effects are obtained by including wear in the model. It is shown that most initial waviness will wear away under steady state operating conditions, and thus hydrodynamic load support will decrease with time. Neither thermal effects nor friction effects alter this behavior. However, a variable sealed pressure may lead to a stable or increasing fraction of hydrodynamic load support.

By making the seal waviness travel relative to the seal ring, it is shown how hydrodynamic lubrication can be sustained regardless of wear. This idea offers possibilities for improved seal design. It is also shown that there are certain waviness shapes that provide a greater load support than a sinusoidal shape.

The seal model is also developed on a two dimensional basis, so that leakage can be included. The model is verified by comparison to previous work.

Preliminary considerations are made for the design of an experimental test rig to be used for studying hydrodynamic effects in contacting face seals.

~~SECURITY CLASSIFICATION OF THIS PAGE(When Data Entered)~~

APPLICATION OF RESEARCH TO THE NEEDS  
OF THE U. S. NAVY

Mechanical face seals are used in numerous applications in Naval machinery. These applications range from propeller shaft seals to boiler feed pump seals. In such equipment the mechanical seal plays a vital role. When such seals fail, repair is costly both in terms of lost time and direct cost, so any improvement in seal life and reliability would be of significant benefit.

As more advanced equipment is designed, it is sometimes difficult to achieve desired performance in more severe service environments with the present state of the art of seal design. Thus an improvement in seal technology would serve this important application.

The immediate objective of the research herein is to further the understanding of mechanical face seal lubrication phenomena. The ultimate objective is to develop the capability of designing contacting face seals having a longer life, greater reliability, and for extreme environments. Thus the objectives of this research are compatible with mechanical face seal needs for Naval machinery.

TABLE OF CONTENTS

<u>Chapter</u>	<u>Page</u>
APPLICATION OF RESEARCH TO THE NEEDS OF THE U. S. NAVY	ii
LIST OF FIGURES	vi
LIST OF SYMBOLS	viii
1 LUBRICATION IN MECHANICAL FACE SEALS	1
Introduction	1
Previous Research	1
Seal Applications of Interest	8
Proposed Model--Elastohydrodynamic Lubrication with Asperity Contact and Wear	9
Sources of Waviness	10
2 THE ONE DIMENSIONAL ELASTOHYDRODYNAMIC EQUILIBRIUM MODEL	14
The Equilibrium Model	14
Additional Considerations	26
Alternative Method of Solution	28
The Equilibrium Solution	29
Effect of Various Parameters on Seal Performance	34
Initial Waviness	34
Number of Waves	36
Roughness Height	36
Stiffness	38
Face Load	42
Initial Liftoff Waviness	42
Parameter Study Summary	44
3 ONE DIMENSIONAL TIME DEPENDENT MODEL	46
Base Case Solution	48
Time Step Size Effect	50
Effect of Number of Deflection Terms	54
Effect of Number of Wear Terms and Number of Points	54
Friction Effects	54
Thermal Effects	61
Time Dependent Pressure	69

TABLE OF CONTENTS (continued)

<u>Chapter</u>		<u>Page</u>
(3)	Comparison to Experimental Results	76
4	ELASTOHYDRODYNAMIC LUBRICATION AND IMPROVED-FACE SEAL PERFORMANCE	78
	Variable Wear Rate	78
	Tangentially Varying Friction Effects	82
	Traveling Wave	85
	Optimum Wave Shapes	
5	TWO DIMENSIONAL ELASTOHYDRODYNAMIC SEAL MODEL	95
	Basic Equations	95
	Boundary Conditions	100
	Leakage and Load Support	102
	Numerical Formulation	103
	Finite Difference Equation	103
	Successive Over Relaxation	105
	Boundary Conditions	106
	Cavity Shape Convergence	113
	Numerical Solution to Findlay Problem	117
6	PRELIMINARY DESIGN OF AN EXPERIMENTAL TEST RIG	123
	Proposed Test Rig Capabilities	123
	Unique Features	124
	Philosophy of Test Rig	125
	Research that Can be Conducted Using the Test Rig	125
	Description of Test Rig	126
7	CONCLUSIONS	133
	One Dimensional Equilibrium Model	133
	One Dimensional Time Dependent Model	134
	Improved Seal Performance	135
	Two Dimensional Model	136
	Experimental Test Rig	136
	REFERENCES	137

LIST OF FIGURES

<u>Figure</u>		<u>Page</u>
1-1	Waviness Wear on a Seal Ring	7
1-2	Shift of Wave Due to Hydrodynamic Pressure	12
2-1	Longitudinal Roughness and Geometry	15
2-2	Hydrodynamic and Asperity Interaction Regions	17
2-3	Equilibrium Film Shape at $\bar{t} = 0$ , Base Case	32
2-4	Hydrodynamic and Asperity Pressure at $\bar{t} = 0$	33
2-5	Effect of Initial Waviness Amplitude	35
2-6	Effect of Number of Waves $n$	37
2-7	Effect of Surface Roughness	39
2-8	Effect of Ring Stiffness	40
2-9	Effect of Face Width	41
2-10	Effect of Face Load	43
3-1	Time Dependent Behavior	
3-2	Hydrodynamic and Asperity Pressure at $\bar{t} = 400$	51
3-3	Hydrodynamic and Asperity Pressure at $\bar{t} = 800$	52
3-4	Time Step Size Effect	53
3-5	Effect of Second Harmonic Deflection Terms	55
3-6	Effect of Number of Wear Harmonics	56
3-7	Effect of Number of Points	57
3-8	Effect of Friction on Load Support	59
3-9	Effect of Increased Friction Factor on Load Support	60
3-10	Convention for Temperature Effect Model	62
3-11	Seal Face Temperature and Pressure	70
3-12	Time Dependent Behavior with Temperature Effect	71
3-13	Effect of Variable Load on Hydrodynamic Load Support	73
3-14	Effect of Variable Load on Hydrodynamic Load Support - Zero Initial Waviness	74
3-15	Effect of Variable Load on Hydrodynamic Load Support	75
4-1	Variation of Fraction of Asperity Contact $\bar{b}_m$ with $\bar{h}$	81
4-2	Effect of Tangential Friction on Deflection	84

<u>Figure</u>		<u>Page</u>
4-3	Effect of Tangential Friction on Load Support	86
4-4	Traveling Wave	87
4-5	Effect of Traveling Wave on Waviness and Load Support	90
4-6	Optimum Five Term Film Shape	93
4-7	Optimum Film Shape Pressure	94
5-1	Two Dimensional Problem	96
5-2	Coordinates for Two Dimensional Problem	98
5-3	Numerical Representation	104
5-4	Boundary Nodes	110
5-5	Cavity Representation and Smoothing	114
5-6	Comparison to Findlay Cavity Shape	122
6-1	Controlled Waviness Mechanical Face Seal Test Rig	127
6-2	Test Chamber and Seal	130
6-3	Waviness Control Cylinder	131

LIST OF SYMBOLS

a	cross sectional area of ring or length of ring
$\bar{a} = \frac{a}{R}$	
$\bar{a}_i \bar{b}_i$	parameters defined where used
$a_s$	diffusivity of seat material
$A = \frac{EJ_x}{GJ_\theta}$	
b	seal face width
$b_h$	fraction of seal width subject to hydrodynamic pressure
$\bar{b}_h = \frac{b_h}{b}$	
$b_m$	fraction of seal width subject to asperity pressure
$\bar{b}_m = \frac{b_m}{b}$	
$B = \frac{R \eta V b}{E J_x c^3}$	dimensionless constant
c	one half maximum roughness height
$c_o$	wear coefficient - $L^2/F$
$e_y$	eccentricity of loads in y direction measured from centroid or shear center as required
E	Young's modulus
$E( )$	expectancy operator
f	friction force
$\bar{f}$	$\frac{fc}{\eta VBR}$

$f_{h_1}, f_{h_2}$	viscous friction
$f(h_s)$	roughness distribution function
$f_m$	friction due to asperity contact
G	shear modulus
h	thickness of ring or $\theta$ grid space
$h(x)$	nominal film thickness
$\bar{h} = \frac{h}{c}$	dimensionless film thickness
$h_d, h_{da_j}, h_{db_j}$	film thickness variation due to elastic distortion and Fourier coefficients for same
$h_f$	waviness caused by friction and drive forces
$h_f, h_{fa_i}, h_{fb_i}$	waviness caused by tangentially varying friction force
$h_i, h_{ia_j}, h_{ib_j}$	film thickness variation due to initial waviness and wear and Fourier coefficients for same
$h_o$	mean film thickness
$h_s$	random portion of film thickness variation
$h_t, h_{ta_i}, h_{tb_i}$	deflection due to temperature and Fourier coeffi- cients
$h_w, h_{wo'}$	wear and Fourier coefficients for wear
$h_{wa_i}, h_{wb_i}$	
$h_{w_{amp_i}}$	amplitude wear wave
H	total film thickness
$\bar{H} = \frac{H}{c}$	
$H_\infty$	unit surface thermal conductance between ring and surrounding fluid

$H_y$	fraction of load supported by hydrodynamic pressure
$I_x$	moment of inertia for a straight beam about radial axis
$I_\theta$	torsional constant for straight beam
$J_x, J_\theta$	same as I values but for a curved beam
$k$	r grid space
$\bar{k} = \frac{k}{r_o}$	
$k_n$	a dimensionless constant that relates drive force to waviness in a seal ring
$k_s$	thermal conductivity of seat material
$k_r$	thermal conductivity of ring material
$\bar{k}_1 = \sqrt{\frac{H_\omega R^2}{k_r b} + n^2 i^2}$	
$K = \frac{k_r}{k_s}$	
$\ell/D$	equivalent journal bearing width to diameter ratio
$L = \frac{2\pi R}{n}$	length of one wave
$m_x$	distributed moment - $FL/L$
$n$	number of the harmonic or number of waves around seal face or direction normal to cavity boundary
$\bar{n} = \frac{n}{r_o}$	

$P$	hydrodynamic pressure in two dimensional model
$\bar{P} = \frac{pc^2}{r_o^2 \omega n}$	dimensionless hydrodynamic pressure in two dimensional model
$p_b$	boundary pressure
$p_c$	cavity pressure
$p_{fh_1}, p_{fh_2}$	hydrodynamic friction force per unit length of circumference $F/L$
$p_{fm}$	asperity friction force per unit length of circumference $F/L$
$\bar{p}_f = \frac{p_{fc}}{\eta V b}$	friction per unit length $F/L$
$p_h$	hydrodynamic pressure - $F/L^2$
$\bar{p}_h = \frac{p_{hc}^2}{R \eta V}$	dimensionless hydrodynamic pressure
$\bar{p}_h(\theta)$	dimensionless pressure per unit angle of seal circumference for two dimensional case
$\bar{p}_h(\theta) = \frac{p_h(\theta)c^2}{r_o^4 \eta \omega}$	
$p_{ha}$	average hydrodynamic pressure across width
$p_i$	inside pressure
$p_m$	pressure due to asperity contact -- equals yield or ultimate compressive strength - $F/L^2$
$\bar{p}_m = \frac{p_{mc}^2}{R \eta V}$	
$p_{ma}$	average asperity pressure across width
$p_o$	outside pressure
$p_o, p_{ai}, p_{bi}$	Fourier series representation of $p_{ma}$

$p_{un}$	unbalanced face pressure
$\bar{p}_{un} = \frac{p_{un} c^2}{R\eta V}$	
$\bar{p}_{aj}^*, p_{aj}^*$	Fourier series approximation to pressure distribution and Fourier coefficients
$p_{bj}^*$	
$q, q_{ai}, q_{bi}$	total heat flow and Fourier coefficients
$q_r$	heat flow into ring
$q_s$	heat flow into seat
$\bar{q} = \frac{qc}{\eta V^2 b}$	dimensionless heat flow
$q_r, q_\theta$	flow in two dimensional model
$\bar{q} = \frac{q}{r_o^{wc}}$	dimensionless flow
$Q$	total leakage for two dimensional case
$\bar{Q} = \frac{Q}{r_o^{2wc}}$	dimensionless leakage
$r$	radial coordinate
$r\theta z$	polar coordinates
$\bar{r} = \frac{r}{r_o}$	dimensionless radial coordinate
$r_o$	outside radius of seal
$r_i$	inside radius of seal
$R$	radius to centroid or mean radius of seal ring
$s_s$	shear strength of ring material
$\bar{s}_s = \frac{s_c}{\eta V}$	dimensionless shear strength

$t$	time
$\bar{t} = \frac{tc_o v^2 R \eta}{c^3}$	dimensionless time
$T$	temperature
$T_{a_i}, T_{b_i}$	Fourier coefficients of ring face temperature
$T_r$	ring face temperature
$T_s$	seat face temperature
$T_\infty$	temperature of fluid surrounding seal ring
$\bar{T} = \frac{k_s c^2 T}{\eta V^2 R}$	dimensionless temperature
$v$	face axial displacement
$V$	sliding speed
$w$	load support per wave
$\bar{w} = \frac{w_c^2}{R^2 \eta V b}$	dimensionless load support
$w_h$	load support due to hydrodynamic pressure
$w_m$	load support due to asperity pressure
$\dot{w}$	wear rate L/T
$W$	load support for two dimensional case
$\bar{W} = \frac{w_c^2}{r_o^4 \omega r \eta}$	dimensionless load support
$\bar{x} = \frac{x}{R}$	dimensionless x coordinate
$x_1$	point where hydrodynamic pressure begins

$x_2$	point where hydrodynamic pressure ends
$x, y, \theta$	ring coordinates
$x_1, y_1$	coordinate system fixed to seat
$x_2, y_2$	coordinate system fixed to ring
$\alpha$	angle of normal to cavity boundary
$\beta$	coefficient of thermal expansion
$\Delta$	a factor to provide a bound on viscous friction
$\bar{\Delta} = \frac{\eta V}{c S_s}$	
$\eta$	viscosity of sealed fluid
$\theta$	angular coordinate
$\theta_c r_c$	point on cavity boundary where curve is tangent to $r$ = constant curve
$\theta_\ell r_\ell$	cavity coordinates
$\lambda_s, \lambda_r$	fraction of grid space cut by boundary
$\mu$	coefficient of friction on face
$\rho_s$	density of seat material
$\psi$	phase angle of wear wave
$\omega$	angular speed of traveling wave or angular velocity of seal ring
$\Omega$	successive over relaxation factor

CHAPTER 1  
LUBRICATION IN MECHANICAL FACE SEALS

Introduction

In applications where a rotating shaft must pass from one fluid region to another, contacting mechanical face seals\* play the essential role of minimizing the transfer of fluid between the regions. Applications of face seals range from water pump seals to process pump seals to propeller shaft seals.

The performance and reliability of contacting mechanical face seals are of great importance for any type of equipment where minimal leakage, high reliability, and long life are necessary. Even for equipment where these factors are not so critical, seal failures and short seal life lead to high operating cost due to down time and maintenance cost.

Even though mechanical face seal technology has been steadily improving over the past several decades, an improvement of the state of the art of seal design would be most beneficial. Although seals having an acceptable life and reliability can be designed for many applications, further improvement in seal life and reliability would result in significant cost savings to the user. Also, there are numerous mechanical face seal applications where seal loading, reliability, life, and leakage requirements are difficult to achieve within the present state of the art. Examples of such applications are seals for pumps for nuclear power plants and seals for large diameter submarine propeller shafts. Additionally, the friction losses in face seals represent a significant fraction of energy consumed for pumping purposes. Within the present state of the art of seal design, it is very difficult to design a low leakage seal that also has a low friction loss.

\*The class of low leakage face seals where there is definite contact and wear of the faces as opposed to hydrostatic or hydrodynamic where a definite clearance is maintained.

The main barrier to the advancement of the state of the art is that the mechanics of seal operation are not well enough understood to be able to reasonably anticipate seal performance as function of design parameters. There are no well established fundamental theoretical bases that can be used to indicate the type of seal design that will give improved performance. Improvements that have been made have been brought about largely by trial and error combined with elementary sealing theories.

In order to be able to predict the performance of contacting face seals as a function of design parameters, it is essential that the lubrication mechanisms between the faces be well understood. At present it is known that hydrodynamic lubrication plays some role in providing load support for oil seals as well as water seals. But, the precise nature of this lubrication is not known. Several theories have been put forth, but it is not possible to use these theories for the design of seals except where face geometry is controllable. This excludes the class of contacting face seals of interest here because wear alters any planned geometry.

An argument can be made here for abandoning contacting face seal designs and using hydrodynamic or hydrostatic non-contacting designs. However, there are many applications where non-contacting face seals cannot be used for different reasons. Also, the contacting face seal offers low leakage at relatively low cost compared to non-contacting seals. Therefore, an improvement in the performance of contacting face seals while retaining their advantages is a worthwhile objective.

In this report, a theory of hydrodynamic lubrication with contact and wear is examined and developed. The hydrodynamic lubrication considered is of the type caused by circumferential waviness. This particular lubrication mechanism was chosen for study for two reasons. First, as later discussed, there is some experimental evidence of such lubrication. Second, waviness is a controllable parameter, and lubrication might therefore be improved through seal design.

In the model developed, the interaction of the hydrodynamic pressure with elastic distortion of the seal ring is considered. The effects

of friction on distortion and its interaction with hydrodynamic lubrication are explored. The behavior of hydrodynamic lubrication, leakage, and wear in relation to controllable seal design parameters such as ring stiffness, material properties, and roughness have been explored. These results are used to attempt to explain the behavior of existing seals as well as to suggest means of improving seal design.

The end result of successful research into this subject will be a mathematical model that can be used to accurately predict seal lubrication and leakage behavior as a function of controllable design parameters and to suggest means by which the performance of contacting face seals can be improved.

#### Previous Research

The contacting mechanical face seal consists basically of two annular rings which rotate relative to each other and are pressed together by spring and fluid pressure. The surfaces that rub together are usually made as flat as possible initially (within a few light bands of flatness) so as to minimize leakage.

At first glance it might be expected that the phenomenon at the seal interface would consist of entirely boundary lubrication using the sealed fluid as the lubricant. That is, due to the flat surfaces, no hydrodynamic pressure buildup would be expected. But it has been demonstrated that hydrodynamic and/or hydrostatic action does occur in face seals and that a) the net resulting lifting force is significantly larger than would be predicted by considering the fluid pressure drop across the annular slit and b) the net lifting force is a function of the average film thickness (which is not the case for fluid pressure drop across the slit if the seal faces were rigid and non-moving). It is these two characteristics of seal operation that cause the seal to have a useably long life. If such behavior did not occur, seals would wear out in a shorter time.

This very important discovery has been the focal point of a considerable amount of research in recent years. Several different theories

have been proposed to explain the generation of pressure in the seal interface region and many experimental investigations have been carried out.

A review paper by Nau [1]\* provides a good source of comparison of the pressure generation mechanisms proposed up to the time the paper was published. Nau states that it is generally accepted that the "majority of seals of all kinds depend upon the process of hydrodynamic lubrication for their satisfactory operation." No conclusion is reached on what mechanism is predominant, however. Denny [2] provided some of the first experiments on measurement of the fluid pressure between the seal faces. Mayer [3] also reports some experiments on the measurement of hydrodynamic pressure.

Several schools of thought for pressure generation mechanisms are evident in the more recent literature. The first of these is that micropads or microasperities (either intentional or by virtue of the materials themselves) cause pressure generation by acting as small step bearings. Hamilton, Walowit, and Allen [4] provide a solution for lubrication based on surface microirregularities and associated film cavities. The theoretical results agree qualitatively with experiment. In a later paper by Anno, Walowit, and Allen [5], tests were made on surfaces with planned microasperities and the results were compared to theory. These tests suggest that the use of planned microasperities is an effective method for lubricating the surfaces of face seals. A later paper by Anno, Walowit, and Allen [6] reported results on protruding and negative microasperities as well as the leakage from a microasperity lubricated face seal. In a paper on generally the same subject Kojabashian and Richardson [7] reported on a micropad model where the statistical distribution of pads produced by wear on a carbon surface was determined. Using this distribution of pads and a step-bearing approximation, performance predictions were made which were generally in agreement with experience.

During the later part of the 60's an extensive seals research program was undertaken by General Electric for NASA. Some of this work is

---

\*See List of References at end of report.

reported in Reference [8], and there are several other reports from the same study. This work is representative of a second school of thought which is that the fluid film and leakage are related to seal waviness, misalignment, and eccentricity. Much of the work has been reported in the literature by Findlay and Sneed.

Findlay's first paper [9] presents a mathematical model (short bearing approximation) for the pressure distribution caused by a wavy seal surface (several waves circumferentially around the face) and cavitation. In a second paper [10], Findlay presents the results of some experimental work carried out for a wavy (actually misaligned) seal. This paper attempts to verify experimentally the leakage predicted by the above cavitation model.

Cavitation of the type predicted by Findlay's theory has been observed by several investigators. Nau has carried out extensive research on cavitation in thin films [11] in general and more recently he has conducted a series of experiments directed toward seals using a glass plate as one of the seal faces [12]. Different cavity patterns could be observed depending on the loading and distortion. Cavitation has also been observed by Orcutt [13] under much different conditions using water as the fluid.

Sneed has published a number of papers dealing with various hydro-mechanical effects in seals. In his first paper [14], Sneed studies the effects of misalignment and surface waviness on leakage for laminar flow. In a second paper [15] treating the same subject for turbulent flow, Sneed found that the effects of waviness and misalignment are less. Sneed has considered several additional related phenomena in other papers [16], [17], [18], [19].

More recently Stanghan-Batch [20] reported results of experiments on hydrodynamic pressure in a carbon face seal operating in oil. He found that there is a periodic variation in pressure at the face that is consistent hydrodynamically with periodic variations in film thickness. He also found that initially flat carbon rings wear in a manner such that two high spots are produced when the ring is measured after testing and that there is some correspondence of these waves with pressure.

This author has made an extensive investigation of the waviness characteristics of face wear on carbon seal rings [21]. It now appears that most carbon rings<sup>1</sup> do not wear uniformly but rather in some wavy pattern, with two peaks being most common (see Figure 1-1). Further investigation [22], [23] has led to the conclusion that the largest portion of this waviness arises from distortion due to driving forces.

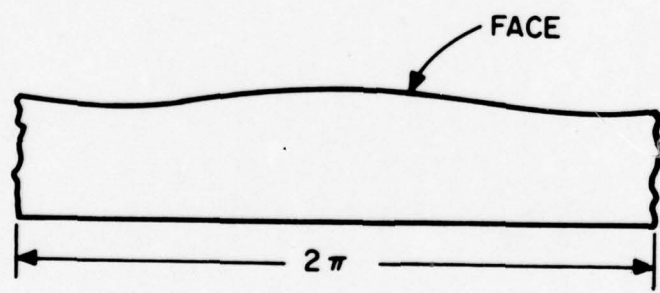
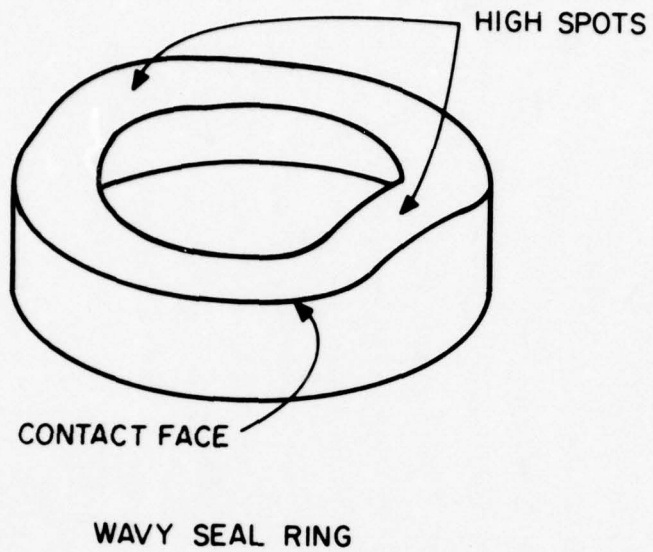
A third school of thought is concerned with radial elastic deformations of the seal faces in relation to generation of a fluid film. In a paper by Cheng and Snapp [24], a detailed analysis is made of the interaction between elastic deformation of the seal surface and the hydrostatic pressure. This is a static analysis and includes no hydrodynamic effects. Davies and O'Donoghue [25] present a theory which accounts for localized (as opposed to major seal face rotation or distortion) elastic deformation in relation to hydrostatic pressure and predict film thickness based on this model. In a following paper [26] Hooke and O'Donoghue present a refined treatment of the analysis in the previous paper.

Burton et al. have published several papers [27], [28], [29], [30] concerned with the role of thermal expansion in contacting sliding surfaces. The relationship of thermal expansion to instability has been examined. The role of wear and insulating films have also been investigated. Lebeck [31] has also investigated thermoelastic instability with wear for the case of the ring geometry used in seals. These investigations are related to the investigation herein in that they provide an understanding of how seal surfaces distort under thermal loading. This distortion interacts with lubrication mechanisms as will be discussed later.

Quite recently, Ludwig [32] has summarized many of the published seal models. He has formulated a new set of models based on interactions of waviness, misalignment, inertia, and secondary seal friction. Ludwig and Allen [33] have worked out the details of a lubrication model involving secondary seal frictions and misalignment.

---

<sup>1</sup>A seal ring made entirely of carbon, that is, having no rigid metal support.



WAVY SEAL RING - DEVELOPED

Figure 1-1. Waviness wear on a Seal Ring

To determine which of the lubrication theories have some validity, the experimental evidence must be examined. First, considering the microasperity load support mechanism, cavitation streamers of the type that result from microasperity lubrication have been observed by Orcutt [13] and researchers at Battelle [34] by using a transparent material for one of the seal rings. Certainly these observations suggest that microasperity lubrication plays some role in the lubrication of face seals, but the actual extent or fraction of the load support is not known.

Several researchers [20], [13], [34] have determined the existence of circumferential pressure and/or film thickness variations which in turn indicates that hydrodynamic lubrication and load support do occur due to waviness of the seal rings. Again, the fraction of load support developed by this mechanism in face seals in actual service is not known.

#### Seal Applications of Interest

The type of seals that are of interest for this research are contacting face seals or those where wear of the seal faces acts as the primary limitation to better seal performance. The term wear is used broadly here to include a gradual wearing away and deterioration of the seal faces and heat checking and blistering of the faces. All of these types of wear can lead to excessive leakage and thus terminate the useful life of the seal. All of these types of wear can be attributed in part to inadequate lubrication at the seal faces.

Seal applications where wear is a limiting factor for performance occur in many instances. For example, when long seal life with low leakage is a requirement, the gradual type of wearing away of the faces becomes important. In seal applications where sealed pressure and sliding speed are high of necessity, again deterioration of the seal faces serves as the primary limitation for desired seal performance. This critical wear situation arises primarily when sealing a low viscosity fluid such as water. Water is the fluid used for the examples herein.

This research is primarily for seals having a low Young's modulus material mating with a high Young's modulus material--typical of the

carbon face seal. Also, only seals having no intentional surface asperities will be considered. Thus, the type of seal of interest is that which is commonly found in field applications.

Proposed Model--Elastohydrodynamic Lubrication with Asperity Contact and Wear

For the type of seal described, a better understanding of the lubrication mechanisms between seal faces is the key to improved seal performance. In such applications it is evident that full separation of the faces does not exist at least for some portion of the seal face or at least for some fraction of operating time because of the existence of the wear. However, there is evidence to suggest that hydrodynamic lubrication still exists for such seals, but the pressure developed is not sufficient to provide adequate face separation.

Because of the experimental evidence and primarily because waviness is a controllable parameter, it was determined that a close examination of the waviness mechanism should be made. It was also determined that unlike many of the models discussed under Previous Research, considerable attention should be given to relating the sources of waviness to real seal parameters and in determining the effects of such non-ideal parameters such as surface roughness and wear on lubrication.

The seal model under study is based on hydrodynamic lubrication due to waviness. Load sharing with asperity contact, wear, and elastic deflection are included in the model. The effect of micropad lubrication will not be directly included. However, since hydrodynamic asperity pad lubrication would simply act to reduce the basic material wear rate, the effects are actually included because basic material wear rates are obtained experimentally and include these effects.

Now, examining the various elements of the proposed model, the presence of asperity to asperity contact in seals can be justified in two ways. First, asperity to asperity contact must exist to account for the wear found in seals operating in non-abrasive environments. Secondly, it can be shown, particularly for seals sealing low viscosity fluids or for heavily loaded seals, that the film thickness required for equilibrium using hydrodynamic pressure only is of the same order of

magnitude as the surface roughness. In some cases the film thickness is less than the surface roughness. Thus some asperity to asperity contact would be expected and is required to support that fraction of the load not supported by hydrodynamic pressure.

Models of asperity load support in conjunction with hydrodynamic support have been developed for bearings by Christensen [ 35], [ 36] and Thompson and Bocchi [ 37]. These models predict a friction and wear behavior for thin film thickness bearings that is consistent with experimental results. These same models have been extended herein to study asperity contact, hydrodynamic load sharing, and wear in mechanical face seals.

For small film thicknesses, the effects of surface roughness on hydrodynamic lubrication must be considered. Christensen [ 36] has developed a statistical method that can be used to calculate hydrodynamic load support where the surface roughness effects are included in the film thickness variation. Thus, models are available for the purposes of accounting for these important effects.

#### Sources of Waviness

Waviness of the seal faces is essential to the hydrodynamic lubrication theory developed. In the discussion of previous research, it was pointed out that experimental evidence shows the existence of such waviness, and there are several possible mechanisms that can act to produce waviness in mechanical face seals. The first of these will be termed initial waviness.

This author [ 21] has made extensive measurements of the waviness of initially flat carbon seals after some period of operation. The conclusion reached is that a large portion of the waviness measured (in the order of 100's of  $\mu$ -in in many cases) is due to the fact that the seal ring is distorted into a wavy configuration due to driving forces. After a period of operation, the face wears relatively flat--while the ring is distorted. Therefore, after the ring is unloaded and returns to its undistorted shape, it appears to be wavy.

The significance of initial waviness to hydrodynamic lubrication is that there is certainly enough face waviness initially to create

converging diverging film regions--even though the seal face is lapped flat. Also, the results described point out the fact that seal rings are quite flexible, and any change in operating conditions can change the waviness. This may lead to a continual source of waviness as is discussed later in this report.

A second mechanism can act to modify the wave. This second mechanism will be termed the phase shift effect. Given an initial waviness (see Figure 1-2), it can be shown that some hydrodynamic load support will develop, the balance of the load being supported by asperity contact. The center of pressure of the hydrodynamic support is shifted from the original center of the wave (see Figure 1-2). Since seal rings are elastic, the resulting equilibrium position for the wave is shifted circumferentially from the original position. The maximum wear rate due to asperity contact occurs at the point of minimum film thickness as shown. Since this point does not coincide with the original peak of the undistorted wave, wear will cause a slow circumferential movement of the wave. Thus the initial wave does not wear as fast because of the shifting.

As the waviness wears away, it is reasonable to expect that friction will increase because of the increased asperity contact required to support the load. Since driving forces create face distortion, any change in friction torque would cause a change in waviness. Thus, this third mechanism could cause a new waviness pattern which in turn could cause hydrodynamic load support and reduce friction.

A fourth mechanism that interacts with the other mechanisms discussed is due to thermal expansion. This author [31] and Burton [27] have shown how localized heating can lead to seal waviness and instability for essentially dry sliding contact. Some of the same principles apply to the lubricated case. The region of asperity contact operates at a higher temperature. This may cause a distortion that even further increases the asperity load. Hydrodynamic action might break down at some point leading to a change in friction and a new pattern of waviness.

It is thought that all four waviness mechanisms may play some role in the hydrodynamic lubrication of face seals. In summary, there is a complex interaction among the following phenomena:

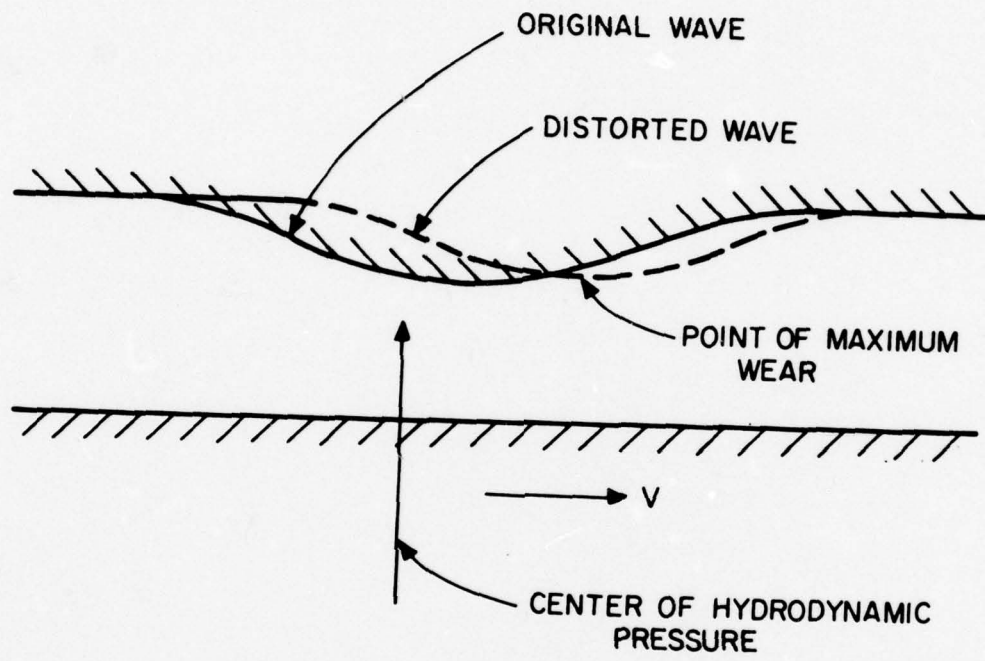


Figure 1-2. Shift of Wave Due to Hydrodynamic Pressure

- 1) Initial waviness
- 2) Waviness due to drive forces
- 3) Wear
- 4) Elastic deformation due to pressure
- 5) Elastic deformation due to temperature effects
- 6) Hydrodynamic lubrication for rough surfaces including cavitation
- 7) Asperity to asperity contact, load support, and friction.

The interactions of these phenomena are all time dependent because of wear.

The proposed model is developed in detail in the next chapter.

## CHAPTER 2

### THE ONE DIMENSIONAL ELASTOHYDRODYNAMIC EQUILIBRIUM MODEL

#### The Equilibrium Model

Considering first the hydrodynamic portion of the equilibrium model, seal faces develop surface roughness patterns that usually appear to be aligned with the direction of sliding (roughness is measured across a section that is perpendicular to the direction of sliding) (see Figure 2-1), although measurements do show a definite roughness perpendicular to this. For the purpose of the initial investigation, the interaction of only the roughness aligned with the direction of sliding or longitudinal roughness with hydrodynamic action will be considered. According to Christensen [36], the total film thickness for this case can be described by a function of the form

$$H = h(x) + h_s(y, \xi) \quad (2-1)$$

where  $h(x)$  is the nominal film thickness and  $h_s$  is the random part of film thickness due to surface roughness. A polynomial approximation of the Gaussian density distribution function is used to describe the surface roughness

$$f(h_s) = \frac{35}{32c^7} (c^2 - h_s^2)^3, \quad -c \leq h_s \leq c \quad (2-2)$$

$c$  corresponds to three standard deviations and represents the peak roughness amplitude. It is assumed that the roughness distribution remains constant with time and coordinate  $x$ .

For the one dimensional problem under consideration, the Reynolds equation in dimensionless form is [36].

$$\frac{d}{dx} \left[ \frac{dp_h}{dx} E(\bar{H}^3) \right] = 6 \frac{d}{dx} E(\bar{H}) \quad (2-3)$$

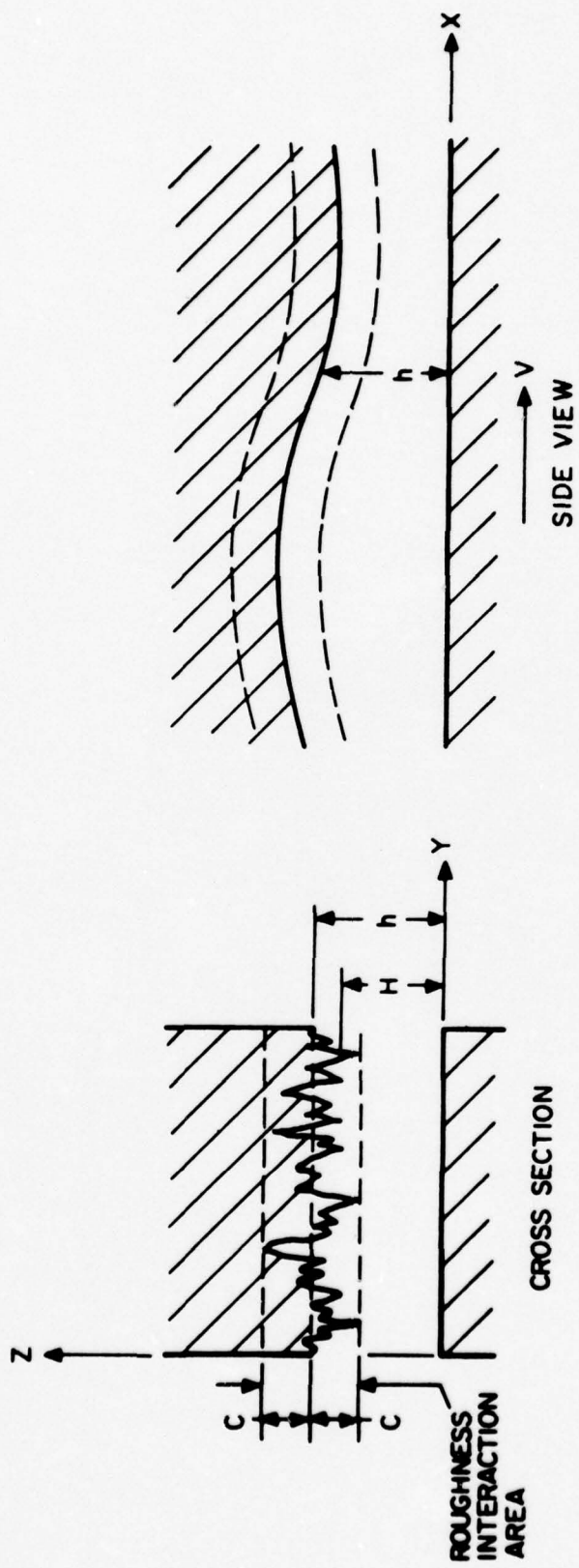


Figure 2-1. Longitudinal Roughness and Geometry

where:

$$\bar{H} = \frac{H}{c} \quad (2-4)$$

$$\bar{x} = \frac{x}{R} \quad (2-5)$$

$$\bar{p}_h = \frac{p_h c^2}{R \eta V} \quad (2-6)$$

and where  $E$  is the expectancy operator which is equal to

$$E(\cdot) = \int_{-\infty}^{\infty} (\cdot) f(h_s) dh_s \quad (2-7)$$

$\bar{p}_h$  is the expected value of hydrodynamic pressure.

For  $h > c$ , using the density function given by equation (2-2), the required expected values are:

$$E(\bar{H}) = \bar{h}(x) \quad (2-8)$$

$$E(\bar{H}^3) = \bar{h}^3 + \bar{h}/3 \quad (2-9)$$

For  $h \leq c$ , the expected values are

$$E(\bar{H}) = \frac{35}{32} \left[ \frac{1}{8} + \frac{16}{35} \bar{h} + \frac{1}{2} \bar{h}^2 - \frac{1}{4} \bar{h}^4 + \frac{1}{10} \bar{h}^6 - \frac{1}{56} \bar{h}^8 \right] \quad (2-10)$$

$$E(\bar{H}^3) = \frac{35}{32} \left[ \frac{1}{40} + \frac{16}{105} \bar{h} + \frac{3}{8} \bar{h}^2 + \frac{16}{35} \bar{h}^3 + \frac{1}{4} \bar{h}^4 - \frac{1}{20} \bar{h}^6 + \frac{3}{280} \bar{h}^8 - \frac{1}{840} \bar{h}^{10} \right] \quad (2-11)$$

For boundary conditions, the Reynolds conditions are used. It is assumed that cavitation ends and a pressure increase begins at the point of largest film thickness  $x_1$  (see Figure 2-2). The absolute maximum value is used. This boundary condition location is somewhat arbitrary. For a one dimensional model, the actual beginning point for the full

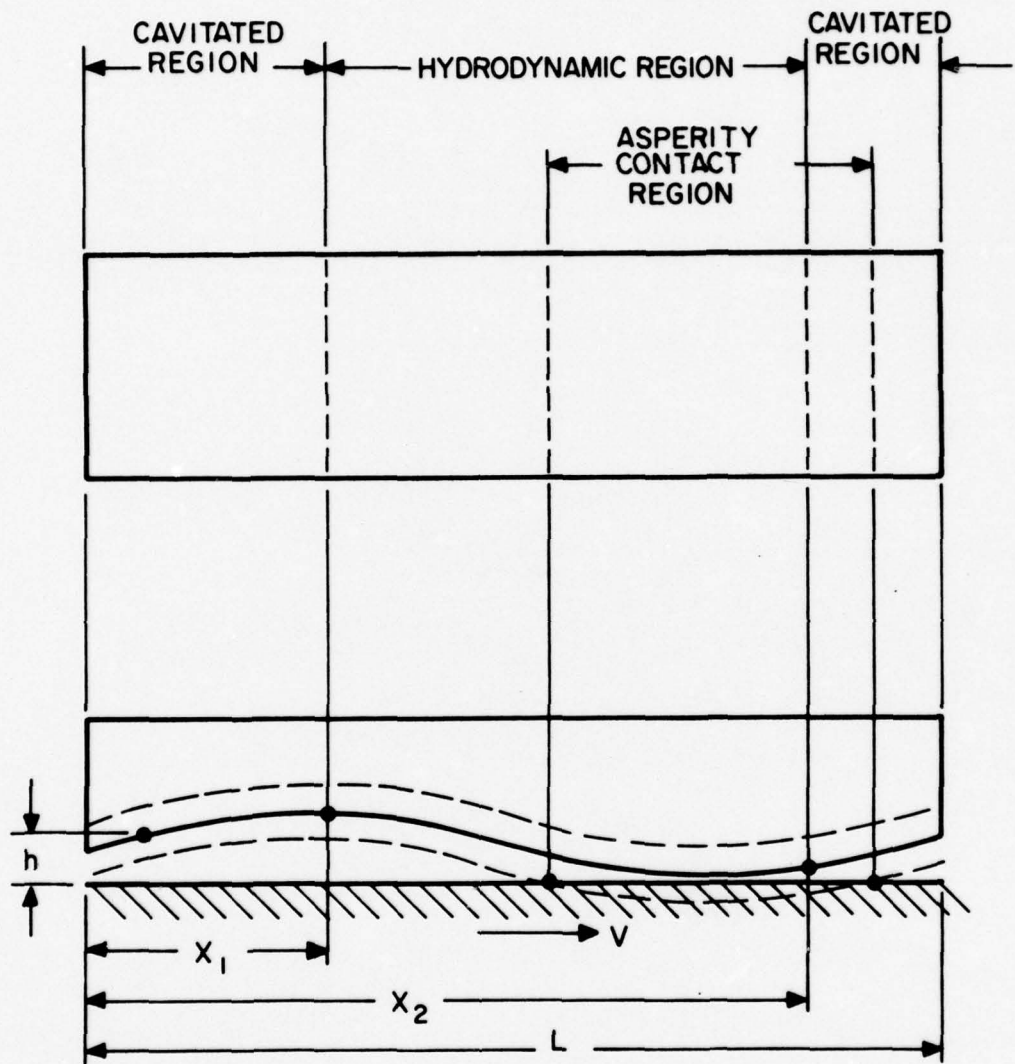


Figure 2-2. Hydrodynamic and Asperity Interaction Regions

film cannot be theoretically established. The convention used for bearings has been used. It is known that load support is not too sensitive to this location. At some point beyond the minimum film thickness,

$$p_h = \frac{dp_h}{dx} = 0 \quad \text{at } x = x_2 \quad (2-12)$$

Within the region of hydrodynamic action there may be an interaction region where  $h < c$ . In this case the appropriate expectancy equations above are used and additional load support is provided by asperity contact.

The length L shown in Figure 2-2 and used in the above equations is the period of one initial wave. The number of initial waves n is arbitrary as far as the solution is concerned. However, it is assumed that there is only one apparent maximum (where pressure buildup begins) within one period.

$$L = \frac{2\pi R}{n} \quad (2-13)$$

The nominal film thickness is assumed to have the following form

$$\begin{aligned} h = h_o + \sum_{j=1}^{\infty} (h_{ia_j} \cos nj\bar{x} + h_{ib_j} \sin nj\bar{x}) \\ + \sum_{j=1}^{\infty} (h_{da_j} \cos nj\bar{x} + h_{db_j} \sin nj\bar{x}) \end{aligned} \quad (2-14)$$

$h_o$  represents the mean film thickness. This Fourier series can represent any possible waveform.  $h_{ia_j}$  and  $h_{ib_j}$  are Fourier series coefficients for the initial waviness and wear at any particular time.  $h_{da_j}$  and  $h_{db_j}$  correspond to a series that describes the change in film thickness caused by elastic distortion of the seal ring.

Assuming for the moment that the coefficients in equation (2-14) are known, then the hydrodynamic pressure distribution can be determined as follows:

1) Find the point of maximum nominal film thickness from equation (2-14). Call this  $x_1$ .

2) The one dimensional Reynolds equations (2-3), integrated one time is

$$\frac{dp_h}{dx} \bar{E}(\bar{H})^3 = 6 \bar{E}(\bar{H}) + C_1 \quad (2-15)$$

where  $C_1$  is an unknown constant.

3) Using boundary conditions, equation (2-12), then

$$\frac{dp}{dx} = 0 \text{ at some } x = x_2 \text{ and}$$

$$C_1 = -6\bar{E}(\bar{H}) \Big|_{x_2} \quad (2-16)$$

4) A second integration of the Reynolds equation gives

$$\bar{p}_h = \int_{x_1}^x \frac{6\bar{E}(\bar{H})}{\bar{E}(\bar{H}^3)} d\bar{x} + C_1 \int_{x_1}^x \frac{1}{\bar{E}(\bar{H}^3)} d\bar{x} \quad (2-17)$$

5) Because  $\bar{p}_h(x_2) = 0$ , substitution of equation (2-16) into equation (2-17) gives

$$0 = \int_{x_1}^{x_2} \frac{6\bar{E}(\bar{H})}{\bar{E}(\bar{H}^3)} d\bar{x} - \left[ 6\bar{E}(\bar{H}) \Big|_{x_2} \right] \times \int_{x_1}^{x_2} \frac{1}{\bar{E}(\bar{H}^3)} d\bar{x} \quad (2-18)$$

6) Equation (2-18) can easily be solved for  $x_2$  by incrementing from  $x_1$  until the equality is satisfied. Then  $C_1$  can be calculated using equation (2-16).

7) The values of the two integrals in equation (2-18) are saved so that  $p_h(x)$  from equation (2-17) can be calculated without additional evaluation of the expectancy functions.

The above procedure saves considerable computer time compared to the Newton iteration method coupled with Runge-Kutta integration used in an earlier version of the computer program.

For the interaction region where  $\bar{h} < 1$ , it is assumed that the asperity contact pressure over the actual area of contact is equal to  $p_m$ , a material constant taken as the compressive strength of the softer material.

$$\bar{p}_m = \frac{p_m c^2}{RnV} \quad (2-19)$$

In the interaction region, the fraction of the seal width subject to  $p_m$  is given by

$$\bar{b}_m = 1 - \bar{b}_h \quad (2-20)$$

where

$$\bar{b}_h = \frac{1}{32} [ 16 + 35\bar{h} - 35\bar{h}^3 + 21\bar{h}^5 - 5\bar{h}^7 ], \quad h < c \quad (2-21)$$

$$\bar{b}_h = 1, \quad h > c \quad (2-22)$$

and where

$\bar{b}_h$  is the fraction of seal width subject to hydrodynamic pressure in the interaction region.

Using these fractions, the average pressures across the seal face are given by

$$\bar{p}_{h_a} = \bar{b}_h \bar{p}_h \quad (2-23)$$

$$\bar{p}_{m_a} = \bar{b}_m \bar{p}_m \quad (2-24)$$

The load support provided by the combined hydrodynamic and asperity pressures is given by

$$\bar{w}_h = \int_0^{2\pi/n} \bar{p}_h \bar{b}_h d\bar{x} \quad (2-25)$$

$$\bar{w}_m = \int_0^{2\pi/n} \bar{p}_m \bar{b}_m d\bar{x} \quad (2-26)$$

$$\bar{w} = \bar{w}_h + \bar{w}_m = \frac{w_c^2}{R^2 \eta V b} \quad (2-27)$$

To support the load,

$$\bar{w} = \frac{2\pi}{n} \bar{p}_{un} \quad (2-28)$$

where

$$\bar{p}_{un} = \frac{p_{un} c^2}{R \eta V} \quad (2-29)$$

where  $p_{un}$  is the unbalanced pressure on the seal face. The total load support for the seal is obtained by multiplying  $\bar{w}$  by the number of waves  $n$  around the seal.

The friction at the interface has several sources. For the full film hydrodynamic region,

$$\bar{p}_{fh_1} = \left[ E\left(\frac{1}{H}\right) + \frac{1}{2} \frac{dp_h}{d\bar{x}} E(H) \right] \bar{b}_h \quad (2-30)$$

$$\bar{f}_{h_1} = \int_{x_1}^{x_2} \bar{p}_{fh_1} d\bar{x} \quad (2-31)$$

For the cavitated areas the friction caused by the fluid is

$$\bar{p}_{fh_2} = E\left(\frac{1}{H}\right) \frac{E(H(x_2))}{E(H)} \bar{b}_h \quad \begin{array}{l} 0 \leq \bar{x} \leq x_1 \\ \bar{x}_2 \leq x \leq \frac{2\pi}{n} \end{array} \quad (2-32)$$

$$\bar{f}_{h_2} = \int_0^{\bar{x}_1} \bar{p}_{fh_2} d\bar{x} + \int_{\bar{x}_2}^{\frac{2\pi}{n}} \bar{p}_{fh_2} d\bar{x} \quad (2-33)$$

The function  $\frac{E(\bar{H}(x_2))}{E(\bar{H})}$  provides the fraction of the possible full film based on continuity. The additional expectancy functions needed are given by

$$E\left(\frac{1}{\bar{H}}\right) = \frac{35}{32} \left[ (1-\bar{h}^2)^3 \ln \frac{\bar{h}+1}{\bar{\Delta}} - \frac{11}{12} + \frac{11}{5} \bar{h} + \frac{23}{4} \bar{h}^2 - \frac{8}{3} \bar{h}^3 - \frac{27}{4} \bar{h}^4 + \bar{h}^5 + \frac{147}{60} \bar{h}^6 \right], \quad \bar{h} < 1 \quad (2-34)$$

$$E\left(\frac{1}{\bar{H}}\right) = \frac{35}{32} \left[ (1-\bar{h}^2) \ln \left( \frac{\bar{h}+1}{\bar{h}-1} \right) + \frac{66}{15} \bar{h} - \frac{16}{3} \bar{h}^3 + 2\bar{h}^5 \right]$$

$$\bar{h} > 1 \quad (2-35)$$

The  $\bar{\Delta}$  in equation (3-35) must be greater than zero, otherwise viscous friction goes to infinity as the film thickness becomes zero. A realistic value for  $\bar{\Delta}$  can be obtained by setting the maximum viscous shear stress equal to the shear strength of the material, or

$$\bar{\Delta} = \frac{\eta V}{c S_s} = \frac{1}{\bar{s}_s} \quad (2-36)$$

The friction due to asperity contact is given by

$$\bar{P}_{fm} = \bar{s}_s \bar{b}_m \quad (2-37)$$

$$\bar{f}_m = \int_0^{2\pi/n} \bar{s}_s \bar{b}_m d\bar{x} \quad (2-38)$$

where

$$\bar{s}_s = \frac{S_s c}{\eta V} \quad (2-39)$$

and where  $S_s$  is the shear strength of the material. The total distributed friction is

$$\bar{p}_f = \left( \bar{p}_{fh_1} \text{ or } \bar{p}_{fh_2} \right) + \bar{p}_{fm} \quad (2-40)$$

where  $\bar{p}_f$  is the distributed friction force in force per unit length of seal circumference

$$\bar{p}_f = \frac{p_{fc}}{\eta V b} \quad (2-41)$$

Total friction is

$$\bar{f} = \bar{f}_m + \bar{f}_{h_1} + \bar{f}_{h_2} \quad (2-42)$$

where

$$\bar{f} = \frac{fc}{\eta V b R} \quad (2-43)$$

The coefficient of friction becomes

$$\frac{f}{w} = \mu = \frac{\bar{f}}{w} \frac{c}{R} \quad (2-44)$$

Once the pressure distribution is known, the effect of pressure on elastic distortion can be determined. Rather than dealing with the actual pressure distribution to find deflection, it is simpler to make a harmonic analysis of the pressure and determine deflection in this way. Thus,

$$\bar{p}^* = \sum_{j=1}^{\infty} \left[ \bar{p}_{a_j}^* \cos nj\bar{x} + \bar{p}_{b_j}^* \sin nj\bar{x} \right] \quad (2-45)$$

where

$$\bar{p}_{a_j}^* = \frac{n}{\pi} \int_0^{2\pi/n} (\bar{p}_{h_a} + \bar{p}_{m_a}) \cos(nj\bar{x}) d\bar{x} \quad (2-46)$$

$$\bar{p}_{b_j}^* = \frac{n}{\pi} \int_0^{2\pi/n} (\bar{p}_{h_a} + \bar{p}_{m_a}) \sin(nj\bar{x}) d\bar{x} \quad (2-47)$$

The face deflection of a ring subjected to a varying face loading is given by equation (2-154), reference [22]. For a pressure distri-

bution expressed in the form of equation (2-45), deflection is given by

$$h_d = \sum_{j=1}^{\infty} \left[ h_{da_j} \cos njx + h_{db_j} \sin njx \right] \quad (2-48)$$

where

$$h_{da_j} = \frac{B p_a^* j^2 (m^2 + A)}{m^6 - 2m^4 + m^2} \quad (2-49)$$

$$h_{db_j} = \frac{B p_b^* j^2 (m^2 + A)}{m^6 - 2m^4 + m^2} \quad (2-50)$$

and where

$$m = nj \quad (2-51)$$

The constant B represents a dimensionless stiffness,

$$B = \frac{R^5 b \eta V}{E J_x c^3} \quad (2-52)$$

where E is the Young's modulus and  $J_x$  is the moment of inertia about a radial axis for the seal ring.  $h_d$  represents the elastic distortion of the ring due to  $p_h$  and  $p_m$ . The difference between the indices j and m accounts for the fact that the elastic distortion depends on the harmonic number for the entire ring.

For given values of  $h_o$ ,  $h_{ia}$  and  $h_{ib}$ , the equilibrium distortion of the ring can be calculated using the following iterative procedure.

- 1) Assuming  $h_d = 0$ , calculate the hydrodynamic and asperity pressure distributions using the method previously outlined.
- 2) Using equations (2-46), (2-47), (2-49), and (2-50), determine the elastic distortion for this distribution.
- 3) Take a fraction of the change (because of stability of the solution) of the elastic distortion computed from equations (2-49) and (2-50), and recalculate the pressure distribution.

- 4) Repeat steps (2 and 3) until there is no further change in elastic deflection. The result is the equilibrium deflection.

Once elastic distortion equilibrium has been found, then load support can be calculated from equation (2-27). Friction can also be calculated from equation (2-42).

To determine the equilibrium position for a particular given face load,  $h_0$  must be varied until the calculated load equals the given load. This solution then represents the equilibrium operating condition for the seal at a particular time.

Considerable difficulty was encountered with the solution for the equilibrium deflection and mean film thickness. Several different approaches were tried to simplify the problem and to speed up convergence.

First, because a fundamental nth harmonic disturbance has been assumed, the elastic deflection will occur only for the n, 2n, 3n, etc. harmonics. Using equation (2-154) of reference [22], it is easy to show that the deflection due to a 2n disturbance is at least an order of magnitude less than the deflection due to the nth harmonic disturbance - even assuming equal magnitude disturbances. Because the magnitude of the disturbance greatly decreases with increasing harmonic number, deflection due to the 2n harmonic and higher can be neglected at least for a first approximation. This considerably reduces the number of unknowns in the problem.

Even with this simplification the method of convergence previously mentioned was unsatisfactory. The method was sometimes unstable. Convergence was based on the sum of the squares of the two components of deflection so that the parameter acted upon did not represent the true parameter used to check the results.

The above method was greatly improved by using a variable fraction of the (old-new) value as a new guess. Convergence was somewhat improved. Also, a limiting condition was imposed to maintain stability. The method was still slow to converge to sufficient accuracy. Accuracy presented a problem at the next level of iteration on the load. If

the solution were not precise, additional iterations at the next level were required to find  $h_o$ .

The next approach used was a type of interpolating iterative scheme treating  $h_a$  and  $h_b$  separately. Each new guess value was based on information from three previous iterations. However, the interaction of the two variables caused the limits to change so that in some cases convergence became impossible.

The final and successful method used was based on the Newton approach using finite differences to approximate derivatives. Although the method worked well for the two variables  $h_a$  and  $h_b$ , the third variable  $h_o$  was also included to speed up the total process. The equations to be solved are the following:

$$F_1(h_{da_1}, h_{db_1}, h_o) = h_{da_1} - h_{dag_1} = 0 \quad (2-53)$$

$$F_2(h_{da_1}, h_{db_1}, h_o) = h_{db_1} - h_{dbg_1} = 0 \quad (2-54)$$

$$F_3(h_{da_1}, h_{db_1}, h_o) = w(\text{required}) - w(\text{calculated}) = 0 \quad (2-55)$$

where  $h_{dag_1}$  and  $h_{dbg_1}$  are the guess values of  $h_{da_1}$  and  $h_{db_1}$ . This leads to a system of three equations in three unknowns that must be solved for each Newton iteration. Four evaluations of the functions  $F_1$ ,  $F_2$ , and  $F_3$  are required for each iteration.

#### Additional Considerations

There are several other aspects of the one dimensional model that require explanation before a solution is presented. First, in the solution for the problem as outlined, it is assumed that the wave shape is identical for each of the  $n$  periods and that there is only one continuous region of hydrodynamic pressure within each of the waves.

Second, because of ring geometry, the number of major high spots in a real seal will usually be 2, 3, or 4, with 2 being the most common case [22]. However, the wave shape from one segment to the next would not be the same in any real seal. It is also true that each of the waves

is not sinusoidal as is assumed here. However, because the harmonic analysis of real seals [22] shows that the seal waviness does occur predominantly at the lower harmonics and can be approximately described by a sine function, the approach used will provide a good qualitative measure of the performance of real seals with unplanned waviness and an even better qualitative measure of performance of real seals with planned waviness. It should be noted that the general problem can be solved for a specific non-sinusoidal waviness pattern; however this is not a useful tool for making a general study of the influence of waviness on performance of contacting face seals.

Third, according to the theory being used herein [36], there is no side leakage in regions of asperity contact. This happens because the longitudinal roughness creates a series of parallel sealing dams across which the liquid cannot flow\*. In some cases for the solution of the equilibrium problem it is possible that the maximum film thickness is less than 1.0. This means that the entire seal face is in asperity contact. When this condition occurs, there is no way for the sealed fluid to flow into the seal face region because there can be no side leakage theoretically. From a practical standpoint, the amount of liquid in the seal interface, which determines in turn the flow and the beginning point of pressure buildup, becomes arbitrary. For this reason, when  $h_{max} \leq 1.0$  it is assumed that all hydrodynamic load support vanishes. That is, because there is no guarantee that the face will receive adequate lubrication to develop hydrodynamic pressure under these conditions, in the interest of realistic modeling, it is assumed that hydrodynamic load support vanishes.

Fourth, in regions of no asperity contact there will be considerable side leakage. However, the one dimensional model assumes zero side leakage. If zero side leakage is assumed, hydrodynamic pressure becomes unrealistically large. To compensate for this error in the one dimensional model, a factor based on narrow bearings is used. The ratio

\*One would expect that some leakage would occur in these regions because of an imperfect seal. However, the side leakage would be much smaller than in regions of no asperity contact.

of load support for 360° narrow bearings relative to infinitely wide bearings is reported by Cameron [38].

For length to width ratios within the range of interest for sealing, and for  $\epsilon = 0.2$  (which is a representative ratio of maximum and minimum film thickness for the seals under study), the load ratio is given approximately by the following relationship

$$\frac{P_{\text{actual}}}{P_{\text{calculated}}} = 0.205 (\ell/d)^{1.8567} \quad (2-56)$$

where

$$\ell/D = \frac{b}{R} \frac{n}{2} \quad (2-57)$$

Even though there is no side leakage in a region of asperity contact, the ratio was applied uniformly across the entire region of hydrodynamic pressure. It is recognized that this approach is approximate, but it does provide a better approximation to reality than simply using the infinitely wide bearing assumption, and it permits the relatively simple one dimensional model to be used to effectively make useful though approximate predictions. The more exacting approach is of course to use a two dimensional solution as is discussed in a later chapter.

#### Alternative Method of Solution

A finite difference method of solution was developed as an alternative to the method described in an attempt to find a better and faster method of solution. Basically, the problem to be solved is the simultaneous solution of the Reynolds equation and the elastic deflection equation. It was thought that by using a finite difference method, a simultaneous solution could be obtained, rather than an iterative solution as just described. However, it can be noted that the finite difference representation of the Reynolds equation, equation (2-3), does not give a separation of the variables  $\bar{p}_h$  and  $\bar{h}$  in linear equation form. Thus the simultaneous solution is not possible.

As an alternative, the Reynolds equation, equation (2-3), was first solved with finite differences based on an assumed or guess value of  $\bar{h}(x)$ . Then the deflection equation (from reference [22])

$$\bar{h}_d^{vi} + 2 \bar{h}_d^{iv} + \bar{h}_d'' = \frac{R_b^4}{EJ_x C} (p_a'' - Ap_a) \quad (2-58)$$

where

$$p_a = p_{h_a} + p_{m_a} \quad (2-59)$$

was solved by finite difference methods for the deflection  $\bar{h}_d$  (rather than using a harmonic analysis of pressure as before) based on the pressure determined from the previous finite difference solution for the Reynolds equation. It was found that the mean film thickness had to be specified for this solution. The above method was repeated until an equilibrium  $h_d(x)$  was found.

To have completed the solution would have required a second level of iteration on the mean film thickness  $h_o$  in order to make the applied load match the load capacity. Thus, as it turned out, the method was quite cumbersome and much less efficient than the first method discussed.

The results from this second method were used, however, to verify the results from the first method. Because the solutions were obtained independently, errors in both methods were discovered and corrected. Thus, the method served a useful purpose even though its development was stopped because of its inefficiency.

#### The Equilibrium Solution - Base Case

Using the model and method of solution developed, an equilibrium solution was found for what will be termed the base case. The base case represents a real seal application, which is that of a hot water carbon face seal for a 92.1 mm (3-5/8") shaft turning at 1800 RPM. Data for the actual seal are used where possible.

Solutions are based on  $n = 3$  and 4.06 micron ( $160 \mu$  in) initial waviness amplitude. These values were chosen so that a significant amount of hydrodynamic load support would occur for the base case. This represents a larger third harmonic waviness than is usually found for this seal. Thus the results to be presented are indicative of the performance that would be expected if a larger than normal amount of

third harmonic waviness were manufactured into the seal or if the surface roughness were less than the assumed value as discussed later. The results are also directly applicable to seal designs where stiffness is larger relative to initial waviness than for the present case.

The base case parameter values are selected as follows:

$422^{\circ}\text{K}$ ( $300^{\circ}\text{F}$ ) $\text{H}_2\text{O}$	sealed fluid
$\eta = 18.7 \cdot 10^{-5} \text{ Pa}\cdot\text{s}$ ( $3.91 \times 10^{-6} \text{ lb}_f \text{sec}/\text{ft}^2$ )	viscosity
$R = 50.8 \text{ mm}$ (2.00 in)	mean radius
$n = 3$	number of waves
$L = 106.43 \text{ mm}$ (4.19 in)	length of one period
$c = 1.02 \mu\text{m}$ (40 $\mu\text{in}$ )	seal surface roughness during operation
$V = 13.4 \text{ m/s}$ (44 ft/sec)	sliding speed
$p_m = 259.25 \text{ MPa}$ (37600 $\text{lb/in}^2$ )	compressive strength of carbon (2-60)
$s_s = 49.4 \text{ MPa}$ ( $7170 \text{ lb/in}^2$ )	shear strength
$b = 4.76 \text{ mm}$ (0.1875 in)	face width
$E = 2.07 \cdot 10^4 \text{ MPa}$ ( $3 \times 10^6 \text{ lb/in}^2$ )	Young's modulus for seal ring
$I_x = 4.91 \times 10^3 \text{ mm}^4$ (0.01179 in $^4$ )	moment of inertia of seal ring cross section about radial axis
$p_{un} = 0.321 \text{ MPa}$ (46.6 $\text{lb/in}^2$ )	unbalanced face load
$\frac{EJ}{GJ_0} = A = 6.0$	ring parameter
$h_i = 4.06 \mu\text{m}$ (160 $\mu\text{in}$ )	initial waviness

The parameter values above are converted into the following dimensionless numbers needed for the solution:

$$\bar{p}_m = \frac{p_m c^2}{R \eta V} = 2.10$$

$$\bar{s}_s = \frac{s_s c}{\eta V} \approx 20,000$$

$$\bar{p}_{un} = \frac{p_{un} c^2}{R \eta V} = 0.0026$$

$$B = \frac{R b \eta V}{E J_x c^3} = 38,000 \quad (2-61)$$

$$\bar{c} = \frac{c}{R} = 2.0 \cdot 10^{-5}$$

$$\bar{b} = \frac{b}{R} = 0.09375$$

$$\bar{h}_i = \frac{h_i}{c} = 4.0$$

The number of points calculated on the pressure curve is approximately 100.

The results for the base case solution are as follows:

% hydrodynamic load support = 36%

$\mu = 0.13$

The pressure and film shape results for the equilibrium solution are shown in Figures 2-3 and 2-4. Figure 2-3 shows the equilibrium film shape. The point of minimum film thickness is shifted somewhat from the original (undeflected) minimum point by the action of the non-symmetrical hydrodynamic load support. A large fraction of the wave penetrates the asperity region as shown. The large fraction is required because of the relatively low hydrodynamic load support (36%) for this base case. Figure 2-4 shows the hydrodynamic and asperity pressure distribution. Because the center of hydrodynamic pressure is shifted to the left, the wave is shifted toward the right. The net first harmonic waviness in Figure 2-3 is about 0.27 amplitude. Thus the seal ring has been flattened considerably (compare the 4.0 initial waviness to the net 0.27 waviness).

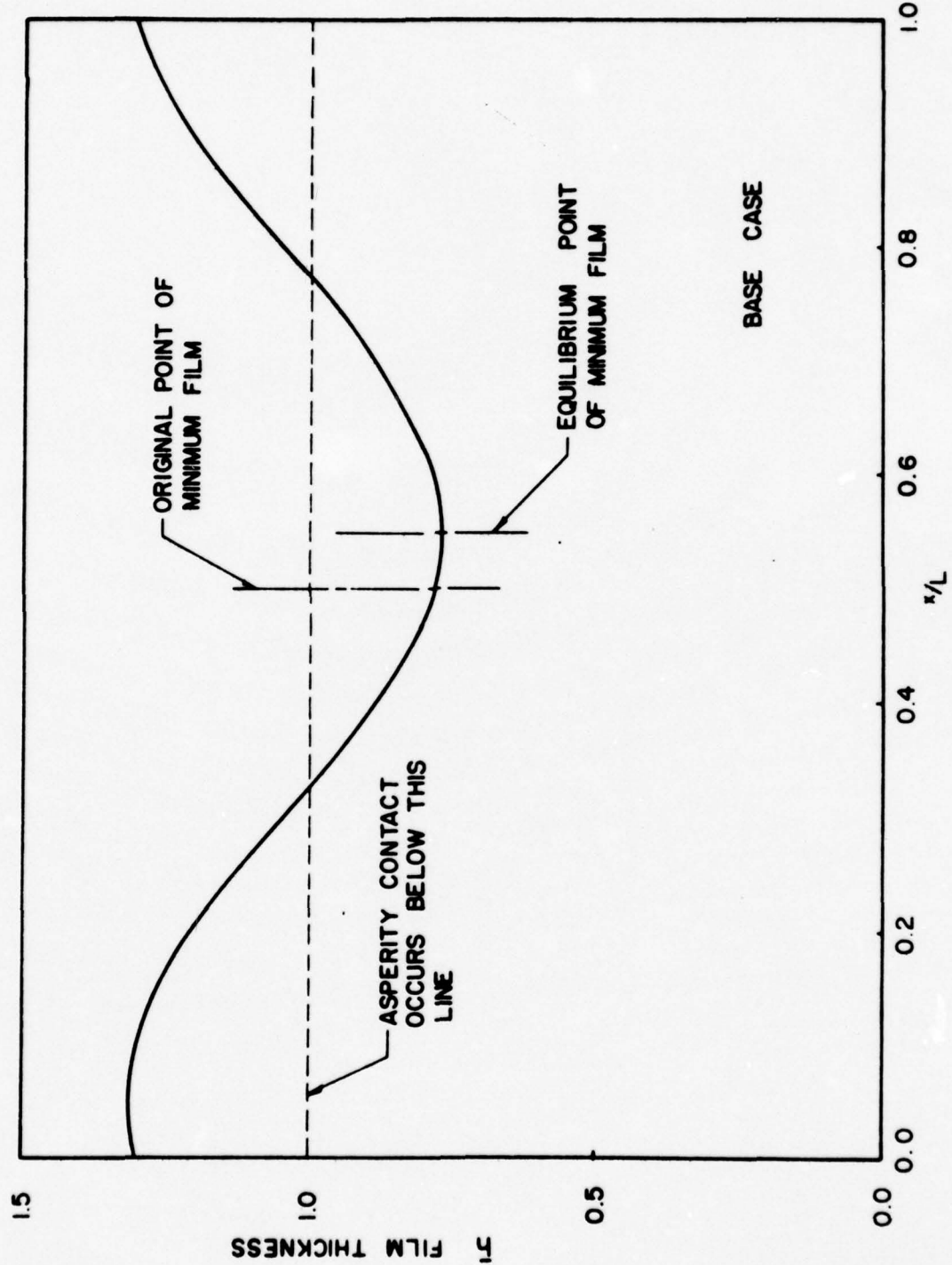


Figure 2-3. Equilibrium Film Shape at  $\bar{T} = 0$ , Base Case

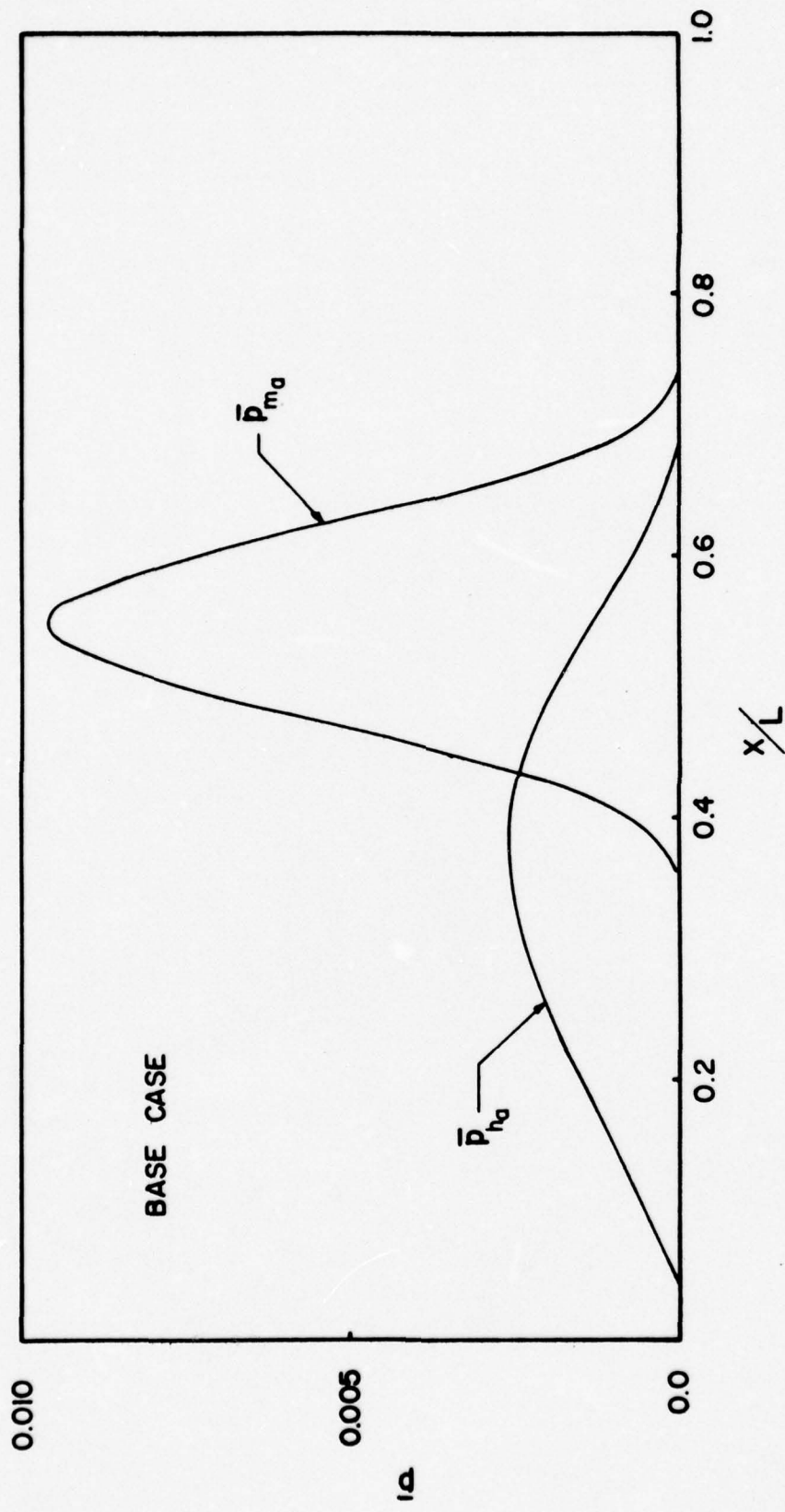


Figure 2-4. Hydrodynamic and Asperity Pressure at  $\bar{T} = 0$

Because of the significant hydrodynamic load support, the wear rate of the material will be reduced compared to the case where there is zero hydrodynamic load support.

#### Effect of Various Parameters on Seal Performance

In order to develop an understanding of the significance of the many parameters on initial load support and leakage, a parameter study has been made. Rather than varying the non dimensionless parameters, the individual parameters such as surface roughness were varied in order to get a better understanding of behavior in relation to the controllable variables of the problem. In all cases, the base case, as described previously, is included as one of the data points for comparison purposes. The curves are based on the base case data with only the one given parameter being changed each time.

##### Initial Waviness

Figure 2-5 shows the effect of initial waviness on % hydrodynamic load support. The base case happens to be very close to the peak load support value ( $\bar{h}_{ial} = 4.3$ ). To the left of the peak, load support drops off because the wave simply flattens out, i.e., net waviness  $\rightarrow 0$ . To the right of the peak, load support falls off because the high peak that results simply causes a greater penetration into the asperity zone so that most of the load is supported by asperity contact. Thus, the hydrodynamic support cannot develop.

Friction coefficient shown in Figure 2-5 simply follows a reciprocal type relationship to the % load support, as would be expected.

A third curve shows a plot of the quantity  $\bar{h}_{max} - 1$ . This is the maximum dimensionless gap that occurs in the film and serves as an indicator of what leakage might be expected. When the initial amplitude is made larger and larger, the seal face rides up on the peaks and the leakage gaps become larger.

Below  $\bar{h}_{ial} = 3.65$  the entire surface is in the region of asperity contact. As discussed previously, it is assumed that hydrodynamic load support would cease to exist in reality for this situation.

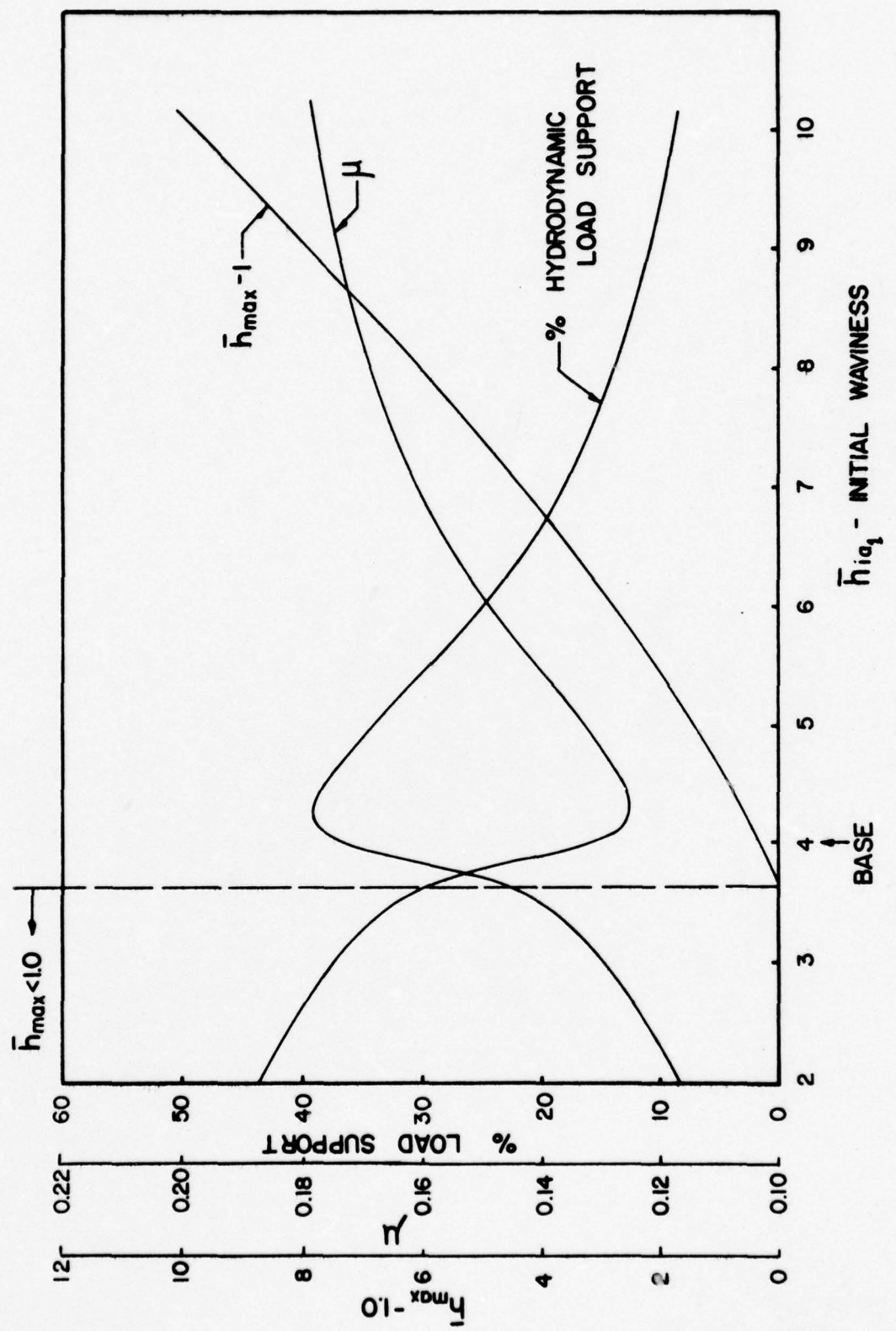


Figure 2-5. Effect of Initial Waviness Amplitude

### Number of Waves

Figure 2-6 shows the effect of the number of waves. As the number of waves increases, the % support decreases and then increases. As the number of waves increases the relative stiffness greatly increases (see equation 2-49). Thus, at  $n=4$ , the points of the waves bear the load because they protrude into the asperity region more than for the  $n=3$  case. Thus, as the number of waves increases, load support begins to increase simply because of the larger number of relatively short hydrodynamic regions.

Below  $n=3$ ,  $\bar{h}_{max} < 1$  so there is no useful hydrodynamic support. The  $\bar{h}_{max} - 1$  curve shows that as the number of waves increases the gap approaches a magnitude of 8, which is twice the initial waviness amplitude. Thus, as  $n$  increases, there is little deflection and the seal face rides up only on the high spots as previously discussed.

The above results are for a constant initial waviness. It is useful to find the particular initial waviness value which gives maximum load support for each number of harmonic  $n$ . These results are tabulated below for the base case data.

$n$	$(\bar{h}_{ia1})_{optimum}$	% hydrodynamic load support
3	4.3	39
4	1.3	49
5	0.7	58
6	0.6	66

As the harmonic number increases, the optimum initial waviness decreases because of the increased relative stiffness. Load support increases with increasing  $n$  because the side leakage effect becomes smaller. The results so far do not show if there is some value beyond which the load support does not increase. However, the results do show that greater support could be obtained by having a rather small amplitude of initial waviness at the higher harmonics.

### Roughness Height

The roughness height chosen for the base case was  $c = 1.02$  micron ( $40 \mu in$ ). This figure was based on an average measurement of roughness

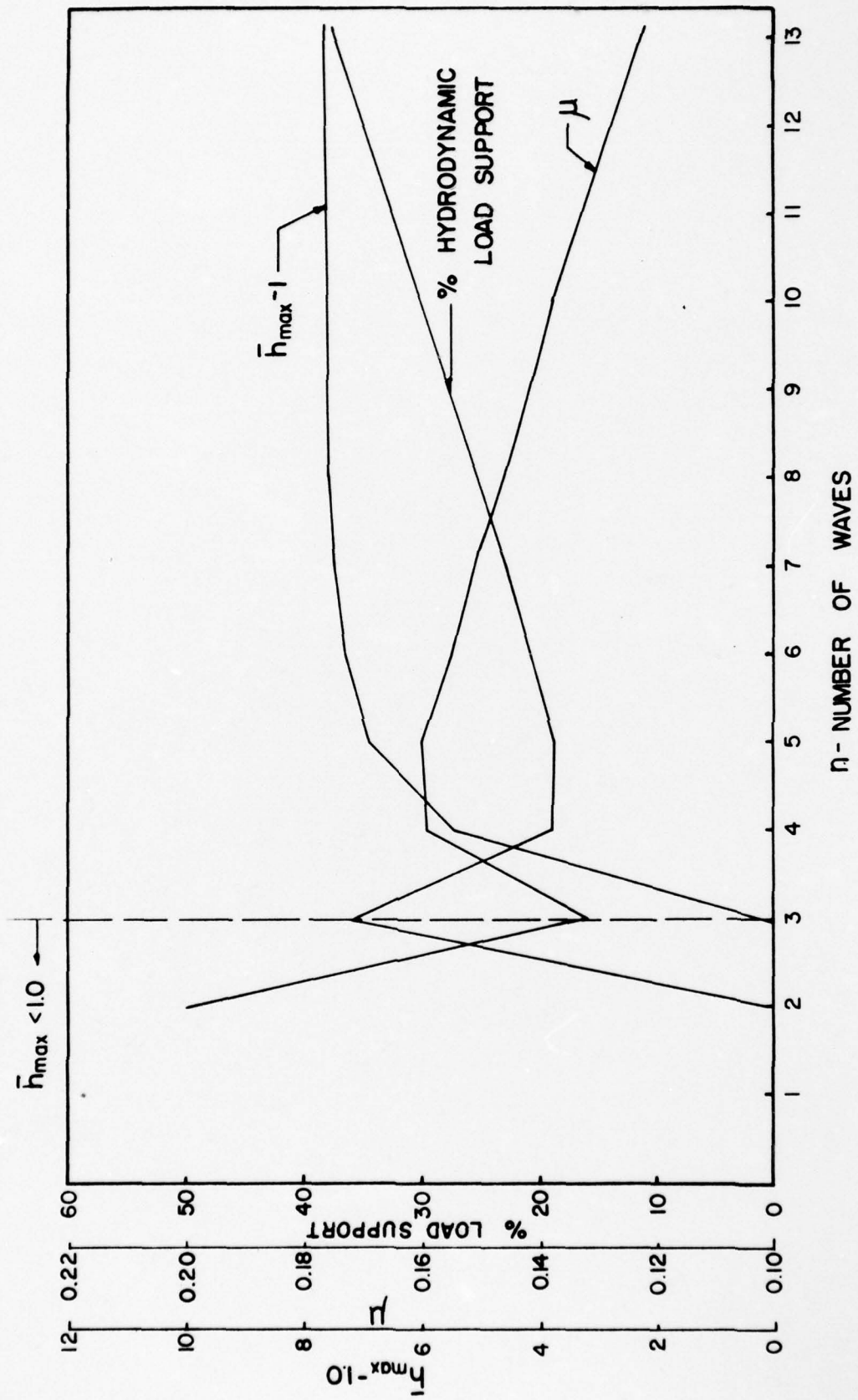


Figure 2-6. Effect of Number of Waves  $n$

on several seals. It is to be noted that some seal surfaces are much rougher and some are much smoother. It is thought that roughness might be controlled to some extent by material selection.

The significance of this discussion becomes apparent when considering the results shown in Figure 2-7, the effect of surface roughness. If surface roughness were 1/2 as much as for the base case, then hydrodynamic load support approaches 100%. The greater surface roughness does not give as much load support because the tangential leakage resistance is lower the greater the roughness height. It should be noted that asperity load support leads to a condition where the minimum film thickness is always approximately some small fraction of the roughness height; thus, decreasing the roughness height in effect decreases the true minimum film thickness.

The maximum film gap plot is given for the quantity  $\frac{C}{C_{\text{base}}} (\bar{h}_{\max}^{-1})$ . This provides a standard base size for the dimensionless gap. The results show that the gap becomes larger as the roughness is decreased. The reason for this appears to be the fact that there is less depth penetration of the asperities by the peaks as the % load increases. Also, the shape of the hydrodynamic pressure curves spreads the load support out more, which causes less deflection.

#### Stiffness

Figure 2-8 shows the results of varying the stiffness parameter B. This parameter has an effect similar to that of initial waviness. In general, the same % support can be obtained for a stiffer ring with a lower amount of initial waviness than for a less stiff ring.

#### Face Width

Figure 2-9 was obtained by varying the face width. The unit load  $p_{un}$  was maintained at the same value. This is similar to what happens in a real seal when the balance ratio is maintained at a constant and the face width is changed. Either increasing or decreasing the face width causes the % load support to decrease relative to the base case. When the face width is increased, additional load support is obtained because of reduced side leakage. However, the increased load support is offset because of flattening of the seal due to, in effect, decreasing

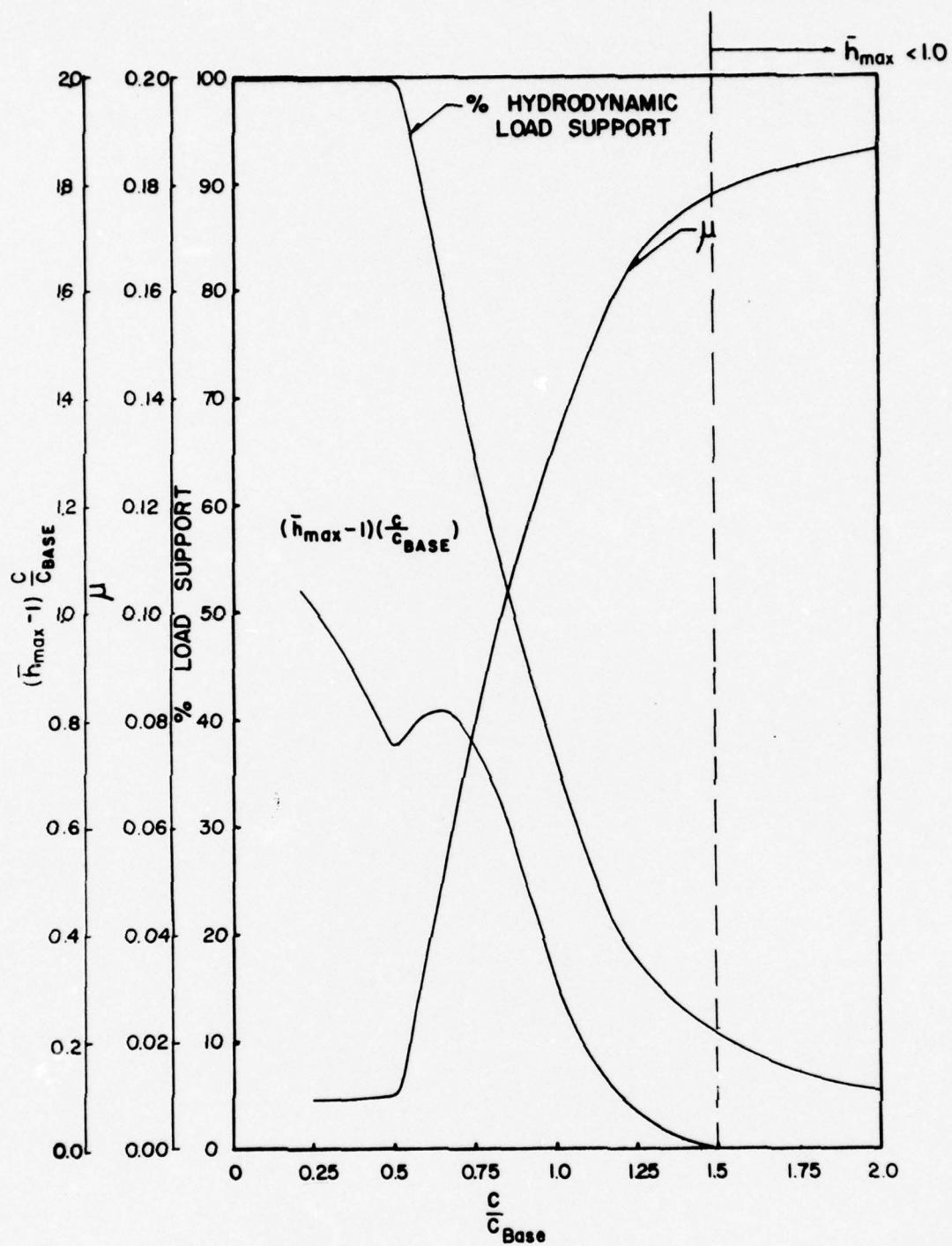


Figure 2-7. Effect of Surface Roughness

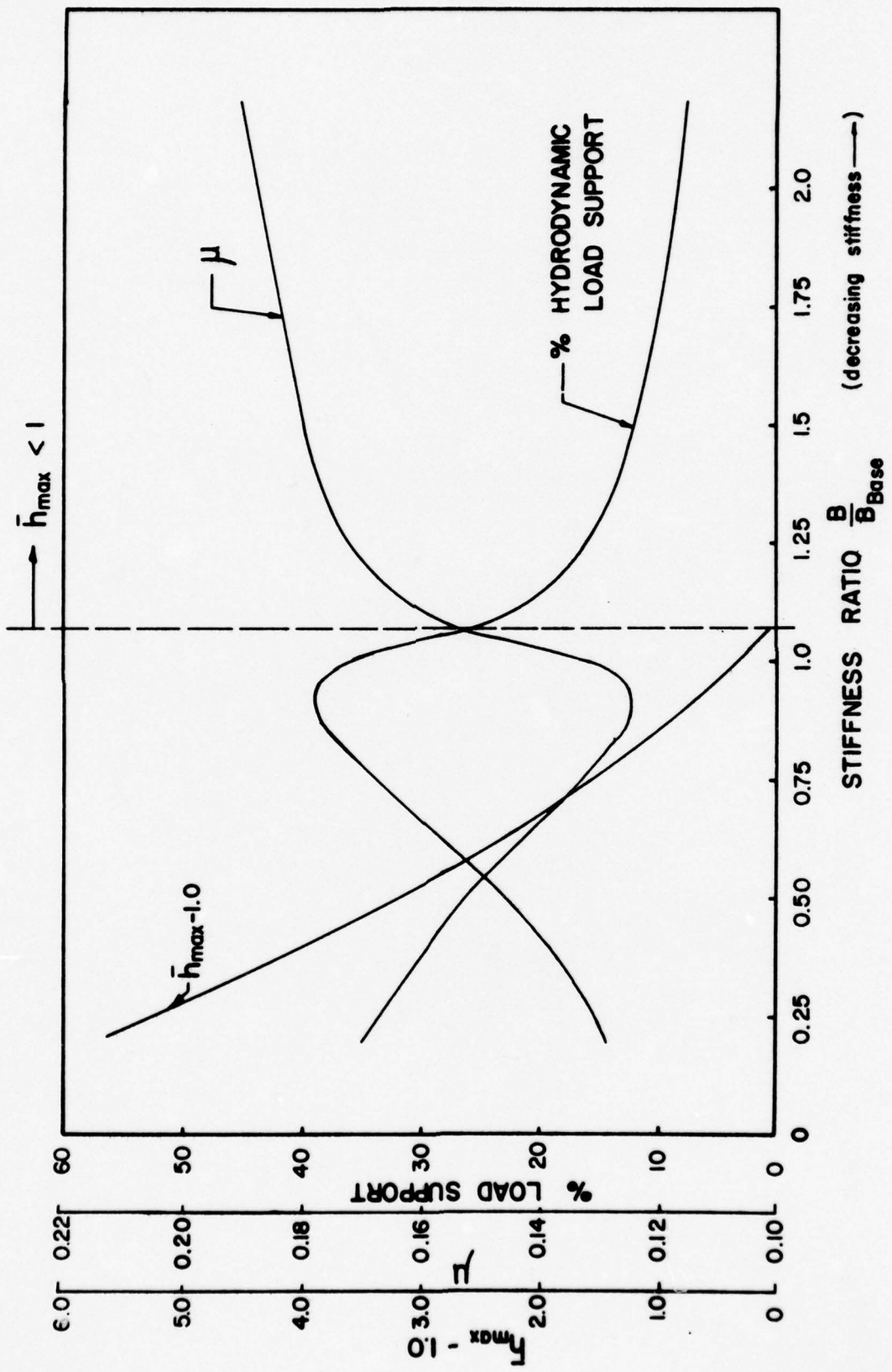


Figure 2-8. Effect of Ring Stiffness

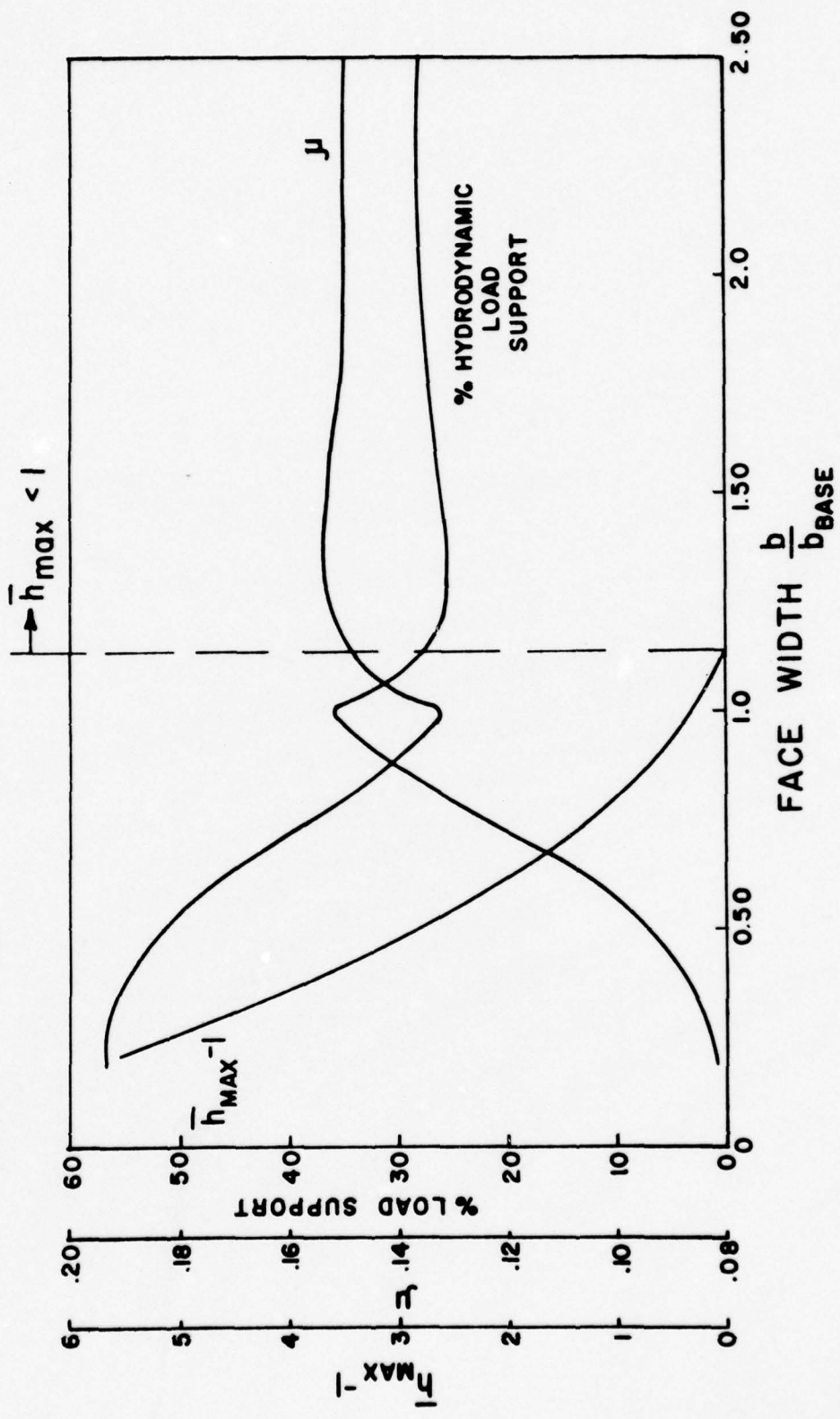


Figure 2-9. Effect of Face Width

stiffness (see parameter B). After a point, the effect is overcome and a small increase in load support occurs. To the left of the base case, the % load support is greatly reduced because of the narrowing face width and because the stiffness parameter B is reduced (which in effect moves the waviness away from its optimum value). The fact that  $\bar{h}_{\max}^{-1}$  increases to the left is due to the increase in stiffness and riding up on the peaks.

#### Face Load

Figure 2-10 shows the effect of varying the unbalanced face load. As expected, % load support decreases quickly with increasing face load. However, decreasing face load also causes a small decrease initially before the large increase in % load support. This decrease is caused by moving away from the optimum net waviness condition. Figure 2-5 shows that load support drops to either side of the optimum, so as the load in the above case is decreased, there is an effective increase in waviness which causes the % load support to drop off until  $p_{un}$  becomes much smaller.

#### Initial Liftoff Waviness

In order to assess how much hydrodynamic action might exist in this particular seal for typical values of initial (or drive force caused) waviness, the amount of initial waviness to just cause  $\bar{h}_{\max} > 1$  (the beginning of hydrodynamic action) was determined for several values of n. These results are tabulated below along with typical values of drive force caused waviness for this particular seal.

n	% Hydrodynamic Load Support	$\bar{h}_{ia_1}$ for $\bar{h}_{\max} = 1.0$	$\bar{h}_{ia_1}$ mean for this seal [22]
2	16	39.	3.4
3	24	3.7	0.70
4	28	0.91	0.23
5			0.14

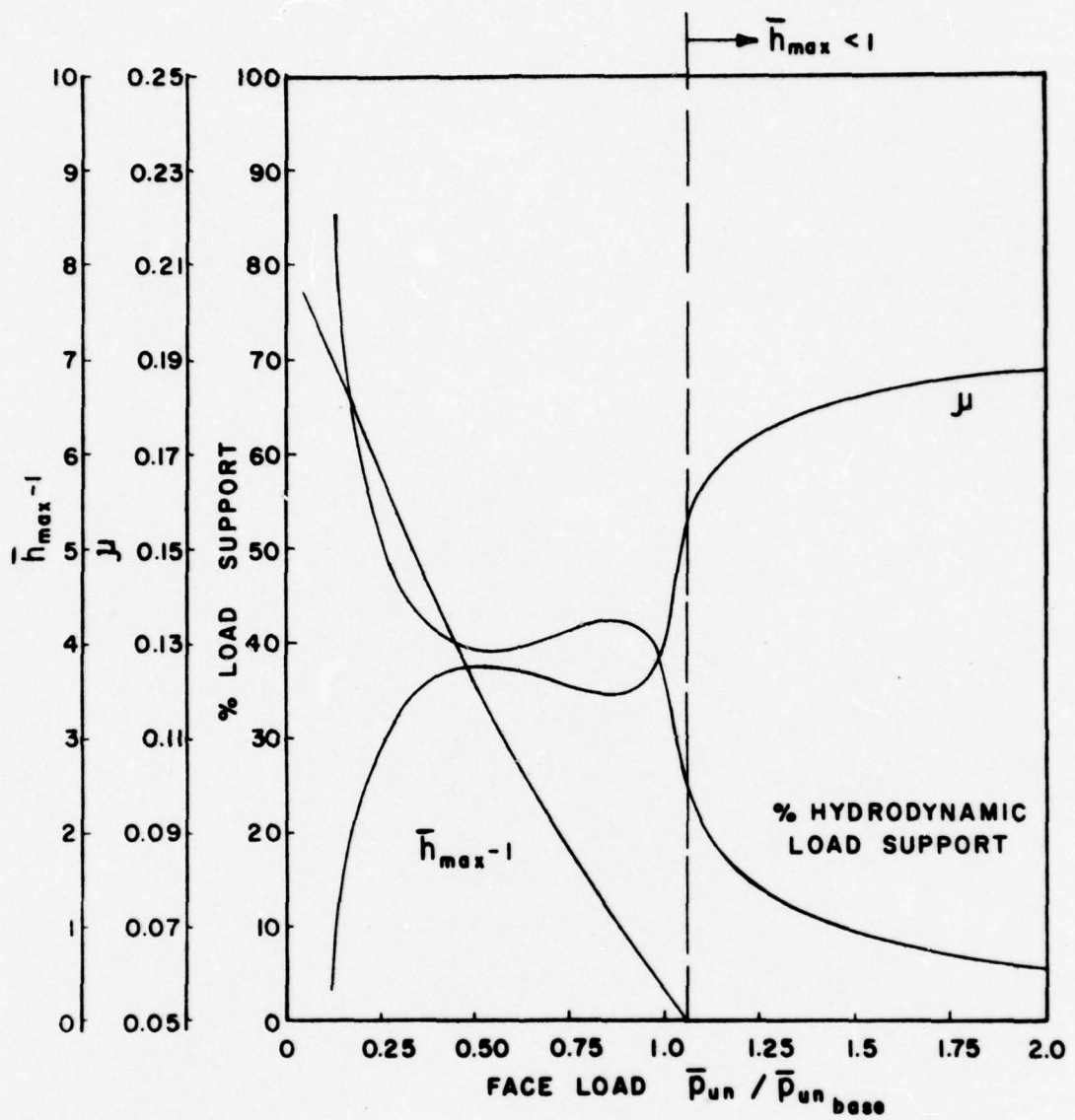


Figure 2-10. Effect of Face Load

From the above results it is clear that for this particular base case, hydrodynamic lubrication may not exist to any appreciable extent at the lower harmonics. However, with small changes in some of the parameters, notably surface roughness or above average waviness, then hydrodynamic load support would be expected. Thus it is expected that in some actual applications for water seals, there may be an appreciable extent of hydrodynamic load support while in others, there may be none.

#### Parameter Study Summary

The results of the previous parameter studies show that the % hydrodynamic load support depends on a number of parameters and that some of these variables greatly interact. The results also show that certain conditions could be chosen for a seal design where the % hydrodynamic load support would be very high even though the maximum gap (and expected leakage) is low. Thus parameter studies could be used to determine an ideal initial waviness condition. From the results it appears that to enhance hydrodynamic load support, the following conditions should be met:

- 1) optimum amount of waviness for a given stiffness;
- 2) number of waves should be large, assuming the initial waviness is adjusted to maximize load support;
- 3) materials should be such that minimum roughness will be produced;
- 4) optimum face width.

As will be shown in a later chapter, there is also an optimum waviness shape.

What is also apparent from the study is that the % hydrodynamic load support depends on some variables that are not specified at all in the design of a seal but in fact are somewhat random. The first of these is surface roughness. For a non-abrasive service, the in operation surface roughness obtained depends primarily on the two materials chosen. Experience has shown that a wide range of in operation surface finish results for the same apparent conditions. The second random variable is initial waviness. Even though seals are lapped initially flat enough such that hydrodynamic lubrication may not normally be set up, there are many factors, such as drive forces, that cause

seal rings to go out of flat to the extent that hydrodynamic lubrication would be initiated. Thus, the influence of some of these random variables over hydrodynamic lubrication may in fact partially explain the apparent random behavior of many seemingly identical seals.

CHAPTER 3  
ONE DIMENSIONAL TIME DEPENDENT MODEL

The results from the equilibrium model solution show that normally some amount of asperity contact can be expected in a water seal. Thus, the original geometry will be altered by wear. It is important to study the effects of wear on hydrodynamic load support to determine under what conditions, if any, the hydrodynamic load support remains.

The time dependent behavior of the seal can be found by using the equilibrium model. It is assumed that time dependent behavior is due solely to wear, or some other external time dependent parameter such as pressure, and that the equilibrium model applies to any point in time for a given worn condition. This assumption requires that changes be slow, because transient effects in the Reynolds equation, such as squeeze effects, are not included.

For the purpose of this study, the most basic of wear relationships is used [39]. It is assumed that wear occurs only where there is asperity contact and that wear is proportional to the average mechanical pressure. Thus,

$$\frac{dh_w}{dt} = C_o p_m V_a \quad (3-1)$$

where  $C_o$  is the wear coefficient which depends on the material pair.  $C_o$  is generally related to material hardness (compressive strength of the material in this study).

$$C_o = \frac{\text{const}}{p_m} \quad (3-2)$$

The parameter  $h_w$  represents the material removed from the soft face of the sealing pair.

In dimensionless form

$$\Delta \bar{h}_w = \bar{p}_m \Delta \bar{t} \quad (3-3)$$

where

$$\bar{t} = \frac{C_o R n V^2 t}{c^3} \quad (3-4)$$

and the other symbols are as previously defined.

The wear  $\bar{h}_w$  is represented by a Fourier series

$$\bar{h}_w = \bar{h}_{wo} + \sum \bar{h}_{wa_i} \cos ni\theta + \bar{h}_{wb_i} \sin ni\theta \quad (3-5)$$

The change in wear over time  $\Delta \bar{t}$  is thus

$$\Delta \bar{h}_w = \Delta \bar{h}_{wo} + \sum \Delta \bar{h}_{wa_i} \cos ni\theta + \Delta \bar{h}_{wb_i} \sin ni\theta = \bar{p}_{ma} \Delta \bar{t} \quad (3-6)$$

The coefficients  $\Delta \bar{h}_{wa}$  and  $\Delta \bar{h}_{wb}$  are found by making a Fourier analysis of  $\bar{p}_{ma}$ . These increments are then added to the running totals  $\bar{h}_{wai}$  and  $\bar{h}_{wb_i}$ . Thus, the method amounts to a simple forward difference method applied on equation (3-1).

The term  $\bar{h}_{wo}$  represents the total wear averaged around the seal face. The term  $\bar{h}_{wo}$  represents the average wear rate which is proportional to the average value of  $\bar{p}_{ma}$ . Thus,

$$\frac{d\bar{h}_{wo}}{d\bar{t}} = \bar{p}_{ma} \quad \text{average around seal} \quad (3-7)$$

From equation (2-26)

$$\bar{p}_{ma} \quad \text{average} = \frac{n}{2\pi} \bar{w}_m = \frac{d\bar{h}_{wo}}{d\bar{t}} \quad (3-8)$$

Now % hydrodynamic load support  $H_y$  is given by

$$H_y = \frac{\bar{w}_h}{\bar{w}} = \frac{\bar{w} - \bar{w}_m}{\bar{w}} \quad (3-9)$$

so that

$$\frac{d\bar{h}_{wo}}{d\bar{t}} = (1-H_y) \bar{w} \frac{n}{2\pi} \quad (3-10)$$

Thus, for a constant applied load  $\bar{w}$ , the average wear rate is simply proportional to one minus the fraction of hydrodynamic support. Average wear

rate is not plotted in the curves to be presented because of this simple relationship to hydrodynamic load support.

Base Case Solution

The parameter values used for the base case time dependent solution are the same as those for the base case equilibrium solution with the addition of the following:

NTERMS = 10	The number of terms in the Fourier series repre- senting $h_w$ .	(3-11)
-------------	--	--------

$\Delta\bar{t} = 20$  The time step size

In terms of  $\bar{t}$ , dimensionless time, real time can be obtained from equation (3-4). Thus,

$$t = \frac{c^3 \bar{t}}{C_0 R n V^2} \quad (3-12)$$

Consider the following example. A typical carbon seal material might wear 12.7 microns (0.0005 in) per 100 test hours under the conditions of the base case (equation (2-60)). Using equation (2-60) and (3-1),

$$C_0 = 8.19 \times 10^{-18} \frac{m^2}{N} (5.65 \cdot 10^{-14} \text{ in}^2/\text{lb}) \quad (3-13)$$

Then from equation (3-12)

$$t = 0.02078\bar{t} \text{ hrs.} \quad (3-14)$$

or 100 dimensionless time units corresponds to about 2.0 hours for this case.

Using the above equations for the time dependence on wear, the computer program was modified for the time dependent case. The results for the base solution are shown in Figure 3-1 where % hydrodynamic load support is plotted as a function of time. The results at time = 0 are of course the same as before. The curve shows that % load support decreases with time. Over the 800 time units (16 hours of real time), the % support drops from 36% down to 24%. All similar runs made for different cases have been observed to behave the same way. The

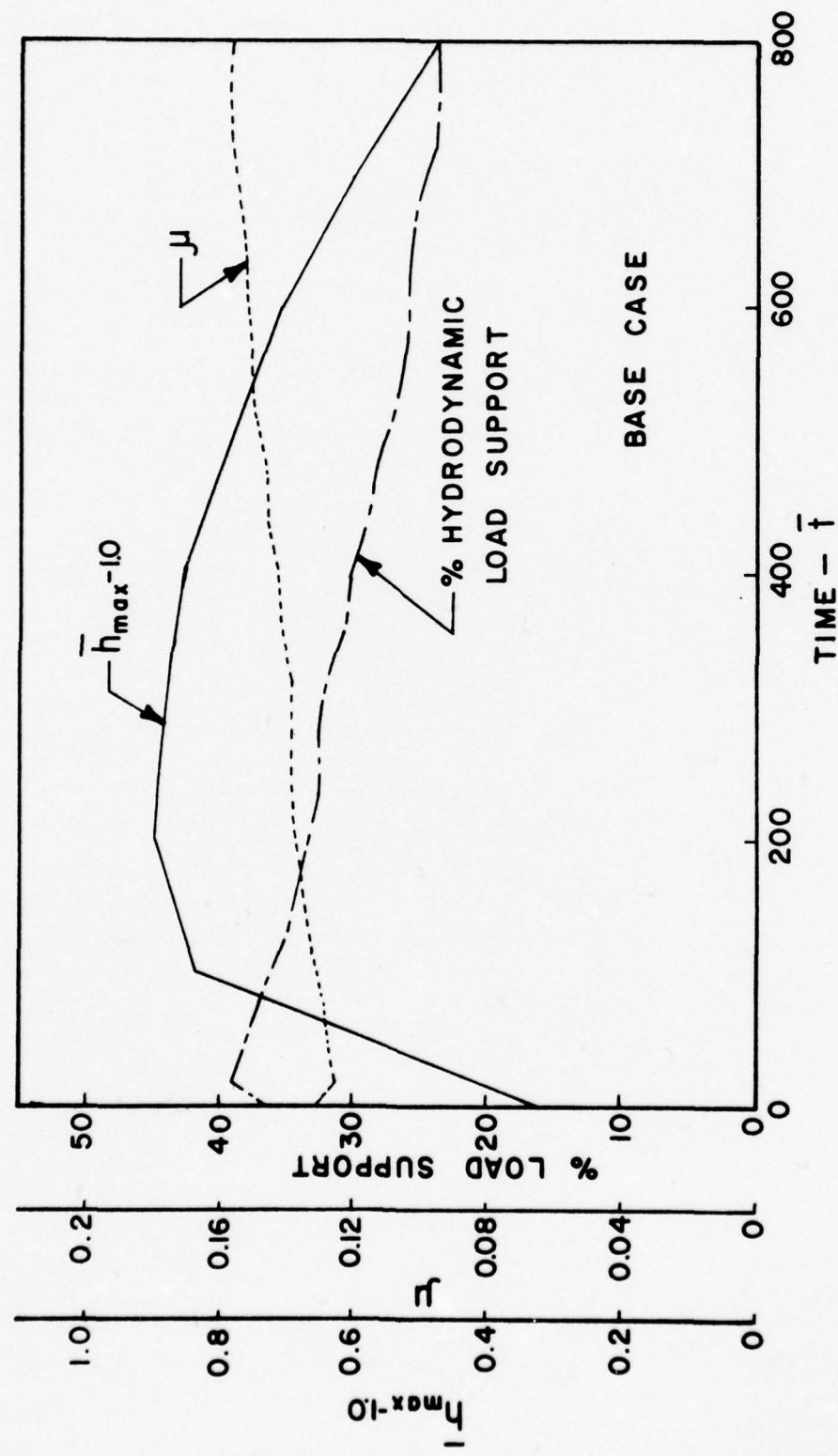


Figure 3-1. Time Dependent Behavior

effect of wear is to alter the profile in such a way that % load support decreases. In fact, the results of some earlier runs show that eventually the seal surface wears flat. Even though the wear harmonics move slowly tantentially, the general effect, based on the factors considered in the model so far, is that % hydrodynamic load support always decreases with time for steady state running conditions.

The curve also shows that the % load support increases for the first time increment. This has been found to invariably be the case with other runs as well. Apparently, the first wear increment improves the profile from the standpoint of hydrodynamic load support, whereas later increments make the profile worse.

Friction behaves in relation to % hydrodynamic load support in exactly the manner expected. The leakage gap  $h_{\max}$ -1 initially increases before later decreasing. The deflection pattern appears to be significantly affected by initial wear, and this causes the greater gap.

Pressure curves after some period of operation are shown plotted in Figure 3-2 and 3-3 (Figure 2-4 applies to  $\bar{t} = 0$ ). It is apparent from the figures that the asperity load support is greater than the hydrodynamic load support. The bumps in Figure 3-2 are due to the Fourier series representation of the wear surface. Because of the high sensitivity of the asperity pressure to the nominal film thickness  $h$  (see equation (2-21)), even a very small error will cause the bumps as shown. A plot of the actual surface would show that the actual magnitudes of the bumps are very small. Figure 3-3 at  $\bar{t} = 800$  shows that the asperity pressure has begun to smooth out more and also that the extent of asperity contact has widened.

To obtain the above solution, it was necessary to establish parameter values which would give the needed accuracy. Thus, several studies were made.

#### Time Step Size Effect

The effect of various time step sizes on % hydrodynamic load support is shown in Figure 3-4. Large time steps above 20 cause the solution to diverge. 20 units appears to be the practical upper limit for the time step size.

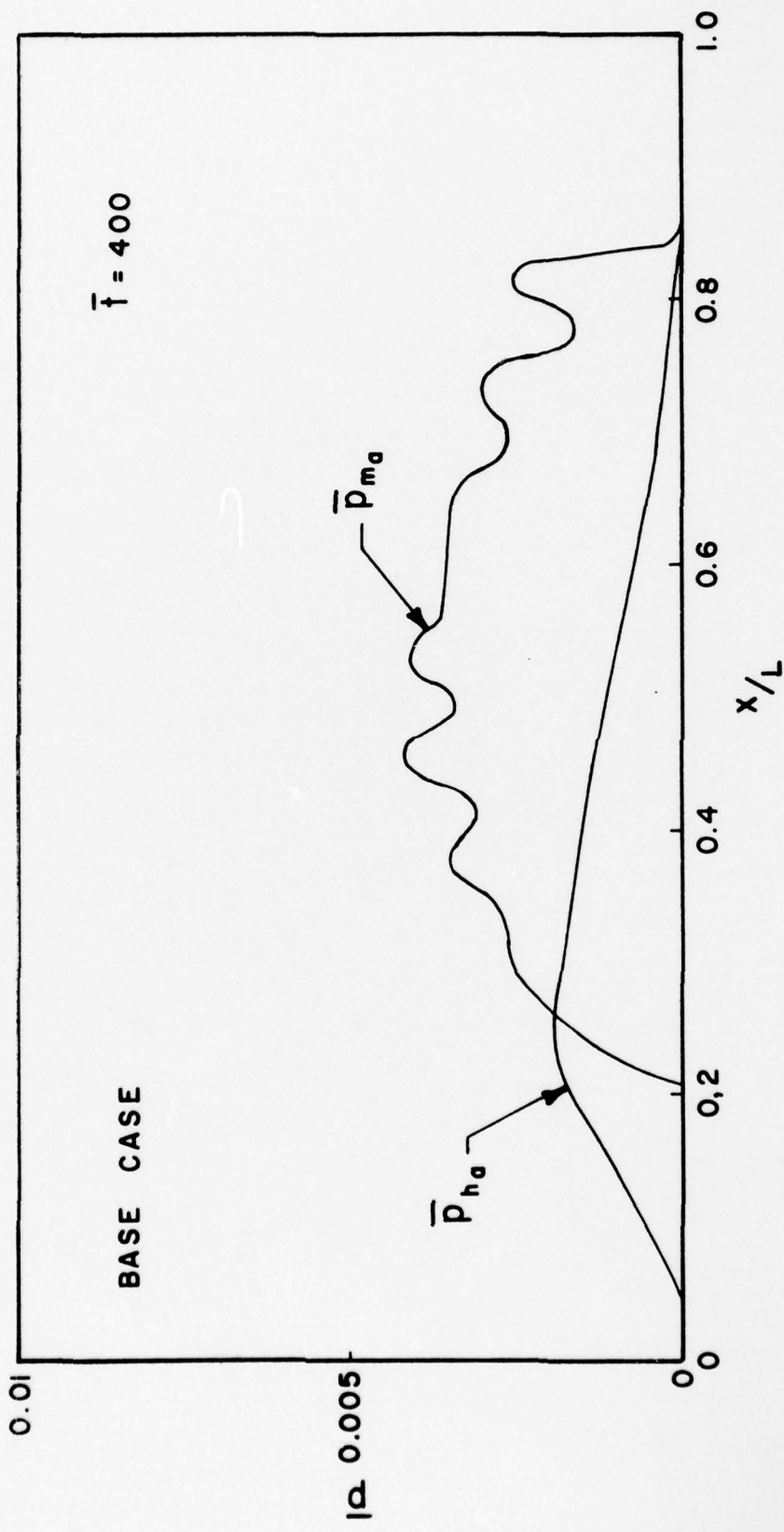


Figure 3-2. Hydrodynamic and Asperity Pressure at  $\bar{t} = 400$

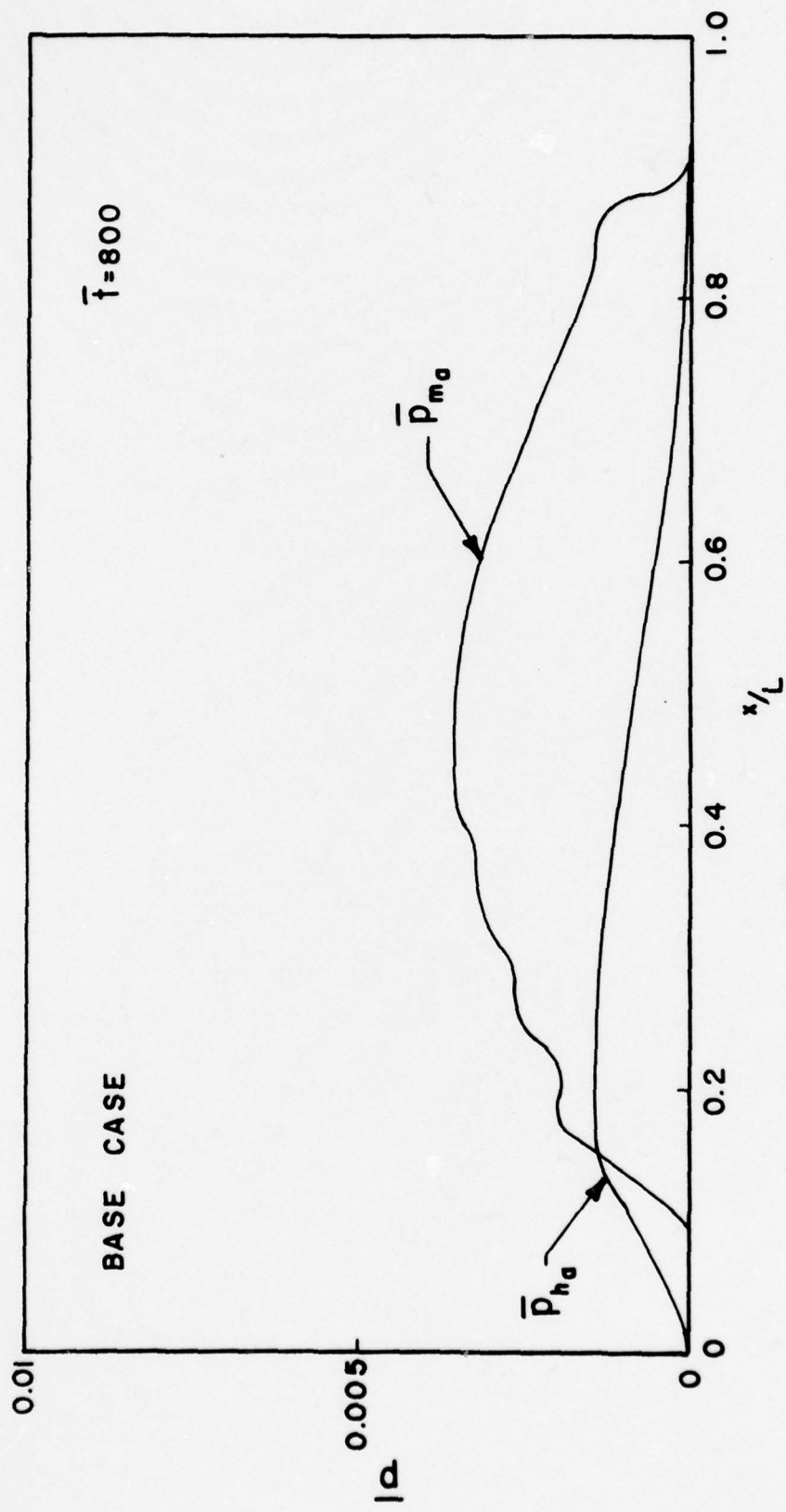


Figure 3-3. Hydrodynamic and Asperity Pressure at  $\bar{t} = 800$

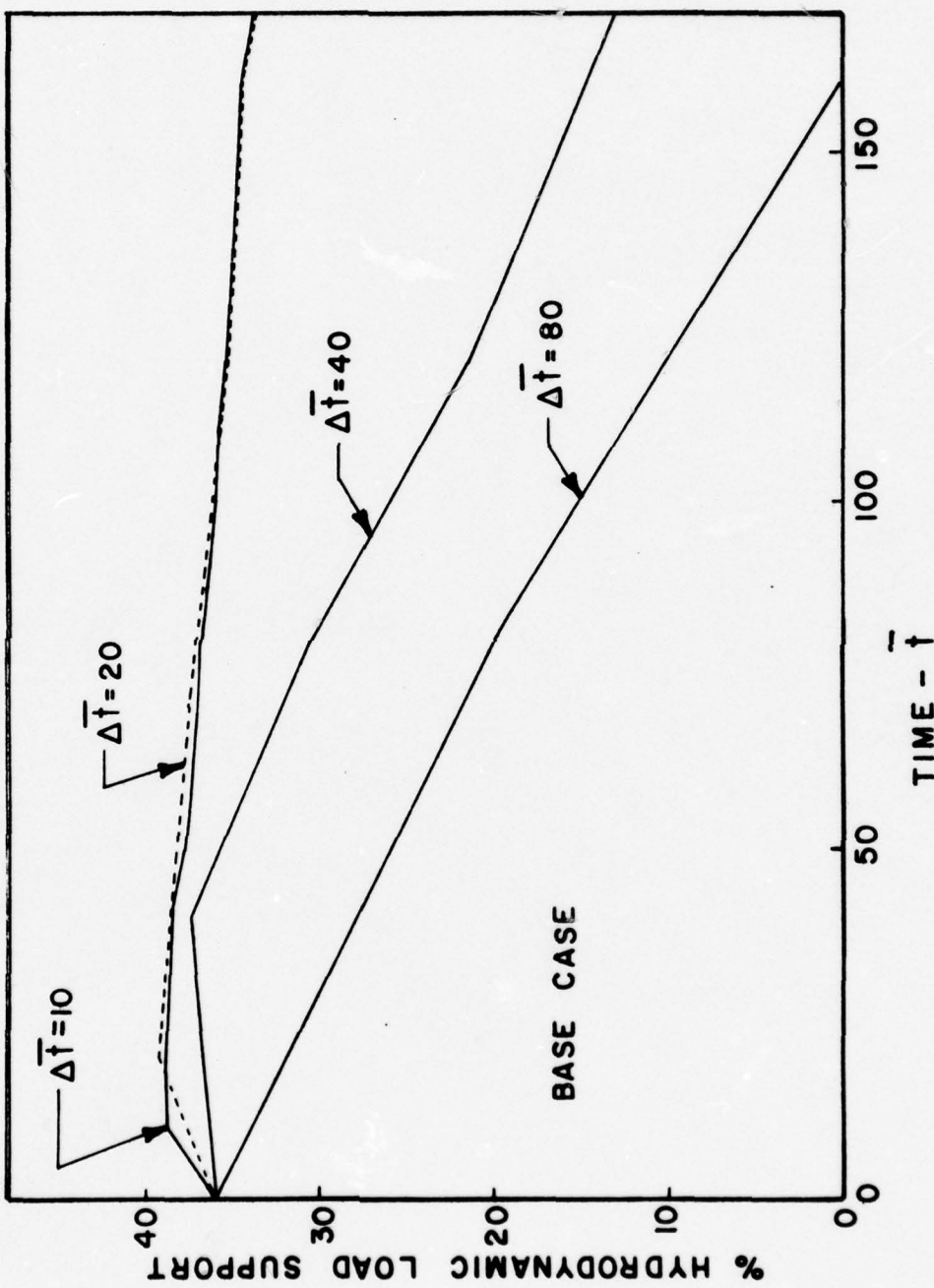


Figure 3-4. Time Step Size Effect

#### **Effect of Number of Deflection Terms**

As discussed under the equilibrium model, it was determined that higher deflection harmonics could be neglected. To verify this, the next higher harmonic deflection terms were included in the computer program. This increased the number of solution variables, equations (2-53), (2-54), (2-55), to five and greatly increased the computing time. The comparative results are shown in Figure 3-5. It is clear that beyond the first few steps, there is no significant difference, and the assumption is justified.

#### **Effect of Number of Wear Terms and Number of Points**

It was observed that under some circumstances the % hydrodynamic load support would begin to oscillate as shown in Figures 3-6 and 3-7. This problem was traced to an incompatibility between the number of wear terms and the number of points computed for the pressure curve. It was found that for a given number of points on the pressure curve, there is a certain maximum number of wear harmonic terms that can be included. Any number beyond this leads to oscillations.

The reason for this behavior has to do with the asperity region and the large changes in pressure over this region (see Figure 2-4). What happens is that the highest harmonic is defined by only a very few points because of the narrowness of the asperity region, initially. Depending on the placement of the points, the highest harmonic content will vary radically because of the inherent error. Only when the number of points is sufficiently increased will the wear term approach a correct value.

Because it is desired to have as many wear harmonics as possible to reduce the error of the type shown in Figure 3-2, it was found that the number of points had to be increased to 100 to accommodate the 10 desired wear harmonics. The results of these deliberations are shown in Figures 3-6 and 3-7.

#### **Friction Effects**

From the results so far, hydrodynamic load support can be expected to decrease over a period of time. However, there are other factors

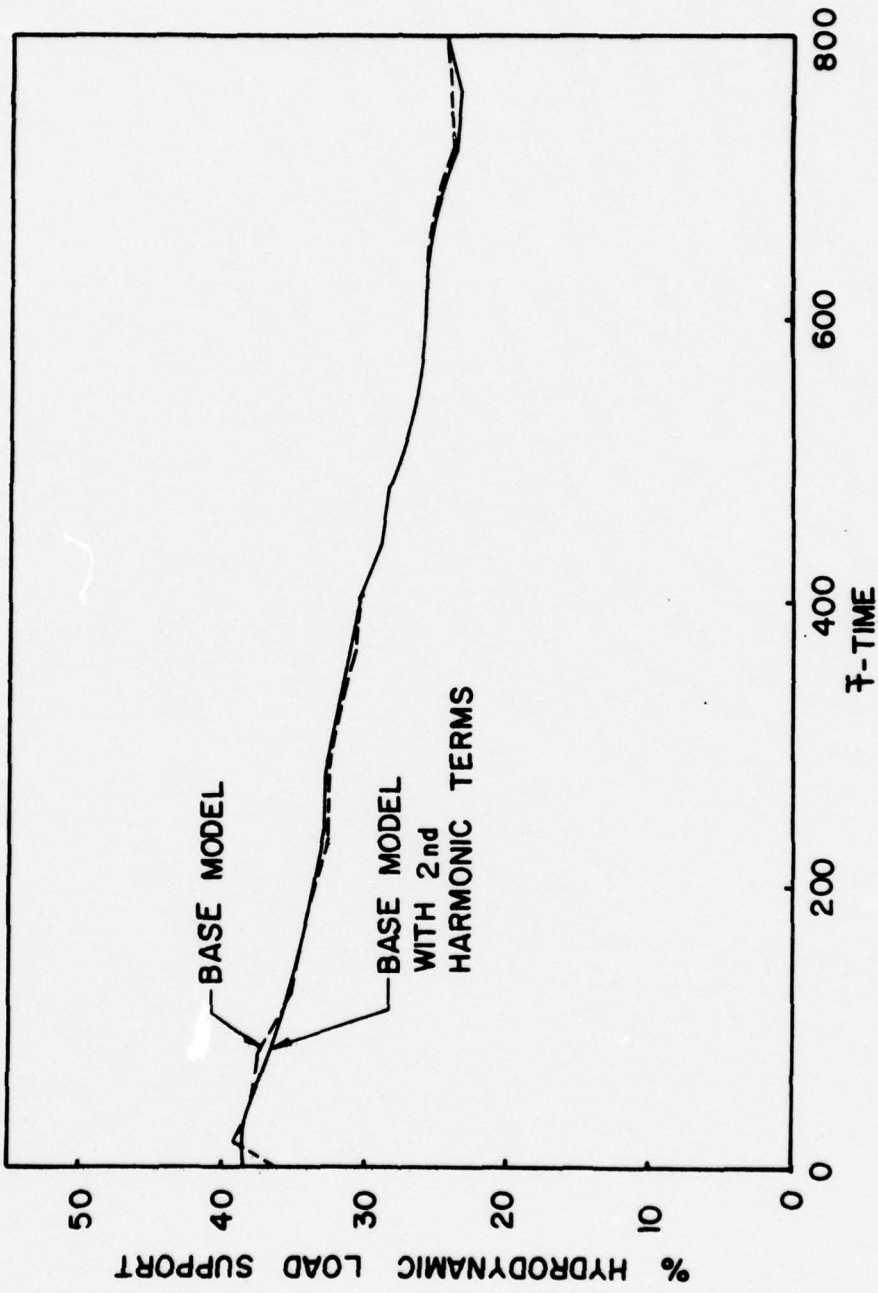


Figure 3-5. Effect of Second Harmonic Deflection Terms

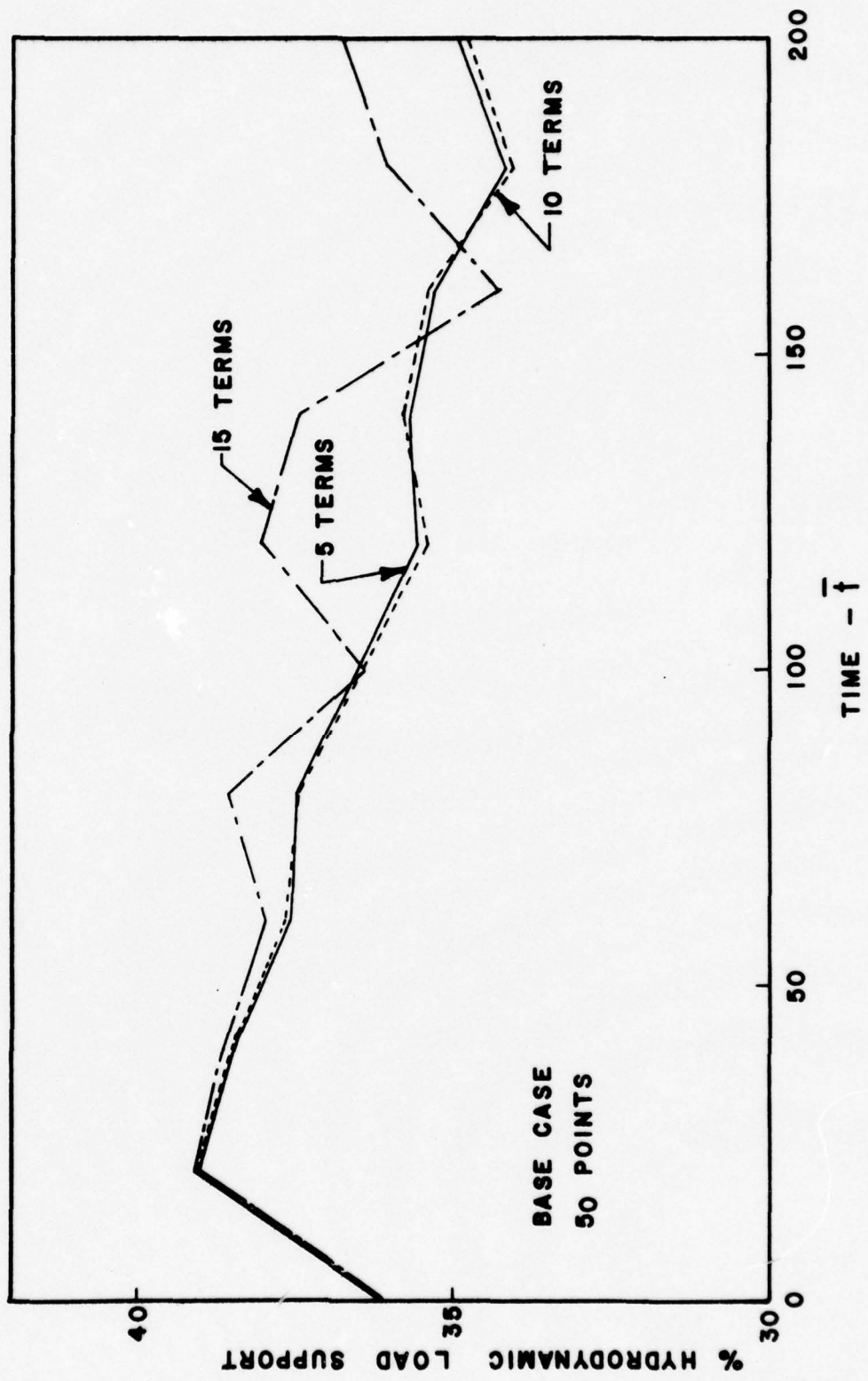


Figure 3-6. Effect of Number of Wear Harmonics

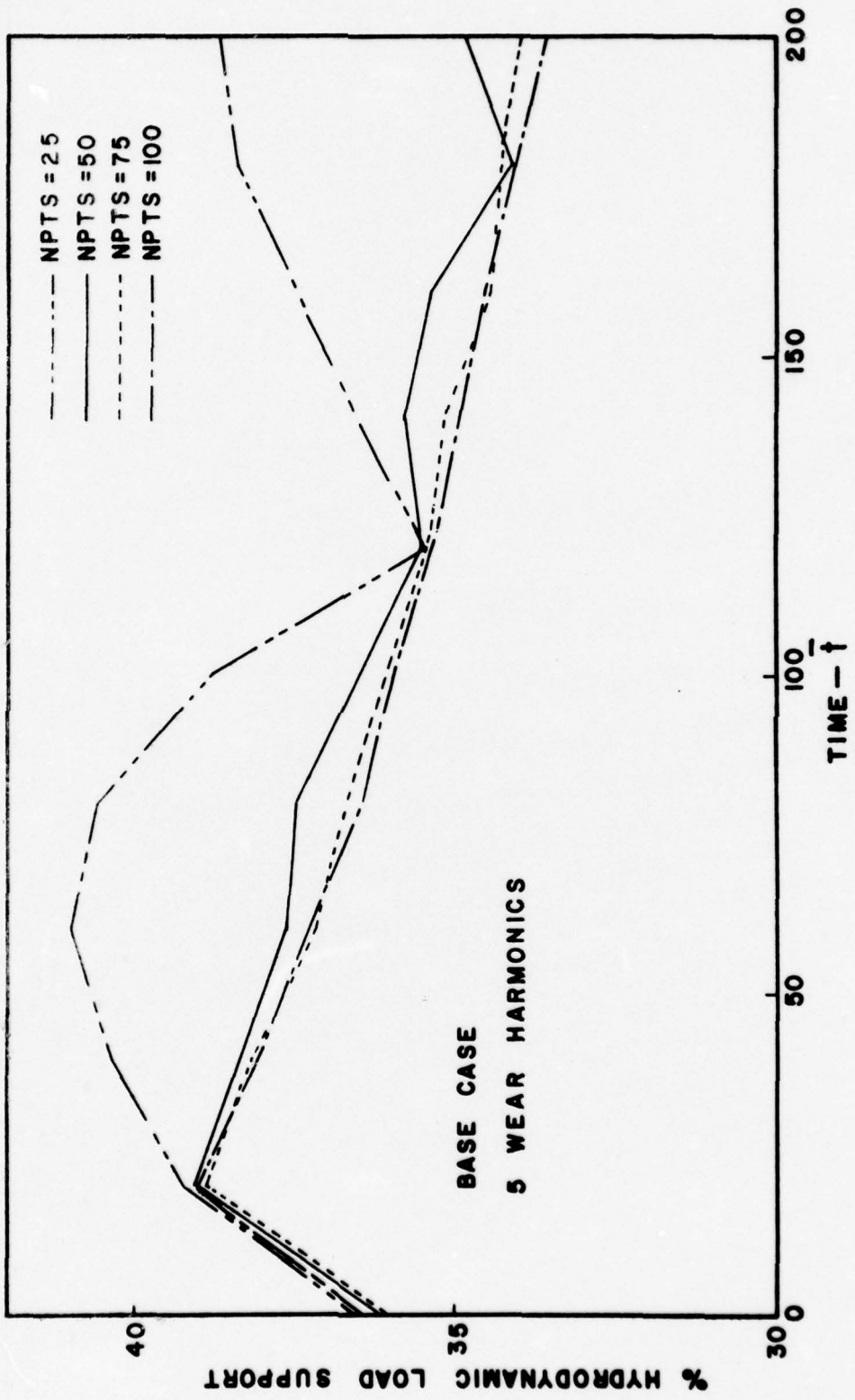


Figure 3-7. Effect of Number of Points

which have not been included in the model so far that could greatly alter this behavior.

The first of these additional factors is friction at the seal face. From a previous study [22], it is known that the common driving arrangements for solid carbon seal rings is such that a change in friction at the face will cause a change in waviness at the face of the seal. Therefore, it is possible that as friction increases with decreasing % hydrodynamic load support, the waviness will increase to offset the decrease because of friction.

To study these possible effects, waviness due to drive forces was included in the model as follows:

$$\bar{h}_f = k_n \frac{c}{R} n B \bar{f} \quad (3-15)$$

where

$k_n$  - a constant that depends on the geometry of the seal ring (see Ref. [22]).

$\bar{h}_f$  - the additional waviness caused by the friction  $\bar{f}$ .

Other symbols have been previously defined.

Friction caused waviness can be introduced into the solution by introducing a fourth variable  $\bar{h}_f$  similar to those in equations (2-53), (2-54), and (2-55). The waviness caused by friction becomes in essence a part of the initial waviness. Thus, now equation (2-14) becomes

$$h = h_o + \sum \left( h_{ia_j} \cos nj\bar{x} + h_{ib_j} \sin nj\bar{x} \right) + \bar{h}_f \cos nx \\ + h_{da_1} \cos nx + h_{db_1} \sin nx \quad (3-16)$$

A solution for a low value of  $k_n$  is compared to the base case in Figure 3-8. There is no significant difference. Values of  $k_n$  were greatly increased for the results in Figure 3-9. Again there is no significant change. It should be noted that values of initial waviness were adjusted as shown in Figure 3-9 so that the starting point would be about the

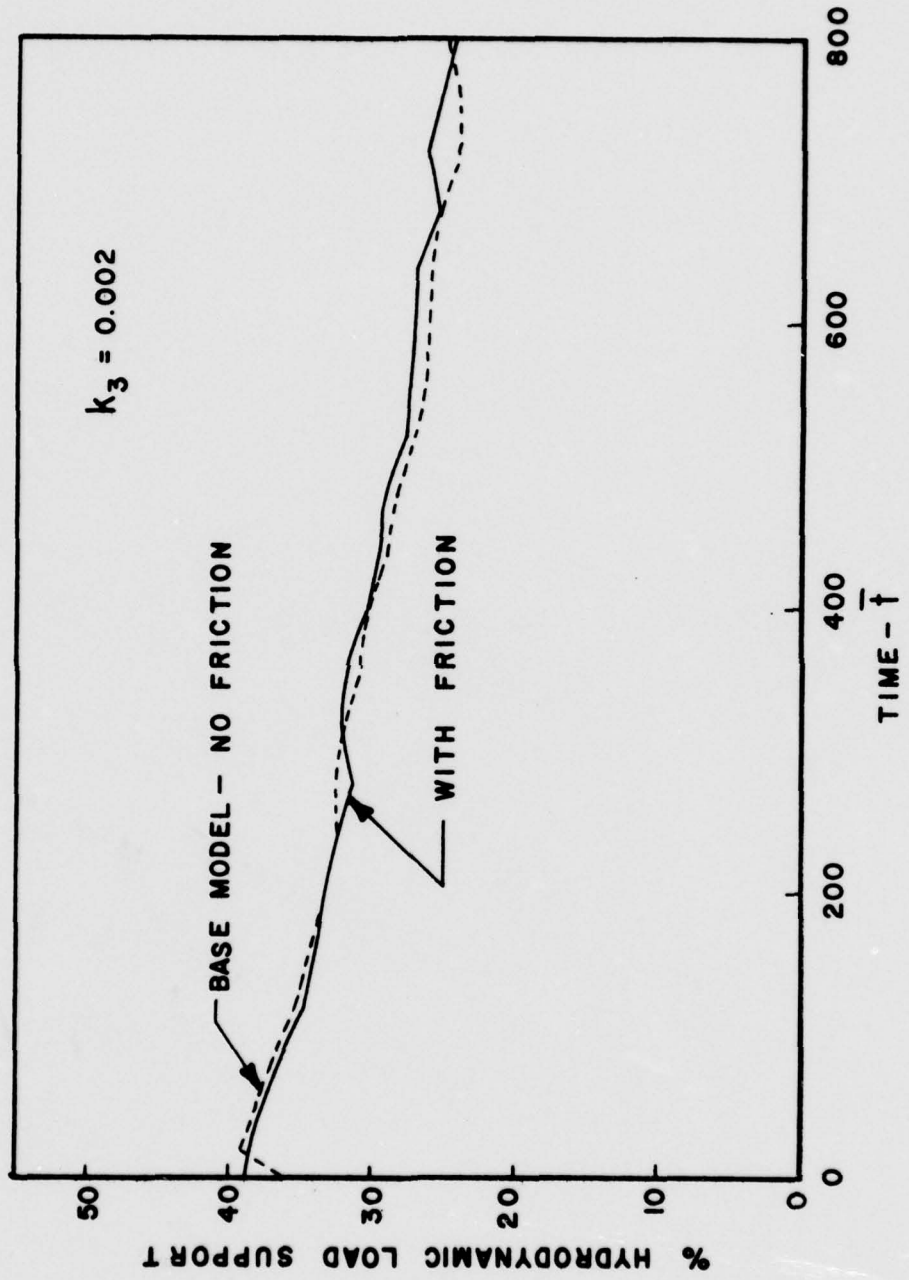


Figure 3-8. Effect of Friction on Load Support

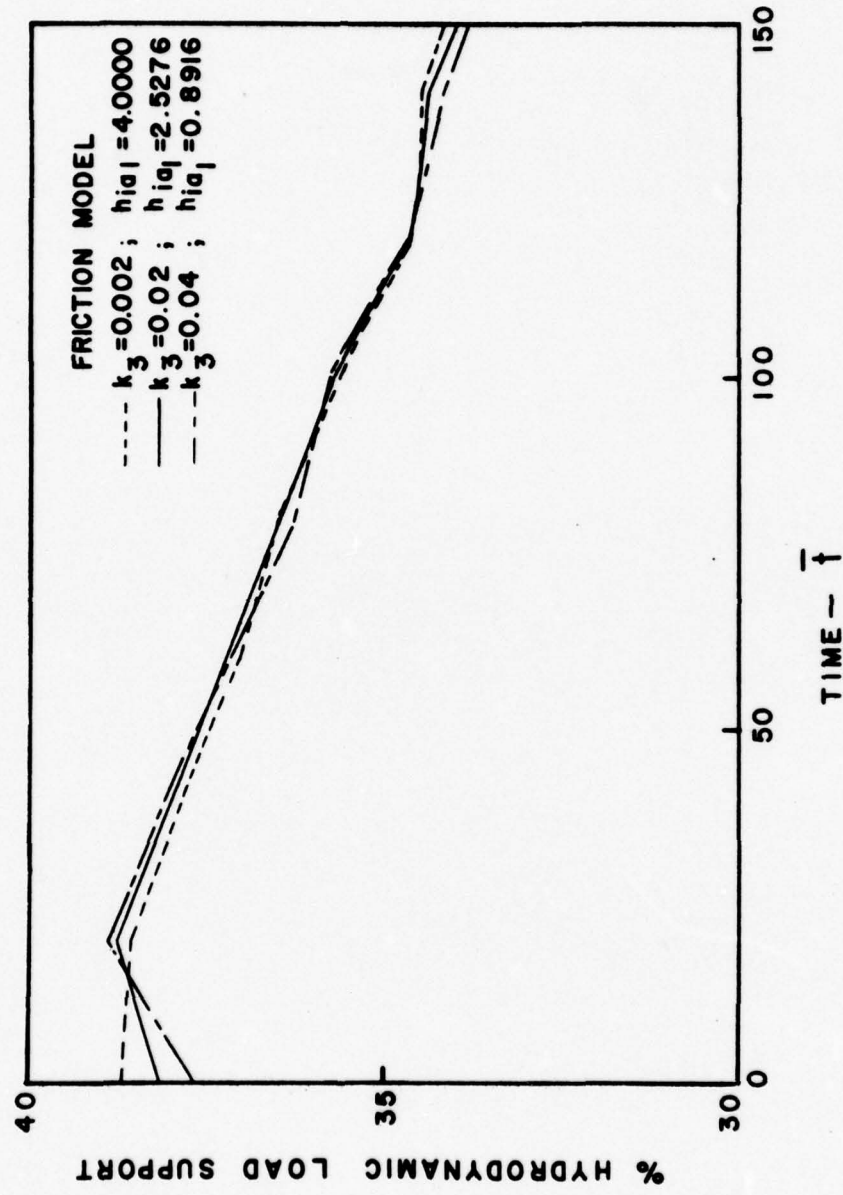


Figure 3-9. Effect of Increased Friction on Load Support

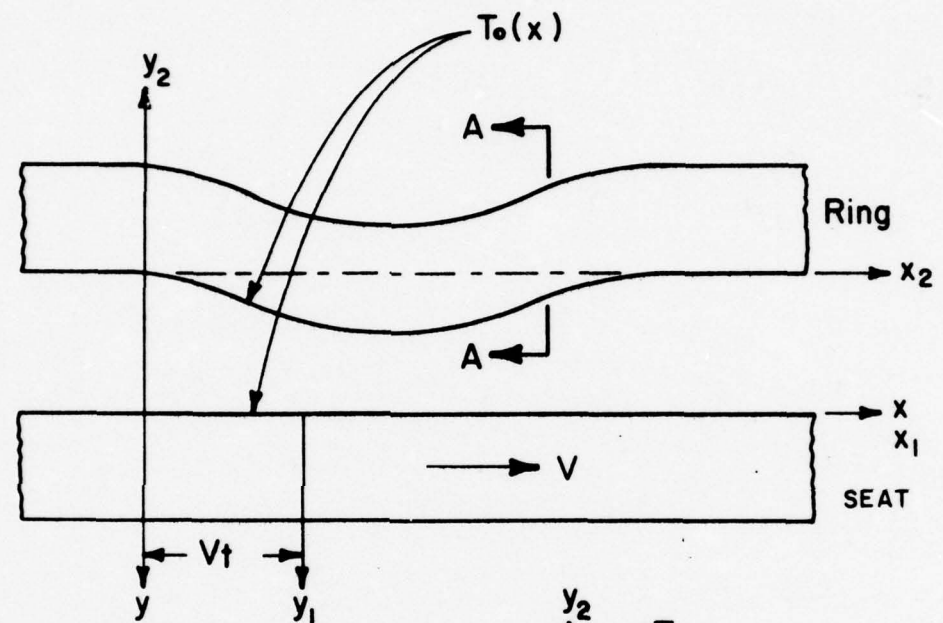
same each time for an easier comparison. It is concluded that the friction interaction with drive force caused waviness is of no significance in the steady state.

#### Thermal Effects

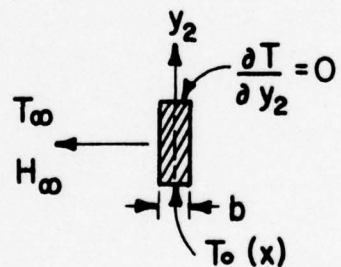
Non uniform heating at the face of the seal leads to waviness. In fact, under extreme conditions an unstable situation can result [27], [28], [29], where contact occurs at only a few points. Although the present case is not extreme, it is reasonable to expect that circumferentially varying temperature and its resulting waviness will affect the equilibrium film shape and may even cause the time dependent behavior to be different.

To explore these possibilities, face temperature and resulting waviness were introduced into the equilibrium problem. The model to do this is based on Figure 3-10. The seat slides past the fixed ring as shown. A tangentially varying friction is developed at the face. This leads to a tangentially varying face temperature and some resulting waviness. The assumptions for the model follow:

- 1) The temperature at the face of the ring and at the face of the seat are equal (zero thermal resistance at the face). This assumption has been used by Burton in his work on Thermoelastic Instability [27], [28], [29].
- 2) The speed of the temperature wave relative to the fixed ring is very low so that non steady state effects in this ring can be neglected. The temperature wave moves slowly because it is caused by the waviness of the seal. The wave can move only by progressive wear which is a relatively slow process.
- 3) The speed of the wave in the seat is large enough that the temperature disturbance does not deeply penetrate the material, and the seat can be considered as a semi-infinite plate [27].
- 4) The seat ring has no convective losses for the alternating component of the temperature wave. These would be very small if included because of the shallow penetration of the temperature disturbance.



$x - y$  FIXED TO RING  
 $x_1 - y_1$  FIXED TO MOVING SEAT  
 $x_1 = x - V_t$   
 $y_1 = y$



SECTION  
A-A

Figure 3-10. Convention for Temperature Effect Model

- 5) Convection losses are significant in the fixed ring because the tangential temperature variation extends through the body.
- 6) Thermal distortion in the seat is negligible relative to the large elastic distortions in the fixed ring and can be neglected.
- 7) Heat transfer due to tangential fluid flow is neglected. The effect of such heat transfer would be to diminish the effects of interest. So, if there are significant temperature effects found, then this tangential heat flow can be included in the model.

Now assume that there exists a temperature variation which is fixed to the ring (Figure 3-10) which is expressed by a Fourier series.

$$T = \sum_i T_{a_i} \cos \frac{n_i x}{R} + T_{b_i} \sin \frac{n_i x}{R} \quad * \quad (3-17)$$

Because

$$x = x_1 + vt \quad (3-18)$$

the temperature wave has the following form relative to the moving seat.

$$T = T_{a_i} \cos \frac{n_i}{R} (x_1 + vt) + T_{b_i} \sin \frac{n_i}{R} (x_1 + vt) \quad (3-19)$$

For the two dimensional semi-infinite plate which represents the seat,

$$\frac{\partial^2 T}{\partial x_1^2} + \frac{\partial^2 T}{\partial y_1^2} = \frac{1}{a_s} \frac{\partial T}{\partial t} \quad (3-20)$$

where

$a_s$  - thermal diffusivity of seat

For the given temperature distribution, Burton [27] has shown that the solution to equation (3-20) is

---

\*Hereafter the summation sign will be dropped for brevity.

$$T_s = T_{b_i} e^{\frac{-\bar{b}_i y_1}{R}} \sin \left( \frac{n_i}{R} x_1 + \frac{n_i V}{R} t + \frac{\bar{a}_i}{R} y_1 \right)$$

$$+ T_{a_i} e^{\frac{-\bar{b}_i y_1}{R}} \cos \left( \frac{n_i}{R} x_1 + \frac{n_i V}{R} t + \frac{\bar{a}_i}{R} y_1 \right) \quad (3-21)$$

where

$$\bar{a}_i = - \left[ \frac{-n_i^2 i^2}{2} + \frac{n_i}{2} \sqrt{n_i^2 i^2 + \frac{V^2 R^2}{a_s^2}} \right]^{1/2} \quad (3-22)$$

$$\bar{b}_i = + \left[ \frac{n_i^2 i^2}{2} + \frac{n_i}{2} \sqrt{n_i^2 i^2 + \frac{V^2 R^2}{a_s^2}} \right]^{1/2} \quad (3-23)$$

Heat flow into the seat at the face is given by

$$q_s = -k_s b \frac{\partial T}{\partial y_1} \Big|_{y_1=0} \quad (3-24)$$

where

$q_s$  - heat flow per unit length of circumference.

Taking  $\frac{\partial T}{\partial y_1}$  of equation (3-21), setting  $y_1 = 0$ , and shifting back to the  $xy$  coordinate system, the following result is obtained:

$$q_s = + \frac{bk_s T a_i}{R} \left( \bar{b}_i \cos \frac{n_i}{R} x + \bar{a}_i \sin \frac{n_i}{R} x \right)$$

$$+ \frac{bk_s T b_i}{R} \left( \bar{b}_i \sin \frac{n_i}{R} x - \bar{a}_i \cos \frac{n_i}{R} x \right) \quad (3-25)$$

---

\*The minus sign in front of this expression is compatible with the direction of  $V$  shown in Figure (3-10). The sign must be reversed for opposite  $V$ .

Thus the heat flow into the seat is known as a function of geometry, properties, and the temperature distribution  $T_{ai}$  and  $T_{bi}$ . It is to be noted that the heat flow is shifted from the temperature variation.

Considering the fixed seat, it is assumed that the ring cross section is thin such that radial heat flow effects can be neglected. The heat transfer model for the ring is based on Figure 3-10. The governing equation becomes

$$\frac{\partial^2 T}{\partial y_2^2} + \frac{\partial^2 T}{\partial x_2^2} = \frac{H_\infty}{k_r b} (T - T_\infty) \quad (3-26)$$

Boundary conditions are shown in Figure 3-10. After finding the general solution by separation of variables and applying the boundary conditions, the temperature is found to be

$$T_r = \frac{\cosh \bar{k}_1 (\bar{a} - \bar{y}_2)}{\cosh \bar{k}_1 \bar{a}} \left( T_{ai} \cos n \bar{x} + T_{bi} \sin n \bar{x} \right) \quad (3-27)$$

where

$$\bar{k}_1 = \sqrt{\frac{H_\infty R^2}{k_r b} + n^2 i^2} \quad (3-28)$$

The heat flow into the face of the ring is given by

$$q_r = - k_r b \frac{\partial T}{\partial y_2} \Big|_{y_2=0} \quad (3-29)$$

$$q_r = \frac{bk_r}{R} \bar{k}_1 \tanh(\bar{k}_1 \bar{a}) \left( T_{ai} \cos n \bar{x} + T_{bi} \sin n \bar{x} \right) \quad (3-30)$$

Thus, expression for the heat flow into both the seat and the ring are now available.

Now, the heat generated at the face is a function of the conditions of lubrication and asperity contact. The friction force is defined by equation (2-40), and friction varies with  $\bar{x}$ . Accordingly, the heat flow

caused by friction is also a function of  $\bar{x}$  and can be represented by a Fourier series.

$$q_{\text{total}} = q_{a_i} \cos n\bar{x} + q_{b_i} \sin n\bar{x} \quad (3-31)$$

assuming for the moment that  $q_{a_i}$  and  $q_{b_i}$  are known from a given lubrication condition, the temperature at the interface can be obtained by equating the sum of the heat flow into the seat and ring to the total heat flow. Thus from equations (3-31), (3-30) and (3-25)

$$\begin{aligned} q_{\text{total}} &= q_{a_i} \cos n\bar{x} + q_{b_i} \sin n\bar{x} = q_s + q_r = \\ &\frac{bk_s T_{a_i}}{R} (\bar{b}_i \cos n\bar{x} + \bar{a}_i \sin n\bar{x}) \\ &+ \frac{bk_s T_{b_i}}{R} (\bar{b}_i \sin n\bar{x} - \bar{a}_i \cos n\bar{x}) \\ &+ \frac{k_r k_1 b}{R} \tanh(k_1 \bar{a}) (T_{a_i} \cos n\bar{x} + T_{b_i} \sin n\bar{x}) \end{aligned} \quad (3-32)$$

For this relationship to be generally true, the coefficients of the sine and cosine terms must vanish independently, or

$$q_{a_i} = \frac{k_s b}{R} \left( T_{a_i} \bar{b}_i - T_{b_i} \bar{a}_i \right) + T_{a_i} \frac{k_r k_1 b}{R} \tanh(k_1 \bar{a}) \quad (3-33)$$

$$q_{b_i} = \frac{k_s b}{R} \left( T_{a_i} \bar{a}_i + T_{b_i} \bar{b}_i \right) + T_{b_i} \frac{k_r k_1 b}{R} \tanh(k_1 \bar{a}) \quad (3-34)$$

In dimensionless form, the above equations became

$$\tilde{q}_{a_i} = \tilde{T}_{a_i} (\bar{b}_i + Kk_1 \tanh(k_1 \bar{a})) + \tilde{T}_{b_i} (-\bar{a}_i) \quad (3-35)$$

$$\tilde{q}_{b_i} = \tilde{T}_{a_i} (\bar{a}_i) + \tilde{T}_{b_i} (\bar{b}_i + Kk_1 \tanh(k_1 \bar{a})) \quad (3-36)$$

where

$$\bar{q} = \frac{qc}{\eta V^2 b} \quad (3-37)$$

$$\bar{T} = \frac{k_s c T}{\eta V^2 R} \quad (3-38)$$

$$K = \frac{k_r}{k_s} \quad (3-39)$$

Given the heat flows, the face temperature terms are given as follows:

$$\bar{T}_{a_i} = \frac{\bar{q}_{a_i} (\bar{b}_i + K \bar{k}_1 \tanh(\bar{k}_1 \bar{a})) + \bar{q}_{b_i} \bar{a}_i}{(\bar{b}_i + K \bar{k}_1 \tanh(\bar{k}_1 \bar{a}))^2 + \bar{a}_i^2} \quad (3-40)$$

$$\bar{T}_{b_i} = \frac{\bar{q}_{b_i} (\bar{b}_i + K \bar{k}_1 \tanh(\bar{k}_1 \bar{a})) - \bar{q}_{a_i} \bar{a}_i}{(\bar{b}_i + K \bar{k}_1 \tanh(\bar{k}_1 \bar{a}))^2 + \bar{a}_i^2} \quad (3-41)$$

Once the temperature terms are found, the thermal deflection can be obtained approximately from equation (2-153) in Reference [22].

$$h_t = - \frac{\beta R^2 T}{a} \frac{1}{n_i^2 - 1} \quad (3-42)$$

where

T - the face temperature

$\beta$  - coefficient of thermal expansion.

In dimensionless form

$$\bar{h}_t = - \frac{\beta R^2 \eta V^2}{k_s c^2} \frac{1}{\bar{a}} \frac{\bar{T}}{n_i^2 - 1}^* \quad (3-43)$$

---

\*a plus  $\bar{T}$  at the face causes a minus  $\bar{h}$ .

There will be two components of  $\bar{h}_t$ ,  $\bar{h}_{ta_i}$  and  $\bar{h}_{tb_i}$  corresponding to  $\bar{T}_{a_i}$  and  $\bar{T}_{b_i}$ .

The inclusion of thermal effects into the hydrodynamic seal model thus introduces the following additional dimensionless variables into the problem:

$$\bar{a} = \frac{a}{R} \quad \text{ring length}$$

$$\bar{k}_1 = \sqrt{\frac{H_\infty R^2}{k_r b} + n^2 i^2} \quad \text{heat transfer constant for the ring}$$

$$K = \frac{k_r}{k_s} \quad \text{ratio of thermal conductivities}$$

(3-44)

$$\frac{VR}{a_s} \quad \text{heat transfer constant for the seat}$$

$$\frac{\beta R^2 \eta V^2}{k_s c^2} \quad \text{thermal deflection constant}$$

The inclusion of thermal effects in the model introduces as many additional unknowns into the problem as the number of terms  $\bar{h}_{ta_i}$  and  $\bar{h}_{tb_i}$ . It can be shown that only the  $\bar{h}_t$  terms for  $i = 1$  are significant. Thus, higher harmonic terms are dropped from the solution, and only two additional terms are introduced.

The method of solution for the equilibrium condition is the same as for the base model except that there are five conditions and five unknowns to be solved for rather than three, using the Newton method.

The temperature equilibrium base case is the same as the original base case except the following additional parameter values and non-dimensional variables are required. These are again based on the actual seal under study.

$a = 21.1 \text{ mm (0.83 in)}$	-seal ring length
$H_\infty = 11.4 \times 10^3 \text{ w/m}^2\text{K}$ (2000 Btu/hr ft <sup>2</sup> °F)	-heat transfer coefficient in water
$k_r = 5.18 \text{ w/m}^\circ\text{K}$ (3 Btu/hr ft °F)	-thermal conductivity of carbon ring
$k_s = 19.0 \text{ w/m}^\circ\text{K}$ (11 Btu/hr ft °F)	-thermal conductivity of ceramic seat
$a_s = 5.16 \times 10^{-6} \text{ m}^2/\text{s}$ (0.20 ft <sup>2</sup> /hr)	-thermal diffusivity of ceramic seat
$\beta = 4.86 \times 10^{-6}/^\circ\text{K}$ ( $2.7 \cdot 10^{-6}/^\circ\text{F}$ )	-coefficient of thermal ex- pansion for carbon

(3-45)

Using the above values plus those in equation (2-60) gives the following additional dimensionless constants for the temperature case:

$$\begin{aligned}\bar{a} &= 0.415 \\ \bar{k}_1 &= 1177 \\ K &= 0.273 \\ \frac{VR}{a_s} &= 1.32 \times 10^5 \\ \frac{\beta R^2 \eta V^2}{k_s c^2} &= 21.5\end{aligned}\tag{3-46}$$

Figure 3-11 shows the pressure, friction, and temperature variations for the equilibrium base case. The temperature buildup lags behind the peak friction, which is expected. The % hydrodynamic load support is 38.5, only slightly different than the original base case. The time dependent results for this case are shown in Figure 3-12. The characteristic behavior is the same as the base case. The factor  $\frac{\beta R^2 \eta V^2}{k_s c^2}$  was in-

creased a factor of ten for the second case shown in Figure 3-12. Again the trend is the same. Thermal distortion at the given and even more extreme operating conditions does not have a great effect on seal performance.

#### Time Dependent Pressure

Some seals are exposed to non-steady operating conditions. Sometimes pressure varies, such as in a submarine seal when diving and

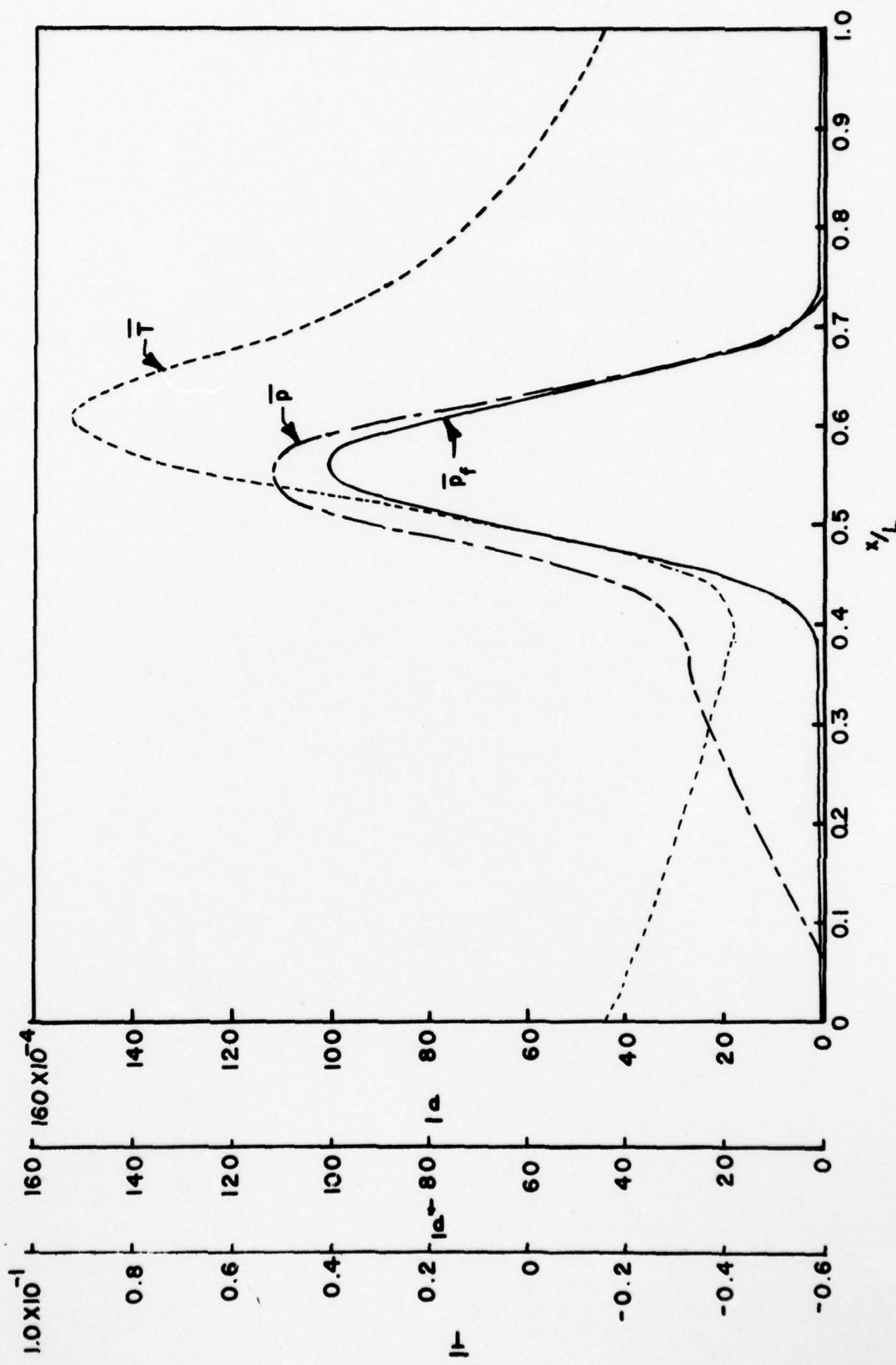


Figure 3-11. Seal Face Temperature and Pressure

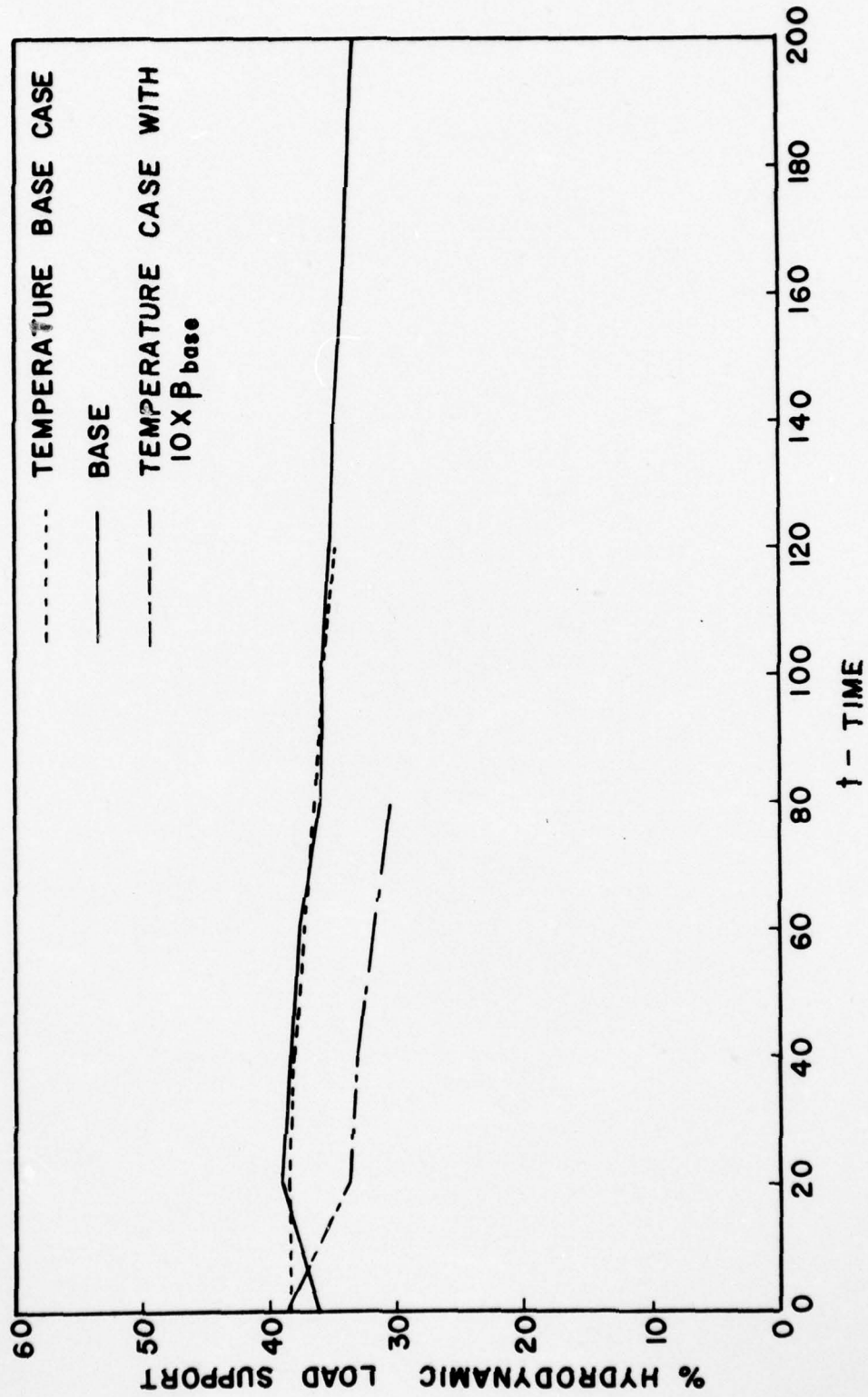


Figure 3-12. Time dependent Behavior with Temperature Effects

surfacing. Also whenever a pump is shut down and restarted, there will be a large pressure variation on the seal.

It is of considerable interest to see how such variations interact with the hydrodynamic lubrication in a seal. To do this, an ideal periodic variation in pressure was introduced into the time dependent program. Friction effects were included in this case because of their influence on waviness through torque interaction. For the first study the load was increased 20% over the base case load on a periodic basis as shown in Figure 3-13. A periodic variation in % hydrodynamic load support is produced as expected. Also, the average % load support appears to decrease with time. Thus, in this case, it is expected that hydrodynamic load support would eventually reach a condition where when the load was large, % support would be zero and when the load was smaller there would be a small % of hydrodynamic load support. Eventual periodic behavior of the load support is expected because of friction interaction. Under steady state conditions with friction, the seal will wear flat. However, when the load is reduced and friction decreases, the change in drive forces will introduce a change in waviness and reestablish a low level of hydrodynamic load support.

Figure 3-14 shows a much different situation. The initial waviness has been reduced to zero. The only waviness existing is due to drive forces. The load is varied  $\pm$  50% of the base case mean value using a sine function. For the low friction factor,  $k_3 = 0.00067$ , the behavior is as described for the ultimate behavior of the previous case. The load support goes to zero each time the load increases to maximum. For the larger friction factor, the behavior is the same except that load support levels are higher. The average load support decreases with time.

The results in Figure 3-15 show still a different behavior. Again here the base case is used except that the load variation is now  $\pm$  50% of the base case mean with a sinusoidal variation. The results show that the average load support is increasing with time. Since this behavior may have important implications in practice, it is to be studied in much greater detail to determine the causes of this behavior. The only possible explanation found so far (other than the possibility of a computational

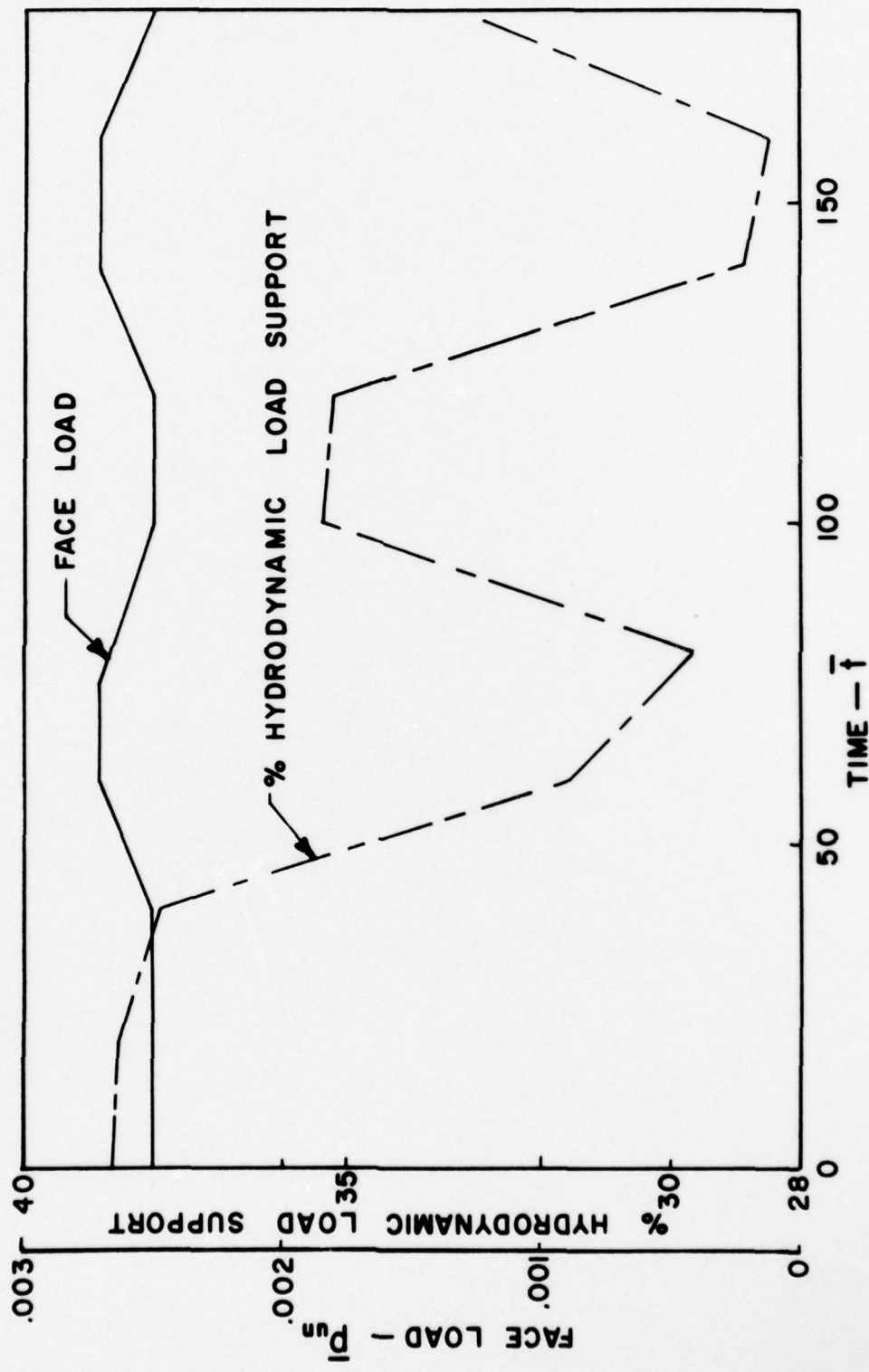


Figure 3-13. Effect of Variable Load on Hydrodynamic Load Support

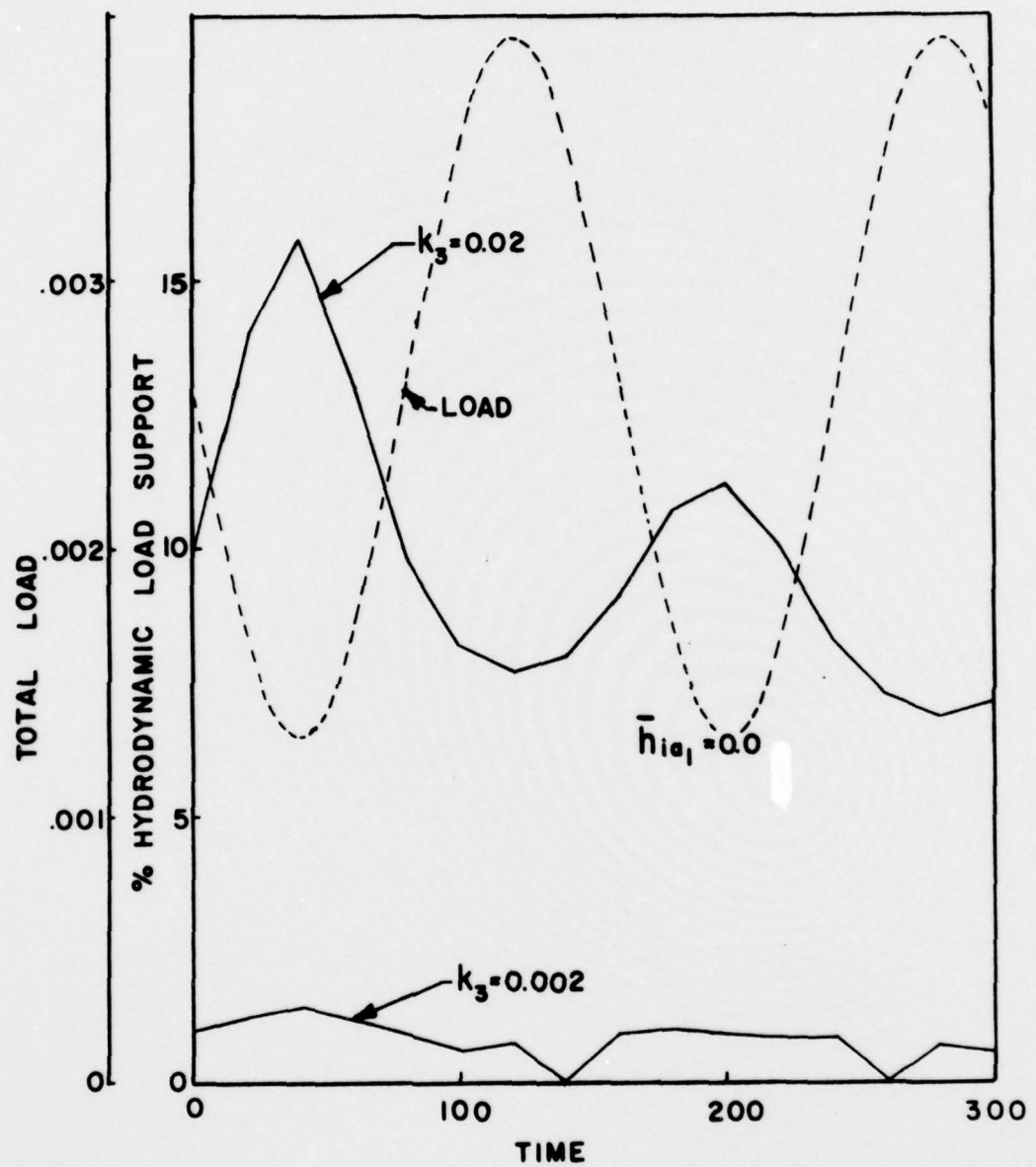


Figure 3-14. Effect of Variable load on Hydrodynamic Load Support - Zero Initial Waviness.

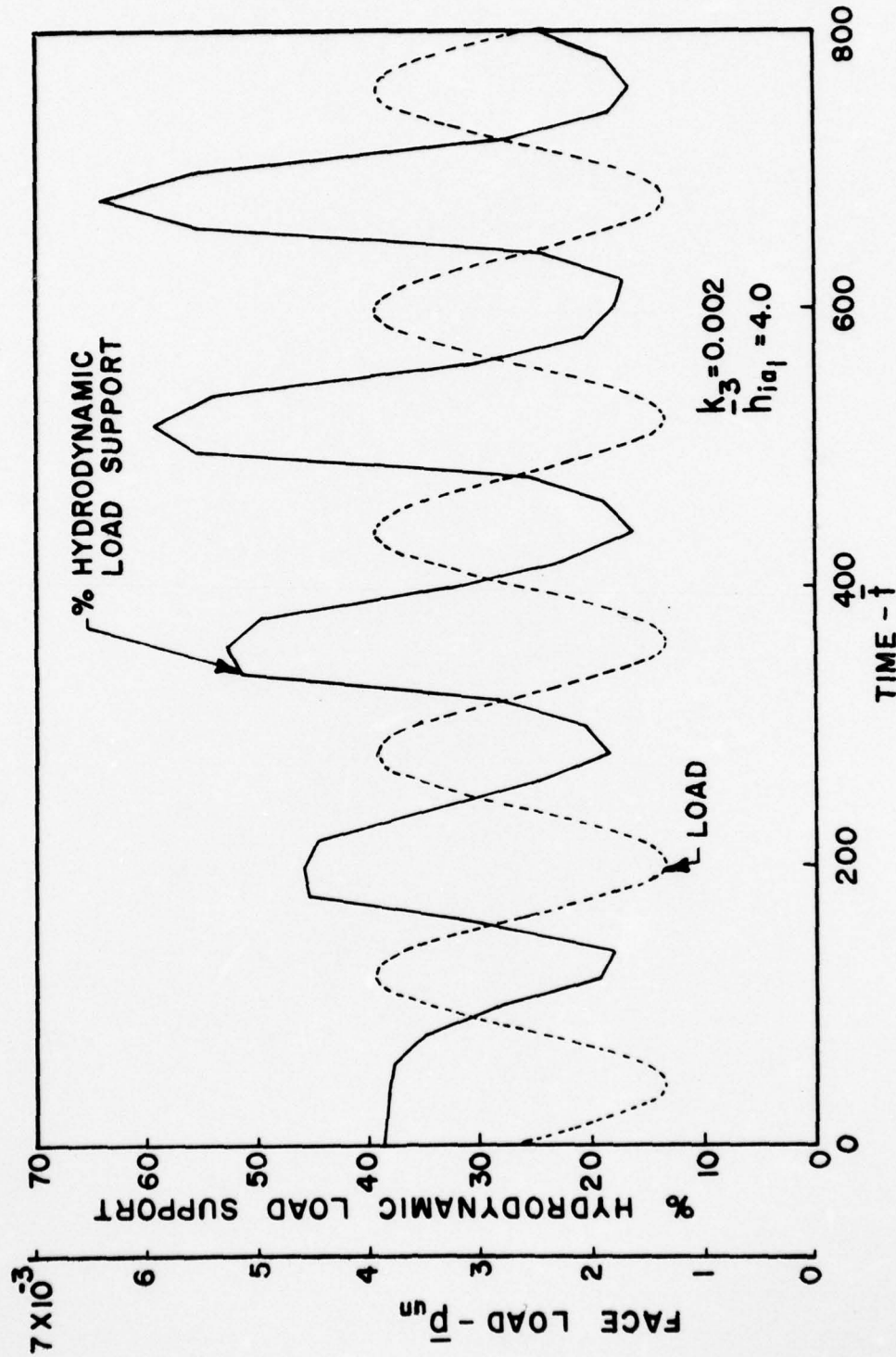


Figure 3-15. Effect of Variable Load on Hydrodynamic Load Support

divergence problem) is that under high load the wear region is in a different location than under low load. It is possible that the cycling leads to a waviness wear pattern that is stable.

#### Comparison to Experimental Results

The only experimental results available where tests have been conducted for a controlled waviness in water are given by Snapp and Sasdelli [40] for a submarine shaft seal. On test A2 in Reference [40], three  $450 \mu\text{in}$  TIR waves were lapped into one of the faces. In addition, a radial taper was included. The seal was run and leakage was recorded.

The Snapp and Sasdelli results were compared to those found using the one dimensional model. Certain parameter values were approximated.

$$p_m = 262 \text{ MPa (38,000 psi)}$$

$$c = 1.02 \text{ micron (40 } \mu\text{in)}$$

$$\eta = 6.81 \cdot 10^{-4} \text{ Pa}\cdot\text{s (9.89} \times 10^{-8} \text{ lb sec/in}^2 \text{) (for 60°F water)}$$

$$V = 5.08 \text{ m/s (1000 ft/min) (Reference [40] high speed test)}$$

$p_{un}$  - based on 100% test pressure

Based on the above values and some approximated values, the following non-dimensional parameters apply:

$$\bar{p}_m = 0.317$$

$$\bar{p}_{un} = 0.00133 \text{ (100% pressure)}$$

$$B = 1.48 \times 10^5$$

$$\bar{S}_s = 2.22 \times 10^4$$

$$A = 2.08$$

$$b/R = 0.0386$$

$$c/R = 4.12 \times 10^{-6}$$

$$n = 3$$

$$\bar{h}_{ia_1} = 5.625$$

Results were computed for 50 and 100% test pressure. Given the equilibrium wave shape, leakage was calculated based on pressure drop across the gap (hydrodynamic effects were neglected). The computed leakage results are compared to those from Figure 13 of Reference [20] below:

<u>% Test Pressure</u>	<u>% Hydrodynamic Load Support</u>	<u><math>\bar{h}_{max}^{-1}</math></u>	<u>Computed Leakage</u>	<u>Measured Leakage [20]</u>
50%	16%	3.37	0.011 $\frac{oz}{min-in}$	0.02 $\frac{oz}{min-in}$
100%	13%	0.0009	0.00	<0.003

The hydrodynamic support developed is so small that its effect on friction would hardly be noticed. The particular wave shape and number of waves used for the test simply do not cause a very large hydrodynamic load support.

At 100% test pressure, the seal face is very much flattened out and leakage becomes quite small, as shown by the table above. At 50% test pressure, a considerable amount of waviness remains and experimental and calculated leakage are in reasonable agreement.

Without having more complete experimental data, a detailed comparison is not possible. However, to the extent that leakage results compare reasonably and that no great difference in friction behavior due to hydrodynamic effects would be expected or was reported as having been observed, the comparison does provide positive support for the theory developed. A better comparison will be possible using the two dimensional program.

CHAPTER 4  
ELASTOHYDRODYNAMIC LUBRICATION  
AND IMPROVED-FACE SEAL PERFORMANCE

As has been discussed earlier, it is expected that elastohydrodynamic lubrication may play only a small role in the long run in many conventional water seals (except as noted previously). Operation over a long period of time flattens out seal waviness due to wear, and hydrodynamic support diminishes. Given that a greater fraction of hydrodynamic load support will reduce seal wear and friction, it is important to determine how contacting seal designs can be altered to take advantage of elastohydrodynamic lubrication. Based on the preceding results, maintaining hydrodynamic lubrication requires that seal waviness be maintained during operation over a long period of time. There are several possible methods to do this. These methods are discussed in detail below.

Variable Wear Rate

One of the first ideas that comes to mind for sustaining waviness is to alter the material properties of the ring. One way to do this is to vary the wear rate of the material. A tangentially varying wear rate could lead to a stable waviness and hydrodynamic lubrication.

The basic wear equation for the asperity contact model is

$$\dot{w} = C_o p_{m_a} V \quad (4-1)$$

where

$\dot{w}$  - wear rate -  $L/T$

$C_o$  - a wear constant

$p_{m_a}$  - average pressure across face

$V$  - sliding speed

The above equation can be modified using dimensionless constants already defined as follows:

$$\frac{\dot{w}}{V} = C_o p_m \frac{\bar{p}_m}{\bar{p}_m - \frac{a}{\bar{b}_m}} \quad (4-2)$$

Now the quotient  $\frac{\bar{p}_m}{\bar{p}_m - \frac{a}{\bar{b}_m}}$  is simply the area of mechanical contact  $\bar{b}_m$ .

$p_m$  is the compressive strength of the material. So,

$$\frac{\dot{w}}{V} = C_o p_m \bar{b}_m \quad (4-3)$$

where  $\bar{b}_m$  depends on the value of  $h$  only.

Suppose now a variable wear rate is introduced so that

$$\frac{C_o}{C_{o_m}} = 1 + \left( \frac{r-1}{r+1} \right) \cos n\theta \quad (4-4)$$

where

$C_{o_m}$  - the mean wear rate

$r = \frac{C_{o_{max}}}{C_{o_{min}}}$  - the ratio of the maximum to the minimum wear rate.

Now, suppose that the wear rate  $C_o$  of the material can be altered without changing its hardness  $p_m$  and without altering the asperity distribution that is assumed constant throughout this work. Let the wear rate  $C_o$  take the above form. Then, eliminate  $C_o$  by substituting equation (4-4) into equation (4-3). In terms of  $\bar{b}_m$ , the result is

$$\bar{b}_m = \frac{\dot{w}}{p_m C_{o_m} V} \frac{1}{1 + \frac{r-1}{r+1} \cos n\theta} \quad (4-5)$$

Now in order that the seal face wear uniformly over a long period of time, which it must if gaps are not going to develop at the sealing face, the wear rate  $w$  must be constant with  $\theta$ . Also assuming that  $p_m$  is constant, as before, and since  $V$  and  $C_{o_m}$  are constant, then the quantity

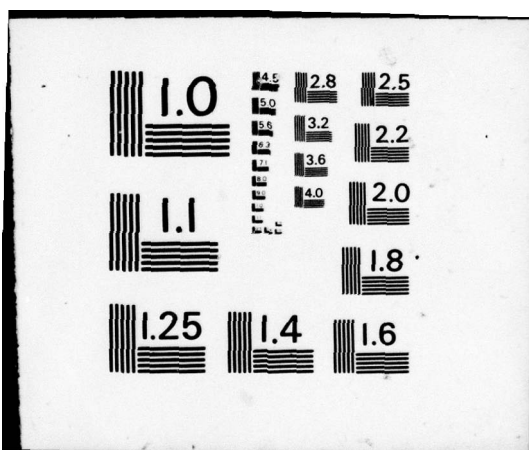
AD-A035 410 NEW MEXICO UNIV ALBUQUERQUE DEPT OF MECHANICAL ENGI--ETC F/G 11/1  
ELASTOHYDRODYNAMIC LUBRICATION WITH WEAR AND ASPERITY CONTACT I--ETC(U)  
JAN 77 A O LEBECK, J L TEALE, R E PIERCE N00014-76-C-0071  
UNCLASSIFIED ME-76(77)ONR-414-1 NL

202  
ADA035410



END

DATE  
FILMED  
3 - 77



$$\frac{\dot{w}}{p_m C_{O_m} V} = D \quad (4-6)$$

must be constant.  $\bar{b}_{m_{max}}$  to  $\bar{b}_{m_{min}}$  can be found from equation (4-5) as

$$\frac{\bar{b}_{m_{max}}}{\bar{b}_{m_{min}}} = r \quad (4-7)$$

Figure 4-1 shows  $\bar{b}_m$  as a function of  $\bar{h}$ . The base model shows that  $\bar{h}$  is about 0.8 with no hydrodynamic load support. Optimistically taking the wear rate ratio  $r$  at 10 and centering about  $\bar{h} = 0.8$  in Figure 4-1, the range of  $\bar{h}$  values provided by a  $\bar{b}_m$  ratio of 10 is from 0.71 to 0.85. This corresponds to a  $0.71 \times 10^{-1}$  micron ( $2.8 \mu\text{in}$ ) waviness amplitude for  $c = 1.02 \mu\text{m}$  ( $40 \mu\text{in}$ ). Thus, a variation in wear rate automatically leads to a variation in film thickness even in the absence of hydrodynamic pressure. This is true if the rings are relatively conformable, i.e., have low stiffness.) Because in the absence of hydrodynamic pressure a film thickness variation exists, it is expected that hydrodynamic effects would only alter this situation to a new stable equilibrium configuration having some hydrodynamic support assuming that other factors do not preclude hydrodynamic load support. However, it is known that this low amplitude will not produce hydrodynamic load support because at a mean film thickness of 0.8, the asperity gaps are so still large as to allow pressure developed by this small amplitude wave to pass or leak through with little pressure buildup. One could operate around a lower value of  $\bar{h}$  to get a greater  $\bar{h}$  range for the same ratio of 10 on  $\bar{b}_m$ . However, the compressive strength of the material would be so low for operation at this low value of  $h$  that the seal ring material would be impractical.

From the above, it is concluded that, based on the asperity model used, there is little chance of developing hydrodynamic load support through varying wear rate. Even if it were possible, as discussed much earlier, whenever asperity contact exists around the entire seal ( $\bar{h}_{max} < 1$ ),

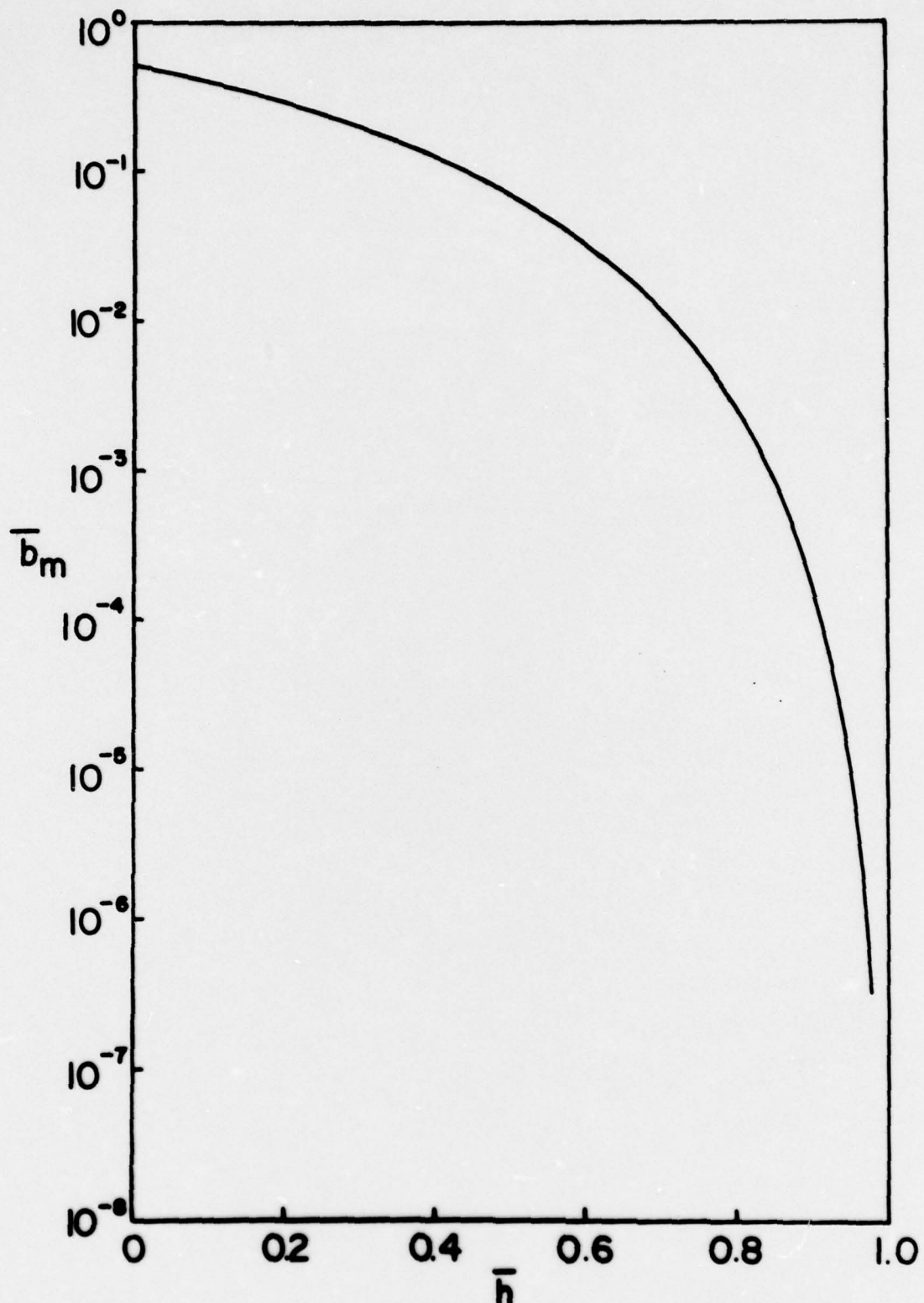


Figure 4-1. Variation of Fraction of Asperity Contact  $\bar{b}_m$  with  $\bar{h}$ .

there is no leakage flow and it is difficult for liquid to pass into the interface zone to sustain hydrodynamic lubrication.

Consider now the wear coefficient  $C_o$  that was assumed to be independent of  $p_m$ . Although this may be possible to do, it is more likely that the wear coefficient will relate to hardness in the conventional manner [39].

$$C_o = k/p_m \quad (4-8)$$

When equation (4-8) is substituted into equation (4-3).

$$\frac{w}{V} = k \bar{b}_m \quad (4-9)$$

or a constant wear rate requires a constant  $\bar{b}_m$  and therefore constant  $\bar{h}$ , and there is no possibility of hydrodynamic load support. (This is not to say that  $p_m$  or  $p_{ma}$  are constant, only their ratio.) This behavior has been verified using the time dependent computer model. Even given an initial waviness and variable hardness and wear rate according to equation (4-4), the waviness disappears and  $b_m$  becomes constant everywhere.

In conclusion, there seems to be no way using the assumed wear model to cause sustained hydrodynamic lubrication by the use of a tangentially variable wear rate or material hardness.

#### Tangentially Varying Friction Effects

It is known from a study of the base time dependent case that the fundamental harmonic waviness moves slowly tangentially as it wears away. The reason for the movement is that the center of mechanical pressure and center of wear are shifted from the centers of the original peak by hydrodynamic effects (see Figure 2-3). If the rate of wear movement could be increased, it might be possible to sustain hydrodynamic lubrication over at least a greater length of time if not indefinitely.

One way to cause an accelerated movement of the wave is by causing a greater phase shift between the center of pressure and the original wave center. This can be accomplished by a deflection that is out of phase with the pressure causing the deflection. One type of deflection of this kind is that due to a tangentially varying friction force.

Figure 4-2 shows how a tangentially varying friction force causes a deflection that is shifted to the left of the original high spot. This mechanism is present in actual seals to some extent because the friction at the face acts eccentrically to the centroid of ring.

To explore the possible effects of tangentially varying friction on hydrodynamic lubrication, it is first necessary to develop the relationship between friction and deflection. From Reference [22], equation (2-30), assuming that  $J_{xy} = 0$  and that a distributed radial moment  $m_x$  acts, then

$$v^{vi} + 2v^{iv} + v'' = \frac{R^3}{EI_x} (m_x''' - Am_x') \quad (4-10)$$

Assume that friction at the face can be represented by a Fourier series.

$$\bar{p}_f = \frac{p_f c}{\eta V b} = \sum_i \bar{p}_{fa_i} \cos ni\theta + \bar{p}_{fb_i} \sin ni\theta \quad (4-11)$$

where  $\bar{p}_f(\theta)$  is the friction force on the face and is defined by equation (2-40). Noting that

$$h = + v \quad (4-12)$$

and

$$m_x = - p_f e_y \quad (4-13)$$

where  $e_y$  is the eccentricity between the face and the centroid, it can be shown using equation (4-10), (4-11), (4-12), and (4-13) that the displacement  $h$  is given by

$$\bar{h}_f = \sum_i \bar{h}_{fa_i} \cos ni\theta + \bar{h}_{fb_i} \sin ni\theta \quad (4-14)$$

where

$$\bar{h}_{fa_i} = - B \frac{c}{R} \frac{e_y}{R} \frac{n^2 i^2 + A}{ni(n^2 i^2 - 1)^2} \bar{p}_{fb_i} \quad (4-15)$$

$$\bar{h}_{fb_i} = + B \frac{c}{R} \frac{e_y}{R} \frac{n^2 i^2 + A}{ni(n^2 i^2 - 1)^2} \bar{p}_{fa_i} \quad (4-16)$$

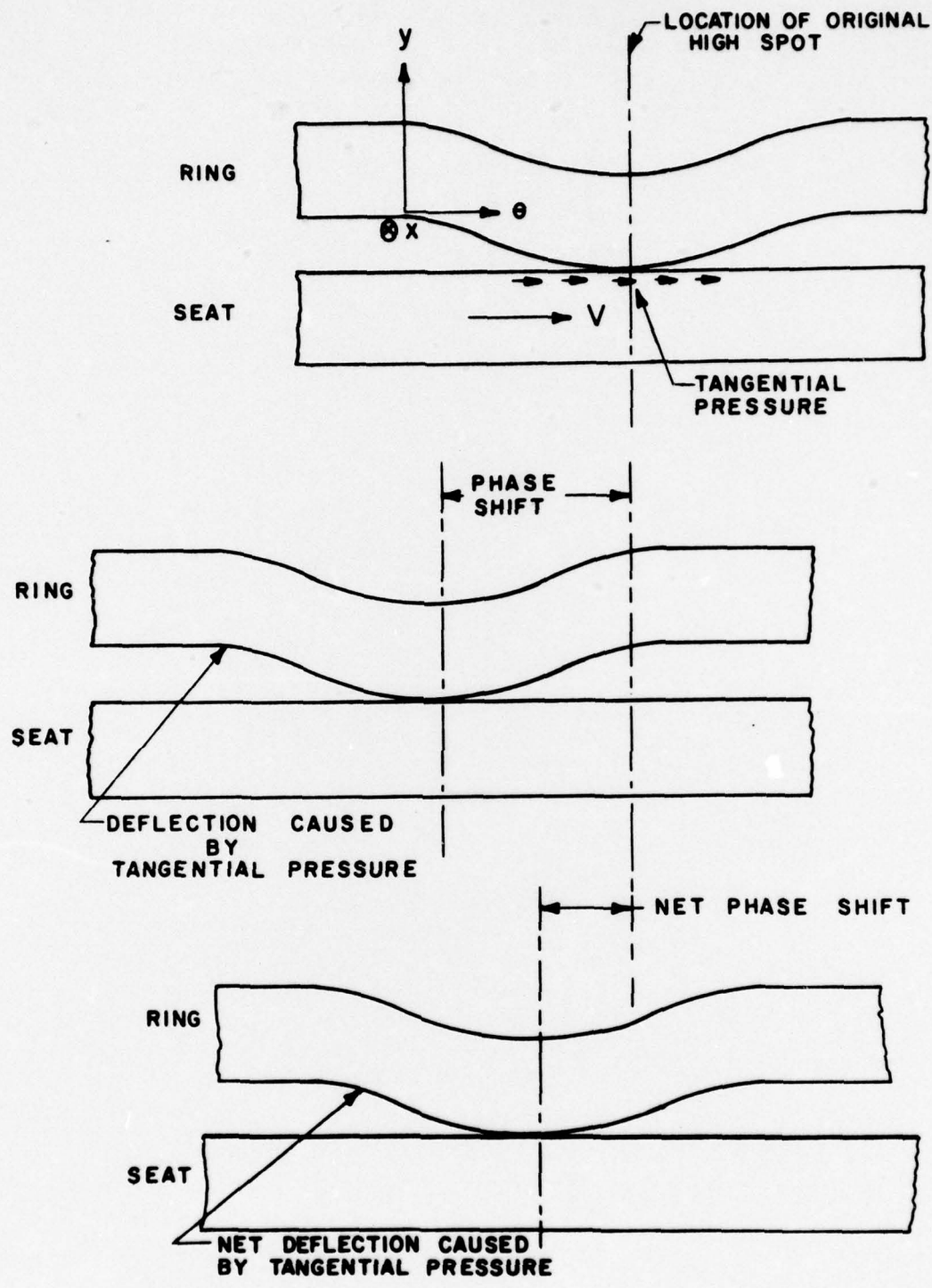


Figure 4-2. Effect of a Tangential Friction on Deflection

The effects of tangentially varying friction can be included in the program by treating  $h_{fa}$  and  $h_{fb}$  in the same way as  $h_{da}$  and  $h_{db}$  in the base case solution. This adds two variables again bringing the total to five. As in the base case, only the first harmonic needs to be included. The higher harmonics are negligible.

The results for this solution are shown in Figure 4-3. The base case is compared to the two tangential friction cases.  $e_y/R = 0.2$  is the actual value for the seal under study.  $e_y/R = 1.0$  was tried to see if a significant effect occurred. It is clear from the results that tangentially variable friction has no significant effect on % hydrodynamic load support.

#### Traveling Wave

A third method of sustaining hydrodynamic load support is the traveling wave. Suppose that a wavy shape is imposed elastically on the seal ring (see Figure 4-4). Then suppose that this wave is made to move slowly relative to this same ring. The result is shown in Figure 4-4. As a result of the slow movement, the wear becomes uniformly distributed around the seal ring and the original wavy shape is essentially unchanged.

This approach offers the possibility of being able to impose any desired shape on the face of a contacting face seal over an extended period of time. The actual mechanism for doing this is taken up in Chapter 6. The optimum shape is discussed in the next section of this chapter. What remains is to establish proof that the concept works and to determine how fast the wave must be moved so as to not significantly alter the wave shape. These topics follow.

Let it be assumed that there is a wave that travels relative to the fixed ring. Associated with any wave is the mechanical or asperity pressure distribution  $\bar{p}_{m_a}$  which will be represented by a Fourier series.

$$\bar{p}_{m_a} = \bar{p}_o + \sum \bar{p}_{a_i} \cos ni\theta + \bar{p}_{b_i} \sin ni\theta \quad (4-17)$$

Now assume that the mechanical pressure distribution does not appreciably change but that it moves relative to the fixed ring at a speed  $\omega$ . Then

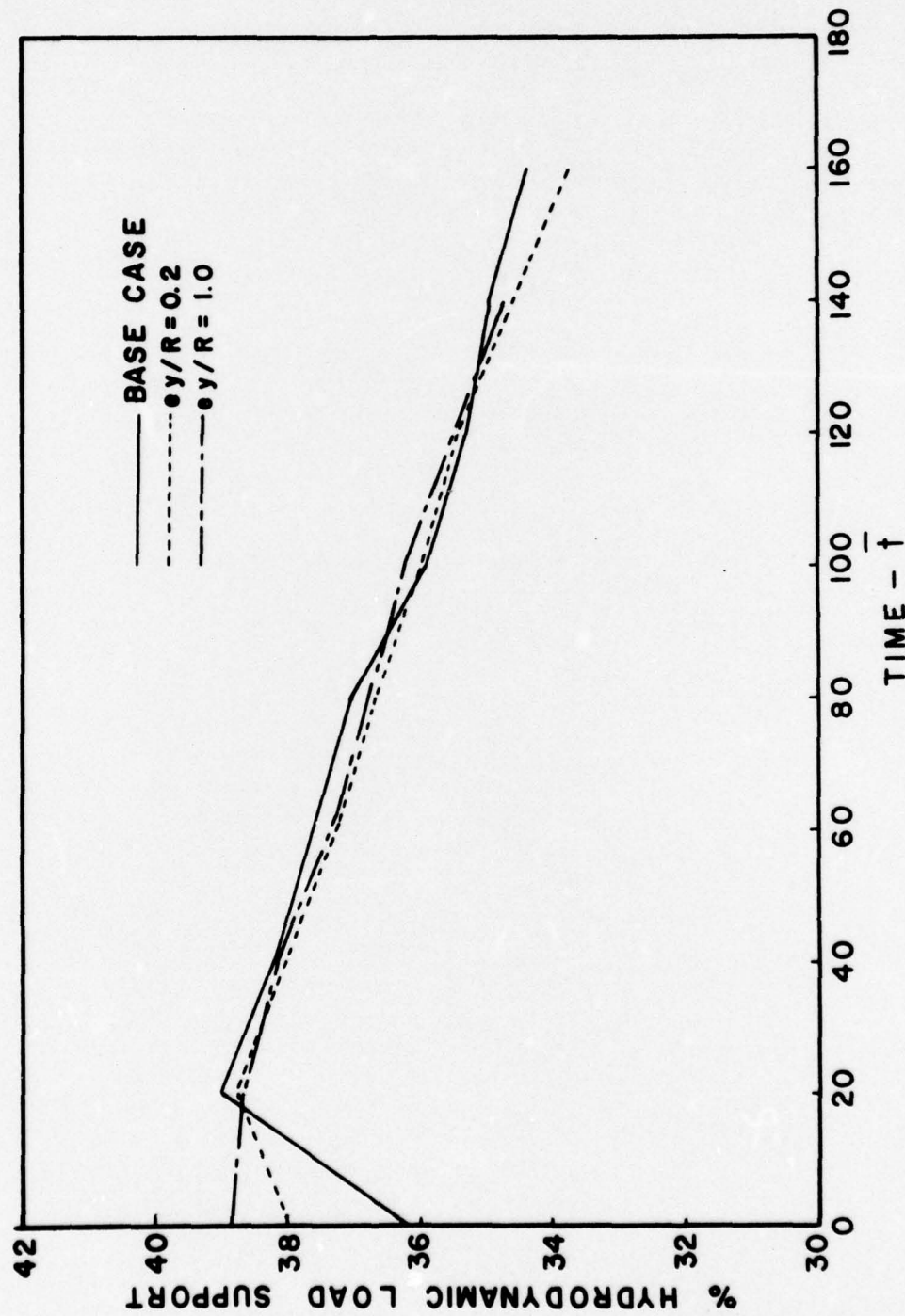
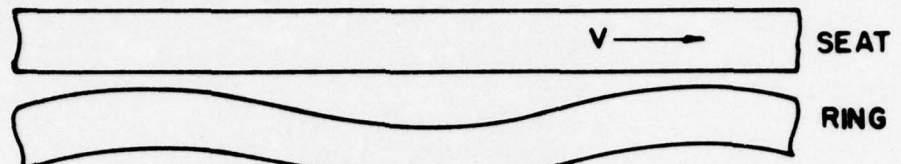


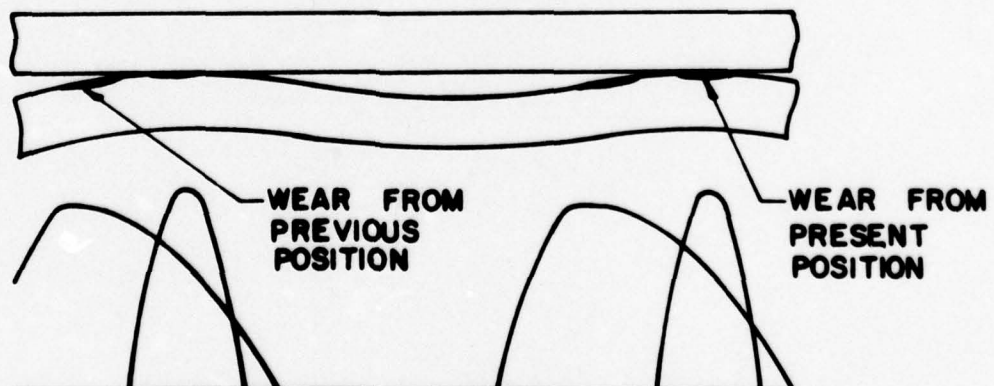
Figure 4-3. Effect of Tangentially Varying Friction on Load Support



DISTORTED RING UNDER ZERO PRESSURE



DISTORTED RING UNDER PRESSURE



DISTORTED RING UNDER PRESSURE  
AFTER WAVE HAS MOVED

Figure 4-4. Traveling Wave

$$\bar{p}_{m_a} = \bar{p}_o + \sum \bar{p}_{a_i} \cos(ni\theta - \omega\bar{t}) + \bar{p}_{b_i} \sin(ni\theta - \omega\bar{t}) \quad (4-18)$$

From before

$$\frac{dh_w}{d\bar{t}} = \bar{p}_{m_a} \quad (4-19)$$

Therefore,

$$\int dh_w = \int \left[ \bar{p}_o + \sum \bar{p}_{a_i} \cos(ni\theta - \omega\bar{t}) + \bar{p}_{b_i} \sin(ni\theta - \omega\bar{t}) \right] d\bar{t} \quad (4-20)$$

Now assuming that wear is zero at time equals zero, then

$$\begin{aligned} \bar{h}_w &= \bar{p}_o \bar{t} + \sum \bar{p}_{a_i} \left( -\frac{1}{\omega} \right) [\sin(ni\theta - \omega\bar{t}) - \sin ni\theta] \\ &\quad + \bar{p}_{b_i} \left( \frac{1}{\omega} \right) [\cos(ni\theta - \omega\bar{t}) - \cos ni\theta] \end{aligned} \quad (4-21)$$

Now, assume that wear is given by a Fourier series

$$\bar{h}_w = \bar{h}_{wo} + \sum \bar{h}_{wa_i} \cos ni\theta + \bar{h}_{wb_i} \sin ni\theta \quad (4-22)$$

Also,

$$\bar{h}_w = \bar{h}_{wo} + \sum \bar{h}_{w_{amp_i}} \cos(ni\theta - \psi) \quad (4-23)$$

Then, equating equation (4-21) and (4-22),

$$\bar{h}_{wa_i} = \frac{\bar{p}_{a_i}}{\omega} \sin \omega t + \frac{\bar{p}_{b_i}}{\omega} (\cos \omega t - 1) \quad (4-24)$$

$$\bar{h}_{wb_i} = -\frac{\bar{p}_{a_i}}{\omega} (\cos \omega t - 1) + \frac{\bar{p}_{b_i}}{\omega} \sin \omega t \quad (4-25)$$

Using equations (4-22), (4-23), (4-24), and (4-25), and assuming for now that  $\bar{p}_{b_i}$  is zero since the reference point is arbitrary when looking at only the  $i$ th term, then

$$\bar{h}_{w_{amp_i}} = \frac{\bar{p}_{a_i}}{\omega} \sqrt{2(1-\cos\omega t)} \quad (4-26)$$

$$\tan\psi = \tan \frac{\omega t}{2} \quad (4-27)$$

The meaning of the above two equations is that the amplitude of the  $i$ th wear wave caused by the traveling wave is itself periodic starting at zero and ending up at zero one time period,  $\omega t = 2\pi$ , later. The amplitude of the wear wave becomes smaller as  $\omega$ , the speed of the wave, increases. Equation (4-27) shows that the phase angle of the wear wave is  $1/2$  that of the traveling wave. Thus, the wear wave moves along at one half of the speed of the traveling wave.

The above expressions have been verified numerically by making the initial base case waviness move with each time step as follows. It was found in the base case that the largest component of  $\bar{p}_m$  is for  $i=1$  as would be expected. Taking the case (shift the wave) where  $p_{b1} = 0$ , then it was found from the base case that

$$\bar{p}_{a_1} = 3.053 \times 10^{-3} \quad (4-28)$$

Now assume that one can allow a maximum amplitude variation in the first harmonic wear term of 0.01. Now the maximum amplitude of the wear amplitude occurs when  $\omega t$  in equation (4-26) equals  $\pi$  or

$$\bar{h}_{w_{amp_{1_{max}}}} = \frac{2\bar{p}_{a_1}}{\omega} \quad (4-29)$$

Thus

$$\omega = 0.61 \text{ (Actually } 0.628 \text{ was used for convenience.)}$$

This is the rate of travel that will cause the maximum amplitude error in the first harmonic to become 0.01. This result is verified by the computer program results of Figure 4-5. The amplitude starts at zero, goes to 0.01, and then returns to zero. The same program also verified equation (4-27). To see what effect the given amount of error has

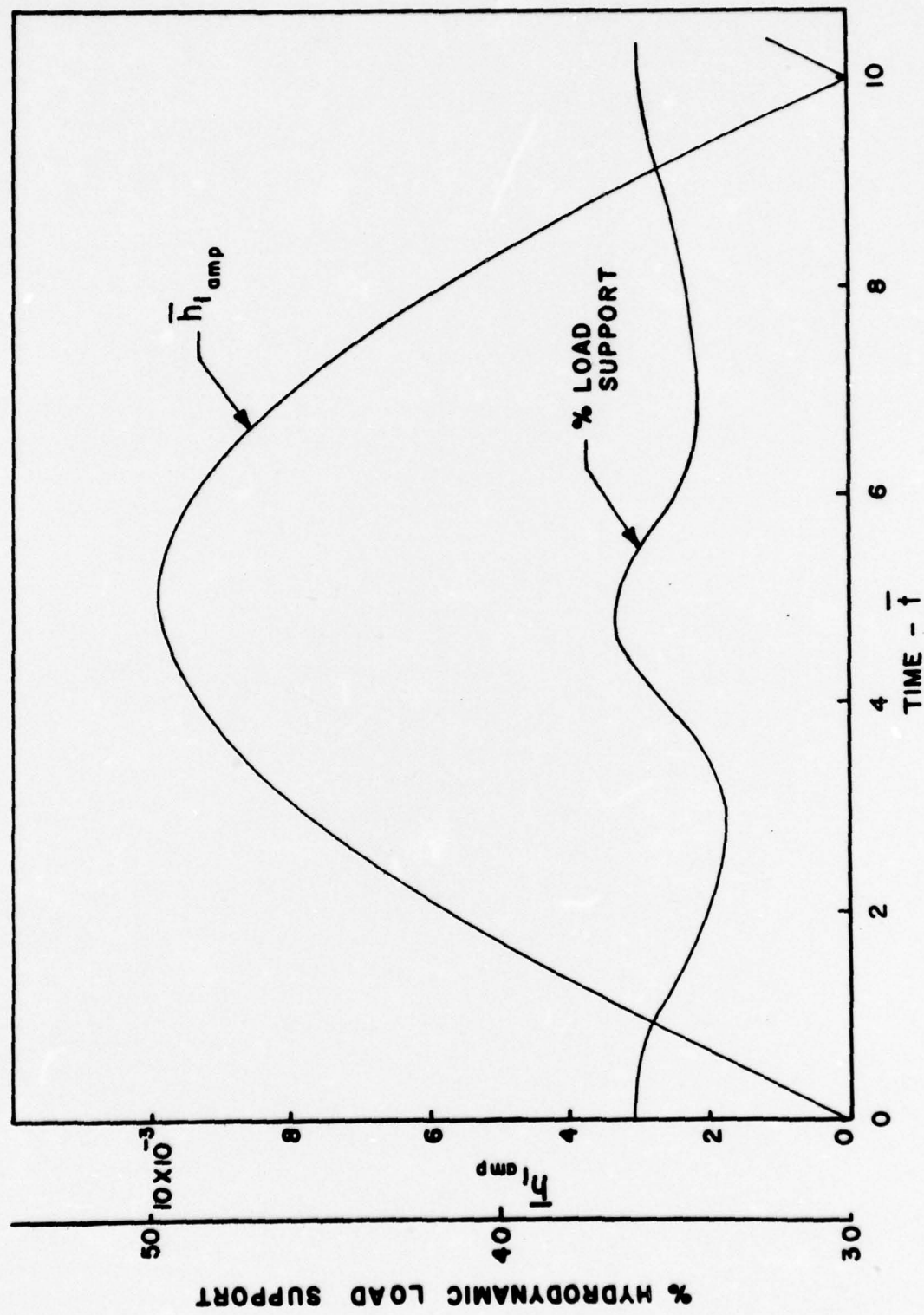


Figure 4-5. Effect of Traveling Wave on Waviness and Load Support

on the hydrodynamic load support, % load support is shown plotted as a function of time. There is some small variation as expected because the 0.01 variation in amplitude is significant. However, after one period of operation, the % hydrodynamic load support returns to its original value. This cycle can be repeated indefinitely without any degradation in load support. This shows that the traveling wave concept is valid.

The actual speed corresponding to this case can be obtained using equation (3-14). For  $\bar{t} = 10$ , this corresponds to  $t = 0.21$  hrs for  $1/n$  or  $1/3$  turns. Thus the time per turn is 0.63 hours. If the wear rate were lower, the required turning rate would be even lower. Also, if a greater deviation in load support were allowed, the turning rate could be even slower. The traveling speed will require additional investigation for the non simple sinusoidal shapes discussed in the next section to see if other shapes are more or less sensitive to a given amount of profile error.

#### Optimum Wave Shapes

The traveling wave concept offers the possibility of using any profile shape desired. There are two important criteria for seal design purposes, minimum wear and minimum leakage. A tradeoff between leakage and wear may be required, but it should be possible to select a traveling wave profile that provides greatly reduced wear with acceptable leakage.

Without the use of a two dimensional solution, leakage cannot be evaluated. The tradeoff question will have to be pursued later after the two dimensional model has been completed. For now it is useful to show that non simple sinusoid shapes are better than sinusoidal shapes from a standpoint of load support and that considerable hydrodynamic load support can be obtained by altering and controlling the surface profile of the seal.

The problem of finding profiles of increased load support was approached as an optimization problem. From equation (2-14), the variable part of the film thickness is given by

$$h = \sum (h_{ia_j} + h_{da_j}) \cos nj\bar{x} + (h_{ib_j} + h_{db_j}) \sin nj\bar{x} \quad (4-31)$$

That is, the variables that control the film are simply

$$HA_j = h_{ia_j} + h_{da_j} \quad (4-32)$$

$$HB_j = h_{ib_j} + h_{db_j}$$

Given an arbitrary set of  $HA_j$  and  $HB_j$ , one can find the initial waviness  $h_{ia_j}$   $h_{ib_j}$  required for equilibrium. The mean film thickness is determined for any  $HA_j$   $HB_j$  by load equilibrium conditions. Thus, the hydrodynamic load support becomes a function of the net waviness.

$$\% \text{ Hydrodynamic Load Support} = f(HA_j, HB_j) \quad (4-33)$$

To find the function  $HA_j$   $HB_j$  that gives a true maximum, many terms are required. To see what possible gain could be realized in load support, the problem was first solved using three variables  $HA_1$   $HA_2$   $HB_2$  ( $HB_1 = 0$  is an arbitrary condition and simply positions the wave). It was found that the load support for the base case conditions could be increased from the 36% for the sine curve of the base case to about 60%, using an optimization technique applied to the three variables.

Using five independent variables,  $HA_1$ ,  $HA_2$ ,  $HA_3$ ,  $HB_2$ ,  $HB_3$ , it was found that load support increased to 70%. The results for the equilibrium film shape for this last case are shown in Figure 4-6. The hydrodynamic and asperity pressures are shown in Figure 4-7.

It is likely that given enough terms, the hydrodynamic load support could be made even higher than 70% and that the curve would become more smooth as more terms were added. It should also be noted from the results of the equilibrium parameter studies that certain other variables can be optimized to bring the % support even higher. 70% hydrodynamic load support represents a factor of 3 reduction in wear rate. The optimization will be pursued further using a two dimensional program so that leakage can be evaluated.

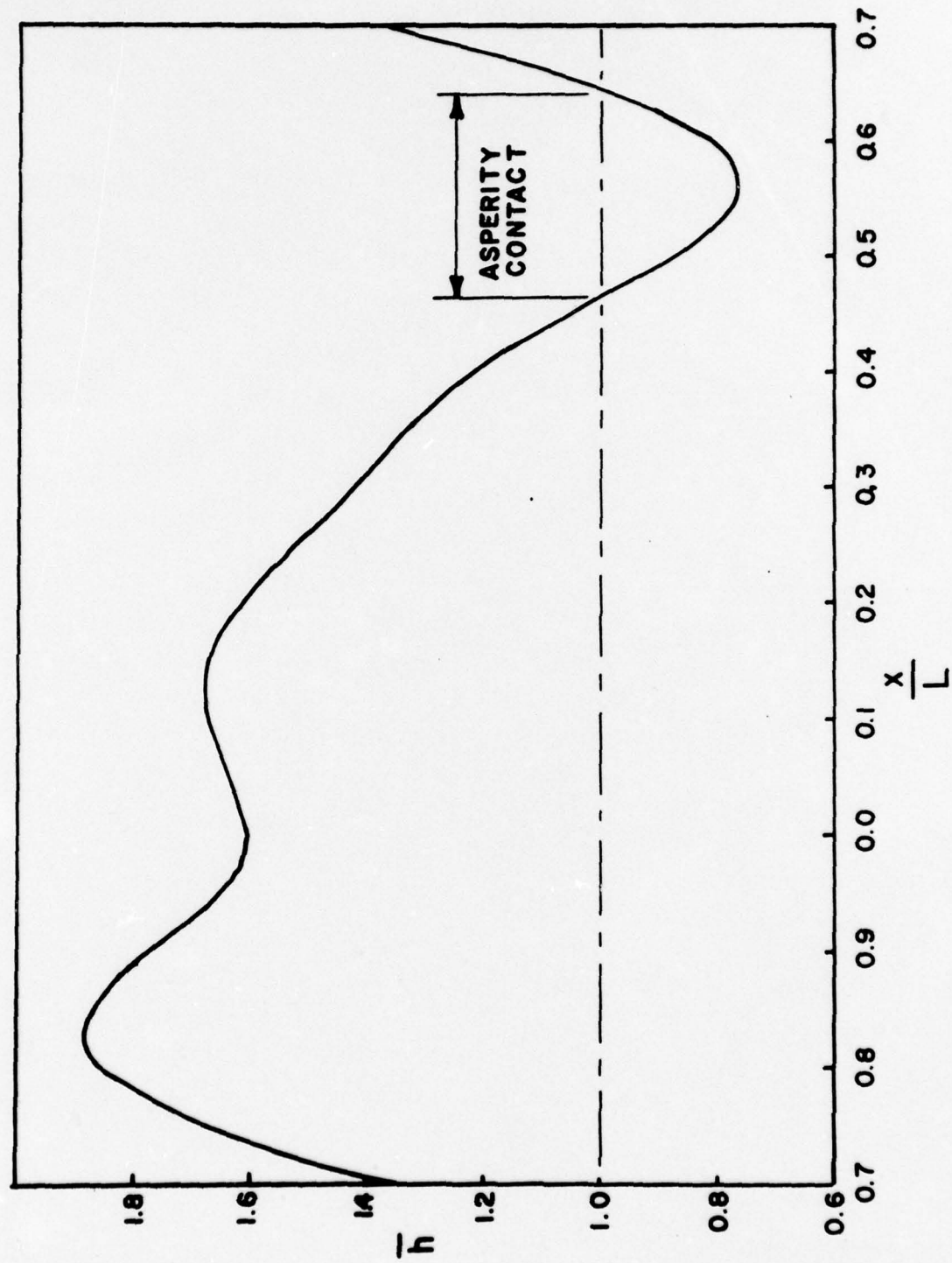


Figure 4-6. Optimum Five Term Film Shape

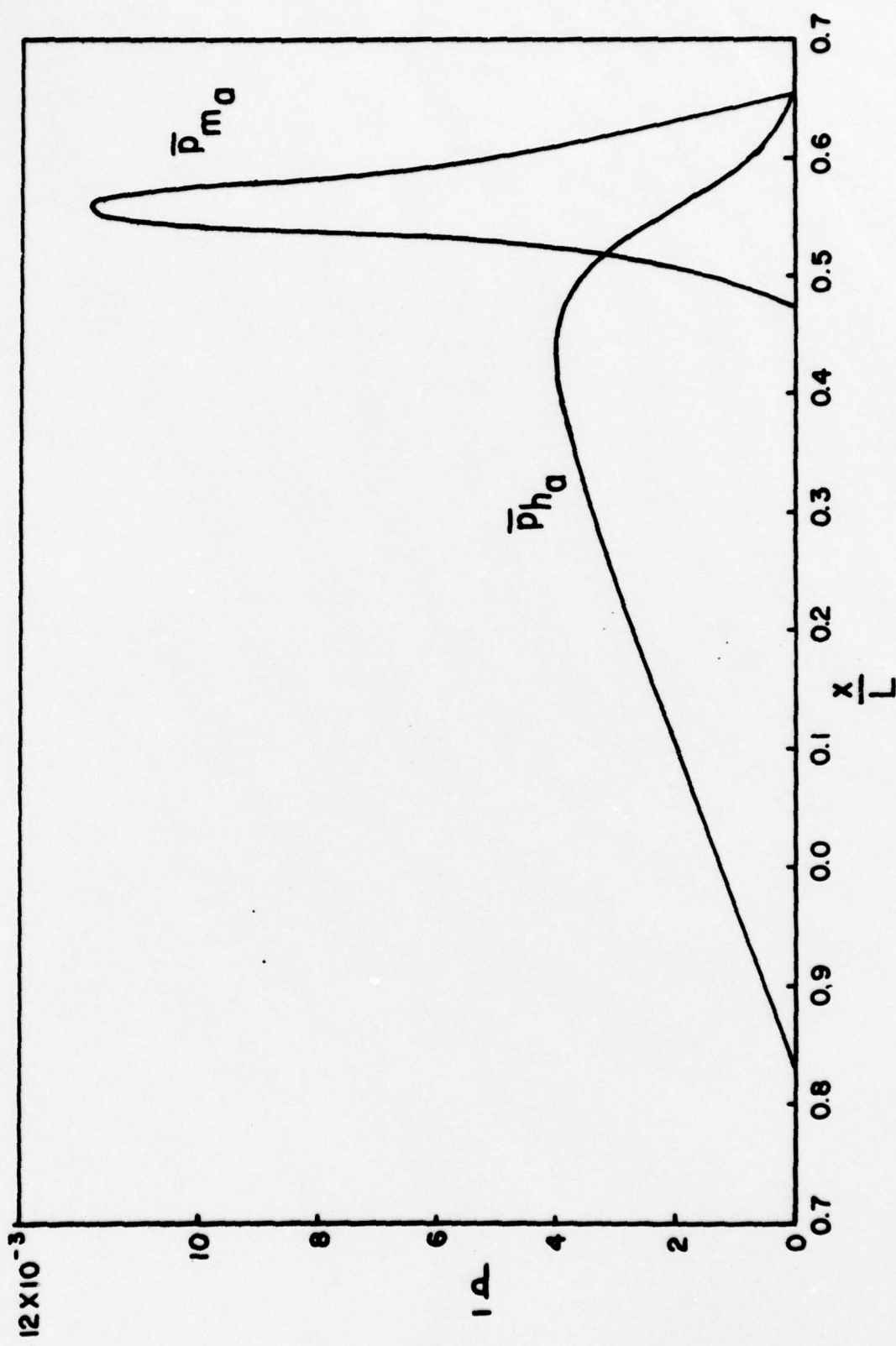


Figure 4-7. Optimum Film Shape Pressure

## CHAPTER 5

### TWO DIMENSIONAL ELASTOHYDRODYNAMIC SEAL MODEL

The primary limitations of the one dimensional seal model are 1) it cannot be used to predict leakage and 2) the accuracy of the load support calculated using the one dimensional model is in question. It is essential to develop a two dimensional model to verify and modify the work based on the one dimensional model as well as to expand on the one dimensional work by the inclusion of leakage.

#### Basic Equations

The essential difference between the one and two dimensional elasto-hydrodynamic problems is in the method of finding  $p_h(x)$ , the hydrodynamic pressure as a function of  $x$ . Other features of the solution will remain the same, so this chapter will concentrate on solving the two dimensional Reynolds equation which gives  $p_h(x,y)$  and thus  $p_h(x)$  needed for the complete solution.

The problem to be solved is illustrated in Figure 5-1. Given an arbitrary film shape with a period of length  $L$  and given inside and outside pressures on the seal, the complete pressure distribution, load support, and leakage must be found. The problem is complicated by the fact that a cavitated region will generally exist, and for the problem of interest, there will be some region of asperity contact. In this section, the mathematics of the solution will be developed.

#### Reynolds Equation

Even though no great error is introduced for most seals by using rectangular coordinates, it was decided to formulate the problem in polar coordinates in case a wide face seal became of interest. The Reynolds equation in polar coordinates is given by

$$\frac{\partial}{\partial r} \left( rh^3 \frac{\partial p}{\partial r} \right) + \frac{1}{r} \frac{\partial}{\partial \theta} \left( h^3 \frac{\partial p}{\partial \theta} \right) = 6Vn \frac{\partial h}{\partial \theta} \quad (5-1)$$

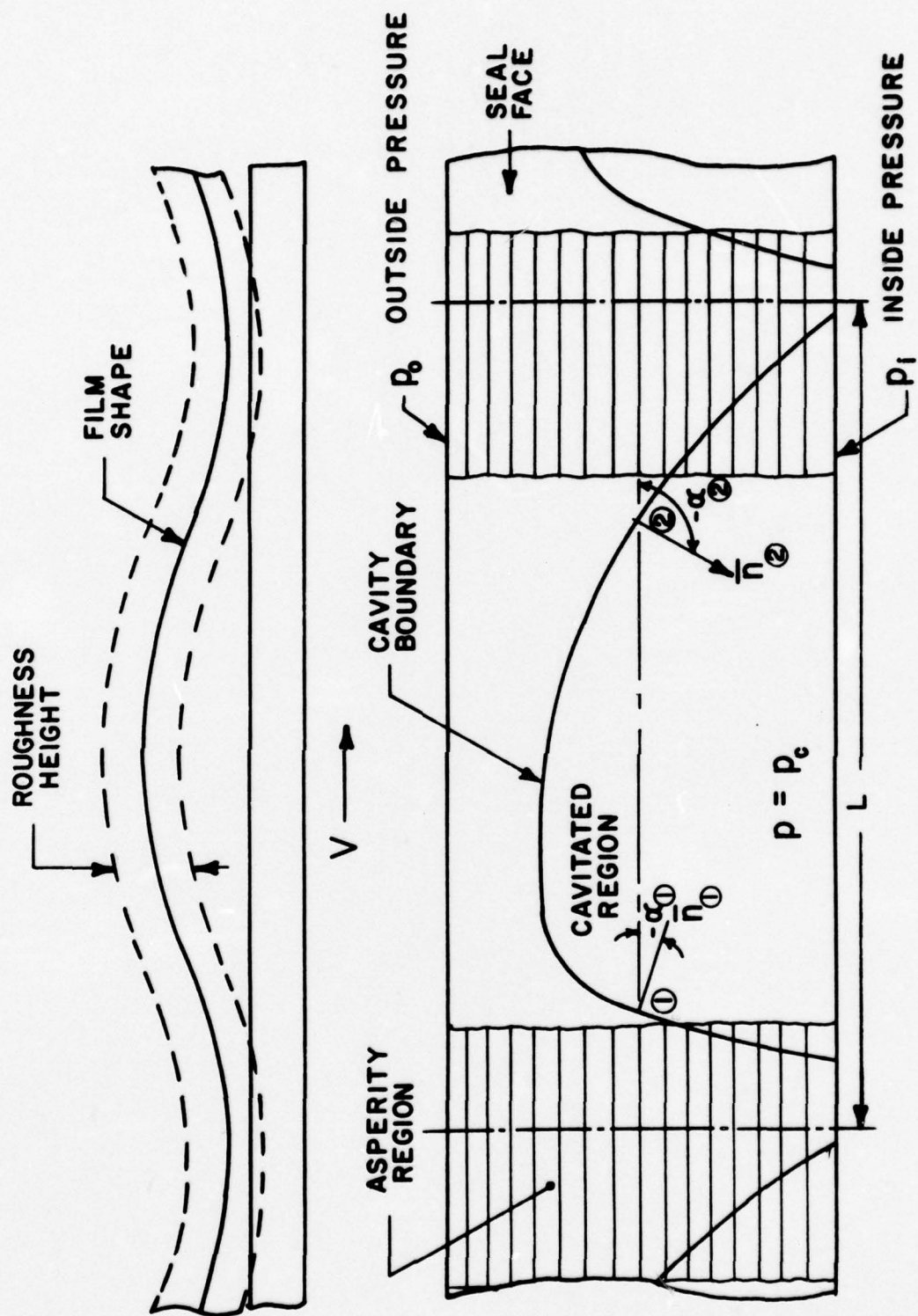


Figure 5-1. Two Dimensional Problem

Flow equations are

$$q_\theta = \frac{-h^3}{12rn} \frac{\partial p}{\partial \theta} + \frac{r\omega h}{2} \quad (5-2)$$

$$q_r = \frac{-h^3}{12n} \frac{\partial p}{\partial r} \quad (5-3)$$

where coordinates are defined in Figure 5-2. The methods of Christensen [36] can be used to include the longitudinal roughness effects into the Reynolds equation. In dimensionless form, the equations for the two dimensional flow region ( $\bar{h} > 1$ ) become:

$$\frac{1}{\bar{r}} \frac{\partial}{\partial \theta} \left( \frac{\partial \bar{p}}{\partial \theta} E(\bar{H}^3) \right) + \frac{\partial}{\partial \bar{r}} \left( \bar{r} \frac{\partial \bar{p}}{\partial \bar{r}} \frac{1}{E\left(\frac{1}{\bar{H}^3}\right)} \right) = 6 \frac{\partial E(\bar{H})}{\partial \theta} \bar{r} \quad (5-4)$$

$$\bar{q}_\theta = - \frac{E(\bar{H}^3)}{12\bar{r}} \frac{\partial \bar{p}}{\partial \theta} + \frac{\bar{r}E(\bar{H})}{2} \quad (5-5)$$

$$\bar{q}_r = - \frac{1}{12E\left(\frac{1}{\bar{H}^3}\right)} \frac{\partial \bar{p}}{\partial \bar{r}} \quad (5-6)$$

where

$$\bar{r} = \frac{r}{r_o} \quad (5-7)$$

$$\bar{H} = \frac{H}{C} \quad (5-8)$$

$$\bar{p} = \frac{p_c^2}{r_o^2 \omega n} \quad (5-9)$$

$$\bar{q}_r = \frac{q_r}{r_o \omega c} \quad (5-10)$$

$$\bar{q}_\theta = \frac{q_\theta}{r_o \omega c} \quad (5-11)$$

$\omega$  = angular velocity

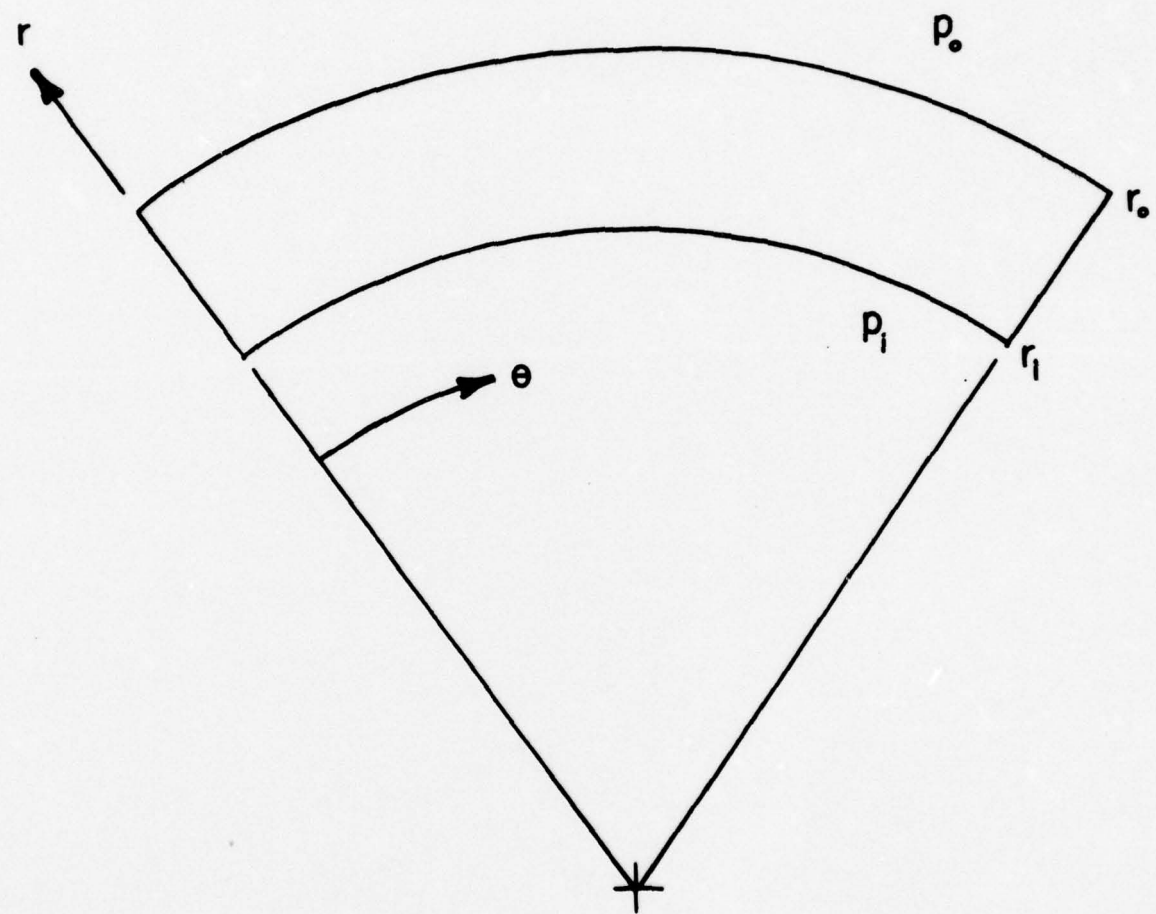


Figure 5-2. Coordinates for Two Dimensional Problem

Also, not previously given

$$E\left(\frac{1}{\bar{H}^3}\right) = \left[ 3(1-\bar{h}^2)(5\bar{h}^2 - 1) \ln\left(\frac{\bar{h}+1}{\bar{h}-1}\right) - 26\bar{h} + 30\bar{h}^3 \right] \frac{35}{32}; \bar{h} > 1$$

$$E\left(\frac{1}{\bar{H}^3}\right) = \left[ \frac{(1-\bar{h}^2)^2}{2\bar{A}^2} (12\bar{h}\bar{A} - \bar{h}^2 + 1) + 3(1-\bar{h}^2)(5\bar{h}^2 - 1) \ln\left(\frac{\bar{h}+1}{\bar{A}}\right) \right.$$

$$\left. + \frac{3}{4} - 13\bar{h} - \frac{15}{2}\bar{h}^2 + 15\bar{h}^3 + \frac{35}{4}\bar{h}^4 \right] \frac{35}{32}; \bar{h} < 1 \quad (5-12)$$

Other symbols and functions are as defined previously.

The common procedure used to solve the above Reynolds equation is to neglect the first term on the left hand side ( $\frac{\partial p}{\partial \theta} = 0$ ). This makes it possible to directly integrate the equation. This is called the short bearing equation. This simplification is used by Findlay [9] and Stanghan, Batch and Iny [4] for a solution to the mechanical seal problem. However, in the present case, this simplification is not possible because, in the asperity region, the equation becomes one dimensional in the tangential direction ( $\frac{\partial p}{\partial r} \rightarrow 0$ ). Thus these two conditions are completely incompatible at the transition between the asperity and non-asperity regions. Therefore, it was decided that the unapproximated two dimensional equation should be used, with the solution being carried out by numerical methods as explained later.

In the one dimensional flow or asperity contact region ( $\bar{h} < 1$ ), the equations are the same as the previous one dimensional case. That is, radial flow becomes zero because the longitudinal roughness acts as a series of dams against the radial flow. In this case tangential flow is given by

$$\bar{q}_\theta = \left( -\frac{E(\bar{H}^3)}{12\bar{r}} \frac{\partial \bar{p}}{\partial \theta} + \frac{\bar{r}E(\bar{H})}{2} \right) \bar{b}_h \quad (5-13)$$

where  $\bar{b}_h$  is the fraction of the area available to flow as before. The  $\bar{b}_h$  term represents a correction to Christensen's original work [36] and

reflects the condition of reduced flow area. This correction was not made for the one dimensional case. However, an inspection of Figure 4-1 shows that  $\bar{b}_h$  remains very close to 1.0 for  $\bar{h}$  even down to 0.7 so the error caused by assuming  $\bar{b}_h = 1$  is small.

For the one dimensional case the Reynolds equation is obtained from the continuity condition:

$$\frac{d\bar{q}_\theta}{d\theta} \approx 0 \quad (5-14)$$

So, from equation (5-13)

$$\frac{d}{d\theta} \left[ \left( -\frac{E(\bar{H}^3)}{12\bar{r}} \frac{dp}{d\theta} + \frac{\bar{r}E(\bar{H})}{2} \right) \bar{b}_h \right] = 0 \quad (5-15)$$

#### Boundary Conditions

The inside and outside boundary conditions are

$$p = p_o \text{ at } r = r_o \quad (5-16)$$

$$p = p_i \text{ at } r = r_i \quad (5-17)$$

where  $p_o$  and  $p_i$  depend on the sealing conditions. In addition to these conditions, previous investigators [42], [9], have shown that a cavity will form in a seal under hydrodynamic conditions. When the pressure attempts to become low or negative, the flow breaks up into a series of streamers which flow across the cavitated region (see Reference [42]). The pressure at which this cavitation begins is called the cavitation pressure  $p_c$  and is usually associated with the vapor pressure of the liquid or the pressure at which absorbed gasses come out of the liquid. For present purposes cavitation pressure is taken as normal atmospheric pressure for seals where either  $p_i$  or  $p_o$  is atmospheric pressure. The first cavity boundary condition is thus

$$p = p_c \text{ at the cavity boundary.}$$

The additional conditions for the cavity boundary are derived from the continuity condition that the flow leaving the left hand boundary

(which forms into a streamer) equals the flow entering the right hand boundary [42] (see Figure 5-1). Also, the Reynolds boundary condition at the left hand end of the cavity is used.

$$\left(\frac{\partial P}{\partial n}\right)_1 = 0 \text{ at left hand cavity boundary} \quad (5-18)$$

where  $n$  is normal to the cavity boundary. Now, for the most general situation, the continuity condition requires that (see Figure 5-1)

$$q_{tangential\ 1} = q_{tangential\ 2} \text{ or } q_t\ 1 = q_t\ 2 \quad (5-19)$$

Now using equations (5-5), (5-6) and (5-18) and using the normal derivative, it can be shown that this condition reduces to the following equation

$$\begin{aligned} & \left(\frac{\partial}{\partial n}\right)_2 \left[ E(\bar{H})_2 \bar{b}_{h2} - E(\bar{H})_1 \bar{b}_{h1} \right] \\ &= \left(\frac{\partial}{\partial n}\right)_2 \left[ E(\bar{H})_2^3 \bar{b}_{h2} \cos^2 \alpha + \frac{1}{E(\frac{1}{\bar{H}})} \sin^2 \alpha \right] \end{aligned} \quad (5-20)$$

Thus, the above equation provides a condition on the normal derivative at the right hand cavity boundary based on continuity. The quantities  $b_{h1}$  and  $b_{h2}$  take on different values depending on whether or not these points are within the asperity contact region.

$$\text{If } \bar{h}_1 > 1 \text{ and } \bar{h}_2 > 1 \text{ then } b_{h1} = 1 \text{ and } b_{h2} = 1 \quad (5-21)$$

$$\text{If } \bar{h}_1 < 1 \text{ and } \bar{h}_2 > 1 \text{ then } b_{h1} = b_{h2} = 1 \quad (5-22)$$

where  $b_h$  values not equal to 1 are calculated from equation (2-21).

If the right hand end is within the asperity region, the normal direction actually becomes tangential and  $\alpha \rightarrow 0$ . Then the following condition applies:

$$6\bar{r} \left[ E(\bar{h}_2) \bar{b}_{h_2} - E(\bar{h}_1) \bar{b}_{h_1} \right] = \frac{E(\bar{h}_2^3) \bar{b}_{h_2}}{\bar{r}} \frac{\partial \bar{p}}{\partial \theta} \Big|_2 \quad (5-23)$$

$$\text{if } \bar{h}_1 > 1 \text{ then } \bar{b}_{h_1} = 1 \quad (5-24)$$

All possibilities are thus taken care of.

#### Leakage and Load Support

Load support as a function of  $\theta$  (required for the complete elasto-hydrodynamic solution) is obtained as follows, given  $p(r, \theta)$ :

$$\bar{p}_h(\theta) = \int_{\bar{r}_i}^{\bar{r}_o} \bar{p} \bar{r} d\bar{r} \quad (5-25)$$

Total load support per wave is given by

$$\bar{W} = \int_0^{2\pi} \bar{p}_h(\theta) d\theta \quad (5-26)$$

where

$$\bar{p}_h(\theta) = \frac{p_h(\theta)c^2}{r_o^4 \eta \omega} \quad (5-27)$$

$$\bar{W} = \frac{w_c^2}{r_o^4 \eta \omega} \quad (5-28)$$

Leakage per wave through the seal is given by

$$\bar{Q} = \int_0^{2\pi} \frac{-1}{12E\left(\frac{1}{H^3}\right)} \frac{\partial \bar{p}}{\partial \bar{r}} (r_o) \bar{r}_o d\theta = \int_0^{2\pi} \frac{-1}{12E\left(\frac{1}{H^3}\right)} \frac{\partial \bar{p}}{\partial \bar{r}} (r_i) \bar{r}_i d\theta \quad (5-29)$$

where

$$\bar{Q} = \frac{Q}{r_o^2 w_c} \quad (5-30)$$

### Numerical Formulation

#### Finite Difference Equation

Equation (5-4) can be expressed by using central differences:

$$\frac{dy}{dx} = \frac{y_1 - y_{-1}}{2\Delta x} \quad (5-31)$$

$$\frac{d^2 y}{dx^2} = \frac{y_1 - 2y_0 + y_{-1}}{(\Delta x)^2} \quad (5-32)$$

Equation (5-4) can be written in the form

$$A \frac{\partial^2 p}{\partial \theta^2} + B \frac{\partial p}{\partial \theta} + C \frac{\partial^2 p}{\partial r^2} - D \frac{\partial p}{\partial r} = E \quad (5-33)$$

where

$$A = \frac{1}{r} E(\bar{H}^3) \quad (5-34)$$

$$B = \frac{1}{r} \frac{\partial}{\partial \theta} E(\bar{H}^3) \quad (5-35)$$

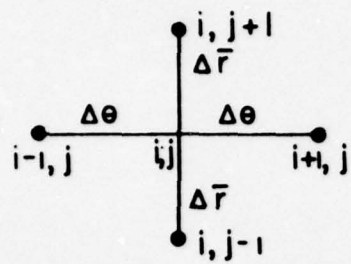
$$C = \frac{\bar{r}}{E\left(\frac{1}{\bar{H}}^3\right)} \quad (5-36)$$

$$D = \frac{1}{E\left(\frac{1}{\bar{H}}^3\right)} + \bar{r} \frac{\partial}{\partial \bar{r}} \left( \frac{1}{E\left(\frac{1}{\bar{H}}^3\right)} \right) \quad (5-37)$$

$$E = 6\bar{r} \frac{\partial}{\partial \theta} E(\bar{H}) \quad (5-38)$$

where the functions A through E are calculated from the various expectancy functions already given and where it is assumed that for now  $h = f(\theta)$  only, i.e., no radial taper.

Applying equations (5-31) and (5-32) to equation (5-33) and using the node pattern shown in Figure 5-3, the finite difference representation of equation (5-33) becomes



BASIC NODE PATTERN

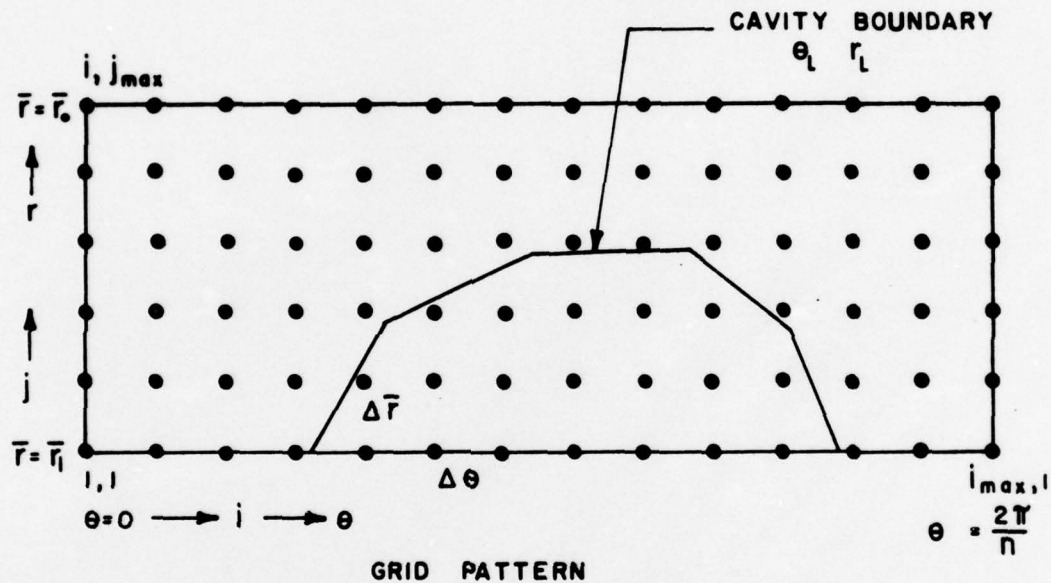


Figure 5-3. Numerical Representation

$$\begin{aligned}
 & p_{i,j} \left( \frac{-2A}{(\Delta\theta)^2} - \frac{-2C}{(\Delta r)^2} \right) + p_{i+1,j} \left( \frac{A}{(\Delta\theta)^2} + \frac{B}{2\Delta\theta} \right) \\
 & + p_{i-1,j} \left( \frac{A}{(\Delta\theta)^2} - \frac{B}{2\Delta\theta} \right) + p_{i,j+1} \left( \frac{C}{(\Delta r)^2} + \frac{D}{2\Delta r} \right) \\
 & + p_{i,j-1} \left( \frac{C}{(\Delta r)^2} - \frac{D}{2\Delta r} \right) = E
 \end{aligned} \tag{5-39}$$

Equation (5-15) for the asperity contact region can be represented in a similar manner, except that the equation is one dimensional.

#### Successive Over Relaxation

The method of solution used for equation (5-39) written for each node is that of successive over relaxation [43]. The steps in the iterative method are as follows:

- 1) Given guess values for  $p_{ij}$
- 2) Find a new  $p_{ij}$  using equation (5-39) and based on current values of  $p_{i-1,j}$   $p_{i+1,j}$   $p_{i,j-1}$   $p_{i,j+1}$ . Call this value  $p_{ij}$  new and the original value  $p_{ij}$  old.
- 3)  $p_{ij}_{SOR} = p_{ij}_{new} (\Omega) + p_{ij}_{old} (1-\Omega)$
- 4) Then  $p_{ij} = p_{ij}_{SOR}$
- 5) Go back to step 1 until all  $p_{ij}$  have been calculated.
- 6) After each time all  $p_{ij}$  have been evaluated, check for the largest error between  $p_{ij}_{SOR}$  and  $p_{ij}$  old. When error is sufficiently small, the solution has been obtained.

By experimentation it has been found that  $\Omega = 1.5$  gives the most rapid convergence to an error of 0.001 in about 20 iterations. The method is very fast numerically because only the coefficients of the terms of immediately adjacent nodes are stored and manipulated for each calculation.

### Boundary Conditions

The numerical representation for the inside and outside boundaries is simply a matter of setting the proper pressure nodes to the boundary values. Also, because of the periodicity of the solution  $p_{1,j} = p_{imax,j}$ . Representation of the cavity boundary conditions is much more difficult.

It was determined that the cavity shape must be accurately defined in this problem because of the coupling with the elastic deflection solution. That is, it was determined that small errors in locating the cavity could lead to convergence problems in the deflection solution later on. The common method [9], [44] to represent the cavity boundary is to force it to fall upon existing nodes. Accuracy can be obtained only by using a very fine grid spacing which is undesirable from a computational time standpoint. In the method selected for use, the cavity boundary position can float between more coarsely spaced nodes, so general equations must then be written to provide the cavity conditions which are dependent upon the particular position of the boundary between the nodes.

It is also a common procedure to force the conditions  $p = p_c$  at the cavity boundary and then adjust the cavity shape so that the derivatives, equations (5-18) and (5-20) are satisfied. In the present case it was determined (from some one dimensional experimentation) that it would be easier to solve the problem if the normal derivative conditions (5-18) and (5-20) were forced first as a part of the solution and then shift the cavity shape until the pressures on the cavity boundary became equal to the cavity pressure.

In order to follow this plan of attack, it is necessary to develop special equations for all nodes which are adjacent to a cavity boundary. Assuming that a cavity position is given, then equations (5-18) and (5-20) can be used to calculate the normal derivative required to satisfy these boundary conditions. Given this normal derivative, it is possible to express the Reynolds equation in a special form for a node adjacent to a boundary. These special equations take place of equation (5-39) where applicable.

There are three boundary intersection possibilities as shown in Figure 5-4. Consider first the case where the boundary cuts off two

adjacent nodes as shown by the  $r-\theta$  intersection of Figure 5-4. It is desired to write the Reynolds equation at P using information at Q and T and the information about the normal derivative. The method used is based on Ames [43].

A Taylors expansion about point P gives

$$p = (p)_P + \Delta\theta(p_\theta)_P + \Delta r(p_r)_P + \frac{(\Delta\theta)^2}{2} (p_{\theta\theta})_P + \Delta\theta\Delta r(p_{r\theta})_P + \frac{(\Delta r)^2}{2} (p_{rr})_P \quad (5-40)$$

$$p_\theta = (p_\theta)_P + \Delta\theta(p_{\theta\theta})_P + \Delta r(p_{r\theta})_P \quad (5-41)$$

$$p_r = (p_r)_P + \Delta\theta(p_{\theta r})_P + \Delta r(p_{rr})_P \quad (5-42)$$

Also,

$$\frac{\partial p}{\partial n} = \frac{1}{r} \frac{\partial p}{\partial \theta} \cos \alpha + \frac{\partial p}{\partial r} \sin \alpha \quad (5-43)$$

Now, it is assumed that the normal derivative at points R, N, and S are the same value for the sake of simplification. It is possible then to write the following expression for the normal derivative at these points. Using equations (5-41), (5-42), and (5-43) and with reference to Figure 5-4,

$$\left. \frac{\partial p}{\partial n} \right|_R = (p_\theta + \lambda_R k p_{\theta r}) \frac{\cos \alpha}{r} + (p_r + \lambda_r k p_{rr}) \sin \alpha \quad (5-44)$$

$$\left. \frac{\partial p}{\partial n} \right|_S = (p_\theta + \lambda_s h p_{\theta\theta}) \frac{\cos \alpha}{r} + (p_r + \lambda_s h p_{r\theta}) \sin \alpha \quad (5-45)$$

$$\begin{aligned} \left. \frac{\partial p}{\partial n} \right|_N &= (p_\theta + \frac{\lambda_r k}{r} \sin \alpha \cos \alpha p_{\theta\theta} + \lambda_s h r \sin \alpha \cos \alpha p_{r\theta}) \frac{\cos \alpha}{r} \\ &\quad + (p_r + \frac{\lambda_r k}{r} \sin \alpha \cos \alpha p_{\theta r} + \lambda_s h r \sin \alpha \cos \alpha p_{rr}) \sin \alpha \end{aligned} \quad (5-46)$$

Using equation (3-40), two additional expressions can be written for p at Q and T.

$$(p)_Q = (p)_P - hp_\theta + \frac{h^2}{2} p_{\theta\theta} \quad (5-47)$$

$$(p)_T = (p)_P - kp_r + \frac{k^2}{2} p_{rr} \quad (5-48)$$

Given  $\frac{\partial p}{\partial n}$  and  $(p)_Q$  and  $(p)_T$ , equations (5-44), (5-45), (5-46), (5-47) and (5-48) represent five equations in the five unknowns  $p_\theta$ ,  $p_{\theta\theta}$ ,  $p_r$ ,  $p_{rr}$ ,  $p_{r\theta}$  which can be solved simultaneously. In dimensionless form the solution is

$$\bar{p}_\theta = AA/DD \quad (5-49)$$

$$AA = \frac{\bar{r}^2 h \bar{k}}{2} \frac{\partial \bar{p}}{\partial \bar{n}} \tan^2 \alpha - (p)_P \left( \frac{h \bar{r}^2}{2} \tan^2 \alpha - \frac{\bar{k}^2}{2h} \right) \sin \alpha \\ + (p)_T \frac{h \bar{r}^2}{2} \tan^2 \alpha \sin \alpha - (p)_Q \frac{\bar{k}^2}{2h} \sin \alpha \quad (5-50)$$

$$DD = 1/2 \bar{k} (\bar{k} \sin \alpha + h \bar{r} \tan^2 \alpha \cos \alpha) \quad (5-51)$$

$$\bar{p}_r = BB/DD \quad (5-52)$$

$$BB = \frac{\bar{k}^2}{2} \frac{\partial \bar{p}}{\partial \bar{n}} - (p)_P \left( \frac{\bar{k}^2}{2h \bar{r}} \cos \alpha - \frac{h \bar{r}}{2} \tan^2 \alpha \cos \alpha \right) \\ - (p)_T \frac{h \bar{r}}{2} \tan^2 \alpha \cos \alpha + (p)_Q \frac{\bar{k}^2}{2h \bar{r}} \cos \alpha \quad (5-53)$$

$$\bar{p}_{\theta\theta} = \bar{p}_{rr} \bar{r}^2 \tan^2 \alpha \quad (5-54)$$

$$\bar{p}_{rr} = CC/DD \quad (5-55)$$

$$CC = \frac{\partial \bar{p}}{\partial \bar{n}} \bar{k} - (p)_P \left( \sin \alpha + \frac{\bar{k}}{rh} \cos \alpha \right) + (p)_T \sin \alpha + (p)_Q \frac{\bar{k}}{rh} \cos \alpha \quad (5-56)$$

$$\bar{p}_{r\theta} = - \bar{p}_{rr} \bar{r} \tan \alpha \quad (5-57)$$

The above expressions can be substituted into equation (5-33). The result is that  $p_{ij}$  ( $(p)_P$  in the above equation) can be expressed in terms of the pressure at the adjacent nodes (T and Q) and the normal derivative. Thus a complete set of equations can be written for all nodes adjacent to a boundary. These are used in place of equation (5-39) where applicable.

The special equations for the two other types of intersection can be derived in a similar way. With reference to the  $\theta$  only intersection of Figure 5-4, the following expressions can be derived for the various partial derivatives:

$$\bar{p}_\theta = AA/DD \quad (5-58)$$

$$AA = \frac{h^2 r}{2} \frac{\partial p}{\partial n} - (p)_P \left[ \frac{\lambda_s h}{2} \left( \frac{h^2 r^2}{k^2} - 1 \right) \sin \alpha \tan 2\alpha - \lambda_s h \cos \alpha \right]$$

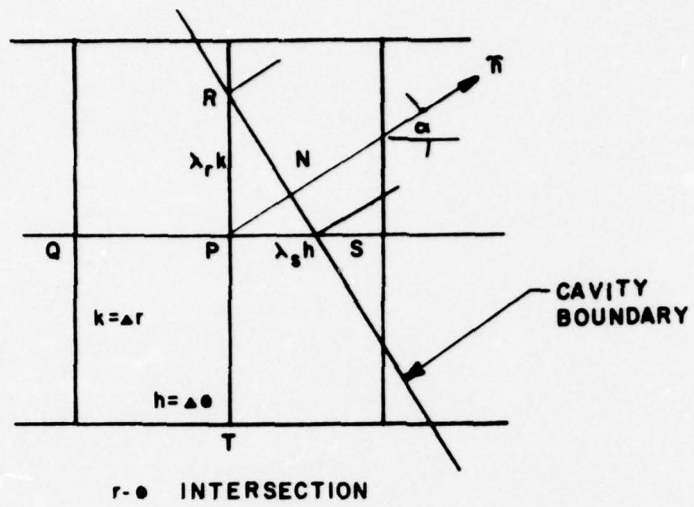
$$+ (p)_Q \lambda_s h (-\cos \alpha - 1/2 \sin \alpha \tan 2\alpha)$$

$$+ (p)_O \frac{h^2 r}{4k} \left( \frac{\lambda_s h r}{k} \tan 2\alpha - 1 \right) \sin \alpha + (p)_T \frac{h^2 r}{4k} \left( \frac{\lambda_s h r}{k} \tan 2\alpha - 1 \right) \sin \alpha \quad (5-59)$$

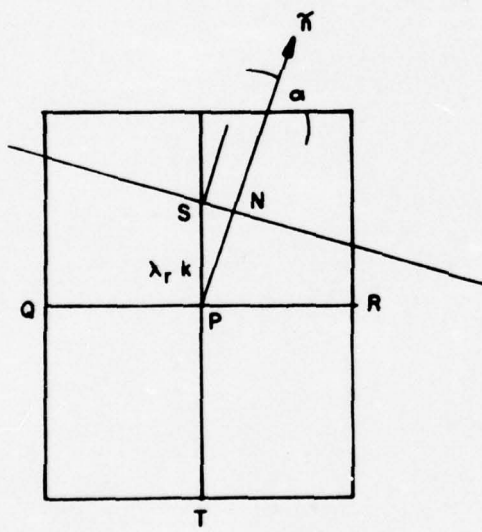
$$DD = h^2 [ (\lambda_s + 1/2) \cos \alpha + 1/2 \lambda_s \sin \alpha \tan 2\alpha ] \quad (5-60)$$

$$\bar{p}_r = \frac{(p)_O}{2k} - \frac{(p)_T}{2k} \quad (5-61)$$

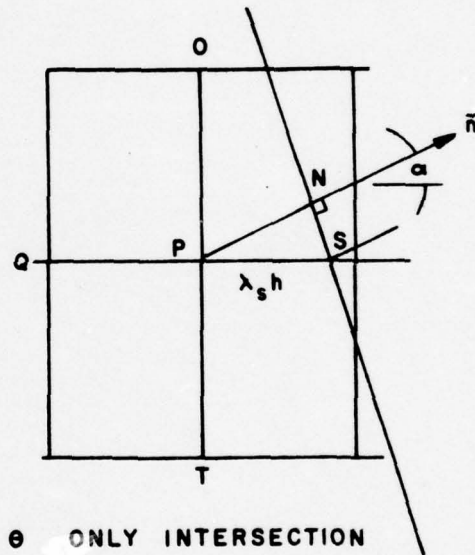
$$\bar{p}_{\theta\theta} = BB/DD \quad (5-62)$$



r-e INTERSECTION



r ONLY INTERSECTION



e ONLY INTERSECTION

Figure 5-4. Boundary Nodes

$$\begin{aligned}
 BB = & h \bar{r} \frac{\partial p}{\partial n} - (p)_P (\cos \alpha + \frac{\lambda_s h^2 r^2}{k^2} \sin \alpha \tan 2\alpha) \\
 & + (p)_Q \cos \alpha + (p)_O \frac{h \bar{r}}{2k} (\lambda_s \frac{h \bar{r}}{k} \tan 2\alpha - 1) \sin \alpha \\
 & + (p)_T \frac{h \bar{r}}{2k} (\lambda_s \frac{h \bar{r}}{k} \tan 2\alpha - 1) \sin \alpha
 \end{aligned} \tag{5-63}$$

$$\bar{p}_{rr} = \frac{-2(p)_P}{\bar{k}^2} + \frac{(p)_T}{\bar{k}^2} + \frac{(p)_O}{\bar{k}^2} \tag{5-64}$$

$$\bar{p}_{r\theta} = CC/DD \tag{5-65}$$

$$\begin{aligned}
 CC = & \frac{h}{2} \frac{\partial \bar{p}}{\partial n} \tan 2\alpha - (p)_P \left[ \frac{1}{2\bar{r}} - \frac{\bar{r}h^2}{\bar{k}^2} (\lambda_s + 1/2) \right] \cos \alpha \tan 2\alpha \\
 & + (p)_Q \frac{1}{2\bar{r}} \tan 2\alpha \cos \alpha . \\
 & + (p)_O \frac{h}{2\bar{k}} (-1/2 \sin \alpha - \frac{\bar{r}h}{\bar{k}} (\lambda_s + 1/2) \cos \alpha) \tan 2\alpha \\
 & + (p)_T \frac{h}{2\bar{k}} (1/2 \sin \alpha - \frac{\bar{r}h}{\bar{k}} (\lambda_s + 1/2) \cos \alpha) \tan 2\alpha
 \end{aligned} \tag{5-66}$$

In a similar manner the expressions for the  $r$  only intersection of Figure 5-4 can be derived.

$$\bar{p}_\theta = \frac{(p)_R - (p)_Q}{2h} \tag{5-67}$$

$$\bar{p}_r = AA/DD \tag{5-68}$$

$$AA = \frac{\bar{k}^2}{2} \frac{\partial \bar{p}}{\partial \bar{n}} - (p)_P \lambda_R \bar{k} \left[ -\sin\alpha + 1/2(1 - \frac{\bar{k}^2}{\bar{r}^2 h^2}) \cos\alpha \tan 2\alpha \right]$$

$$+ (p)_T \bar{k} \lambda_R (1/2 \cos\alpha \tan 2\alpha - \sin\alpha)$$

$$+ (p)_R \frac{\bar{k}^2}{4\bar{r}h} (-1 - \frac{\lambda_R \bar{k}}{\bar{r}h} \tan 2\alpha) \cos\alpha$$

$$+ (p)_Q \frac{\bar{k}^2}{4\bar{r}h} (1 - \frac{\lambda_R \bar{k}}{\bar{r}h} \tan 2\alpha) \cos\alpha \quad (5-69)$$

$$DD = \bar{k}^2 \left[ (\lambda_R + 1/2) \sin\alpha - \frac{\lambda_R}{2} \cos\alpha \tan 2\alpha \right] \quad (5-70)$$

$$\bar{p}_{\theta\theta} = \frac{(p)_Q + (p)_R - 2(p)_P}{h^2} \quad (5-71)$$

$$\bar{p}_{rr} = BB/DD \quad (5-72)$$

$$BB = \bar{k} \frac{\partial \bar{p}}{\partial \bar{n}} - (p)_P (\sin\alpha - \frac{\lambda_R \bar{k}^2}{h^2 \bar{r}^2} \cos\alpha \tan 2\alpha)$$

$$+ (p)_T \sin\alpha + (p)_R \frac{\bar{k}}{2\bar{r}h} (-1 - \frac{\lambda_R \bar{k}}{\bar{r}h} \tan 2\alpha) \cos\alpha$$

$$+ (p)_Q \frac{\bar{k}}{2\bar{r}h} (1 - \frac{\lambda_R \bar{k}}{\bar{r}h} \tan 2\alpha) \cos\alpha \quad (5-73)$$

$$\bar{p}_{r\theta} = CC/DD \quad (5-74)$$

$$\begin{aligned}
 CC = & -\frac{\bar{r}\bar{k}}{2} \frac{\partial \bar{p}}{\partial \bar{n}} \tan 2\alpha - (p)_P \left[ -\frac{\bar{r}}{2} + \frac{\bar{k}^2}{\bar{r}h^2} (\lambda_r + 1/2) \right] \sin \alpha \tan 2\alpha \\
 & + (p)_T \left( -\frac{\bar{r}}{2} \sin \alpha \tan 2\alpha \right) \\
 & + (p)_R \frac{\bar{k}}{2h} \left[ 1/2 \cos \alpha + \frac{\bar{k}}{\bar{r}h} (\lambda_R + 1/2) \sin \alpha \right] \tan 2\alpha \\
 & + (p)_Q \frac{\bar{k}}{2h} \left[ -1/2 \cos \alpha + \frac{\bar{k}}{\bar{r}h} (\lambda_R + 1/2) \sin \alpha \right] \tan 2\alpha \quad (5-75)
 \end{aligned}$$

#### Cavity Shape Convergence

Given a cavity shape, all of the finite difference equations can be set up and solved for as described. Then, using equation (5-40) and numerical values of the derivatives, the pressure at any point on the boundary can be determined. The cavity shape must then be adjusted so that  $p = p_C$  at the cavity boundary.

Many different methods of shifting and adjusting the cavity were tried. The basic objective is to converge on the correct shape with the least number of iterative pressure solutions. The best of the methods of convergence will be described first. With reference to Figure 5-5, the method follows.

- 1) Represent the cavity by any number of  $r_\ell, \theta_\ell$  points. This is a guess shape.
- 2) Find all of special nodes which are adjacent to the cavity boundary. Find all of the normal intersection points and  $\lambda_R$  and  $\lambda_s$  for use in equations (5-49) through (5-75). Set up all of the boundary node equations. Set up all of the other node equations using equation (5-39).

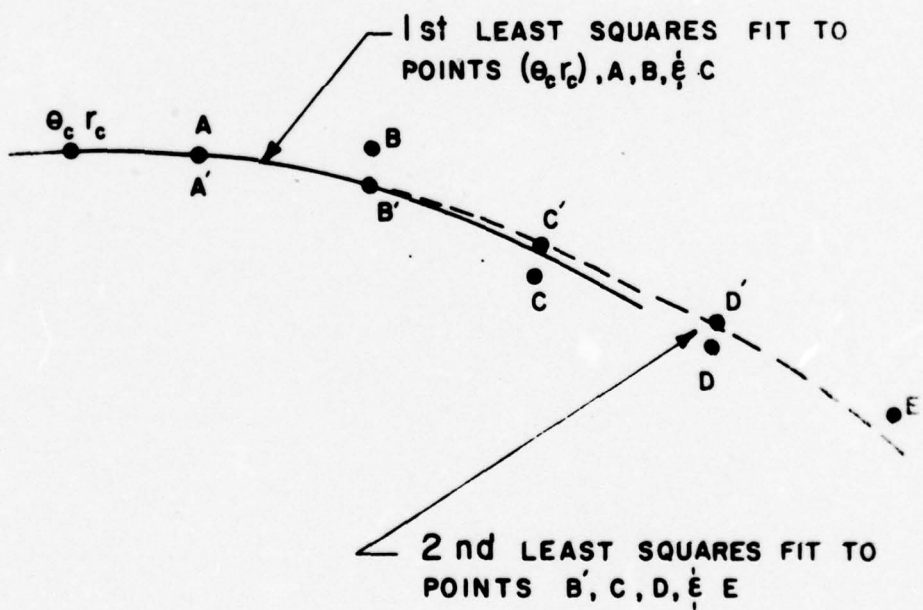
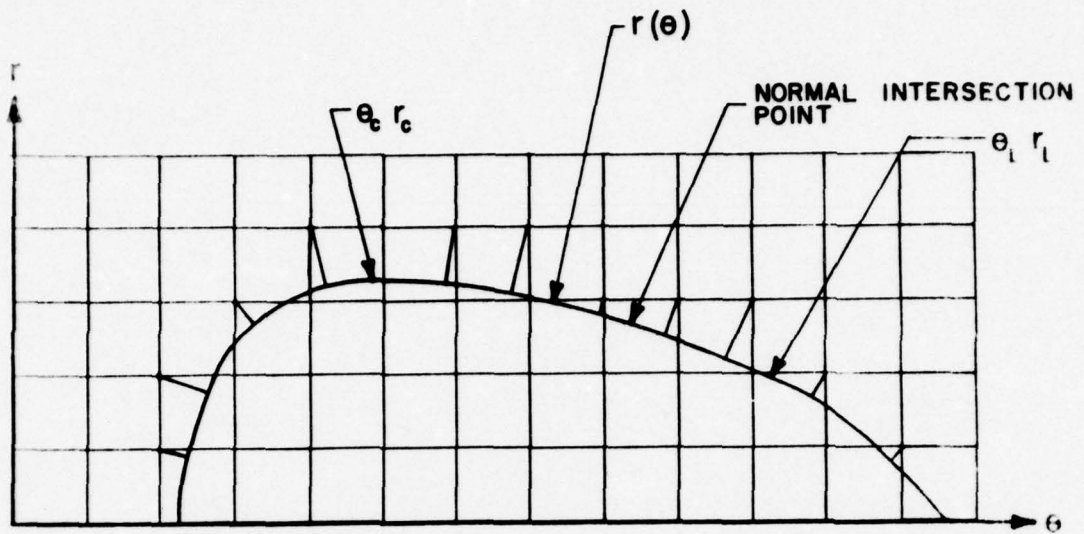


Figure 5-5. Cavity Representation and Smoothing

- 3) Solve for the complete pressure field by using the above equations and successive over relaxation.
- 4) Find the pressure at all of the normal intersection points shown in Figure 5-5 by using equation 5-40).
- 5) Find the normal derivative at each of the normal intersection points. These are zero for the left side and given by equation (5-20) for the right hand side.

$$\text{If } \left. \frac{\partial p}{\partial n} \right|_{\ell} > -0.2 \quad \text{let } \left. \frac{\partial p}{\partial n} \right|_{\ell} = -0.2$$

(This was determined by trial and error.)

- 6) Find the amount of move in the normal direction required to make the boundary pressure equal to zero at each point  $\ell$ .

$$\Delta n = \frac{p_b - p_c}{\frac{\partial p}{\partial n}} \quad (5-76)$$

Given  $\Delta n$ , then

$$\theta_{\ell} = \frac{1}{r} \Delta n \cos \alpha + \theta_{\ell} \text{ old} \quad (5-77)$$

$$r_{\ell} = \Delta n \sin \alpha + r_{\ell} \text{ old} \quad (5-78)$$

Now there is a new set of  $r_{\ell} \theta_{\ell}$  points.

- 7) Find the maximum value of  $r_{\ell}$ . Then average the maximum point and its two adjacent points. Call these  $\theta_c r_c$ .
- 8) Make  $\frac{dr}{d\theta} = 0$  at  $\theta_c r_c$  and starting at this point use a least squares fit based on a second degree polynomial. Fit two or more new points each time making the point and slopes match each time. Use only one or two new values from each fit. Do not allow the curve to become convex-in. A proper cavity shape must be convex-out. Continue this until all points on the right hand side and all on the left hand side have been recalculated. This smooths the curve. The method is shown in Figure 5-5. The primes are the new smoothed points.

- 9) Go back to 1) with the adjusted curve and repeat until the pressure at the boundary matches the cavity pressure sufficiently close.

The above method was arrived at after trying many other different methods. Proper and rapid convergence is difficult to achieve for the following reasons.

- 1) The boundary is highly interactive. That is, moving only one point on the boundary changes the pressure at all other points on the boundary--sometimes radically.
- 2) The boundary shape tends to become irregular and thus defeats convergence. Sudden changes in the angle  $\alpha$ , which are natural in a piecewise linear representation of the cavity boundary, causes non-convergence. Thus, the smoothing feature was added.

Convergence is slow with the present method, and further improvements will be necessary before the two dimensional solution can be coupled with the equilibrium time dependent solution. Several alternative approaches to the solution are being investigated.

For future reference, some of the other less successful methods tried for boundary convergence included the following.

- 1) Representation of the cavity by a small number of points and moving only one point each time according to a Newton method. This was defeated because of the high degree of interaction.
- 2) Finding  $\frac{\partial P_b}{\partial n}$  at each point by moving the entire upstream boundary and then moving accordingly. Then the entire downstream boundary was moved in the same way.
- 3) A linear method of smoothing that simply rounded the corners and did not allow any concave out portion of the curve. This did not do a good job of smoothing.
- 4) Higher degree polynomial fits. Several variations were tried. Invariably, a concave outward portion of the curve would result.

### Numerical Solution to Findlay Problem

To verify the two dimensional computer program, a comparison was made with the results of Findlay [9]. Findlay presents the cavity shape, leakage, and load support for the following non-asperity case (Findlay's parameters):

$$\Lambda = \frac{6\eta\omega}{p_{ref}} \left( \frac{r_o}{h_i} \right)^2 = 2000$$

$$\epsilon = h_{\text{amplitude}}/h_{\text{mean}} = 0.1$$

$$p_o = \frac{p_o}{p_{ref}} = 2$$

$$p_i = \frac{p_i}{p_{ref}} = 1$$

$$p_c = \frac{p_c}{p_{ref}} = 1$$

(5-79)

Findlay's numerical solution values (interpolated from the graphs) are:

$$c_L = \frac{w_{\text{Findlay}}}{p_{ref} r_o} = 1.76$$

$$q_r = \frac{12\eta Q}{h_i^3 p_{ref}} = 34$$

(5-80)

The Findlay solution and the solution herein can be compared by assuming certain arbitrary constants. Let

$$h_i = 20 \mu \text{ in} \quad - \text{ mean film thickness}$$

$$p_{ref} = 14.7 \text{ psia}$$

$$c = 40 \mu \text{ in}$$

(5-81)

Then, from the definition of  $\Lambda$

$$\eta \omega r_o^2 = 1.96 \cdot 10^{-6} \text{ lb} \quad (5-82)$$

The pressures used in the present solution are gauge pressures, so

$$p_o^{\text{Findlay}} = 2 \times 14.7 \text{ psia}$$

$$p_i^{\text{Findlay}} = 14.7 \text{ psia}$$

$$p_o = 14.7$$

$$p_i = 0 \quad (5-83)$$

and from equation (5-81) and (5-82)

$$\bar{p}_o = 0.012$$

$$\bar{p}_i = 0.0$$

$$\bar{p}_c = 0.0 \quad (5-84)$$

The waviness equivalent to the Findlay case is

$$h = 0.5 + 0.05 \cos 2\theta$$

Also,

$$\bar{r}_o = 1$$

$$\bar{r}_i = 0.8 \quad (5-86)$$

Findlay's load support is based on absolute pressure. Load support  $w$  used herein is based on gauge pressure. The necessary conversion is

$$C_L - \pi(1 - r_i^2) = \frac{r_o^2 \eta \omega \bar{w}}{p_{\text{ref}}} \quad (5-87)$$

For leakage, the necessary conversion is

$$q_r = \frac{12\eta r_o^2 w c \bar{Q}}{h_i^3 p_{ref}} \quad (5-88)$$

Using parameter values (5-84) (5-85) and (5-86), a two dimensional solution was carried out as described by the methods in this chapter. The pressure obtained is shown in Table 5-1. The region of zero pressure represents the cavity. Pressures near the cavity may not be small because the solution does not force the cavity boundary to fall on the node itself.

Several different comparisons have been made between the Findlay solutions and the solutions herein. These are shown in Table 5-2. First using equations (5-87) and (5-88), total leakage and load support are calculated. Agreement is very good. Using the present solution method of solving for the cavity shape by adjusting to get the pressure at the boundary to equal the cavity pressure, a comparison of boundary pressure errors was made between the Findlay cavity shape and the cavity shape from the solution herein. These comparisons are shown in Table 5-2. Not only is the maximum error smaller for the present solution, but the average absolute error is also smaller. This result suggests that the present solution cavity shape may represent an improvement over the Findlay solution. The cavity shapes are shown compared in Figure 5-6. Agreement is very good.

In conclusion, the comparison to the Findlay result has verified the computer solution developed in this chapter. The major objective for the near future is to concentrate efforts on speeding up convergence to the cavity shape as discussed previously.

Pressure Distribution

TABLE 5-2  
 Comparison of Results of Solution herein to  
 Findlay [9] Solution

	<u>Findlay</u>	<u>Present Solution</u>
$\bar{w}$	0.0076	0.0077
$\bar{\Omega}$	0.0042	0.0038
$ p_b _{max}$	0.50 $\bar{p}_o$	0.27 $\bar{p}_o$
$ p_b _{avg}$	0.12 $\bar{p}_o$	0.05 $\bar{p}_o$

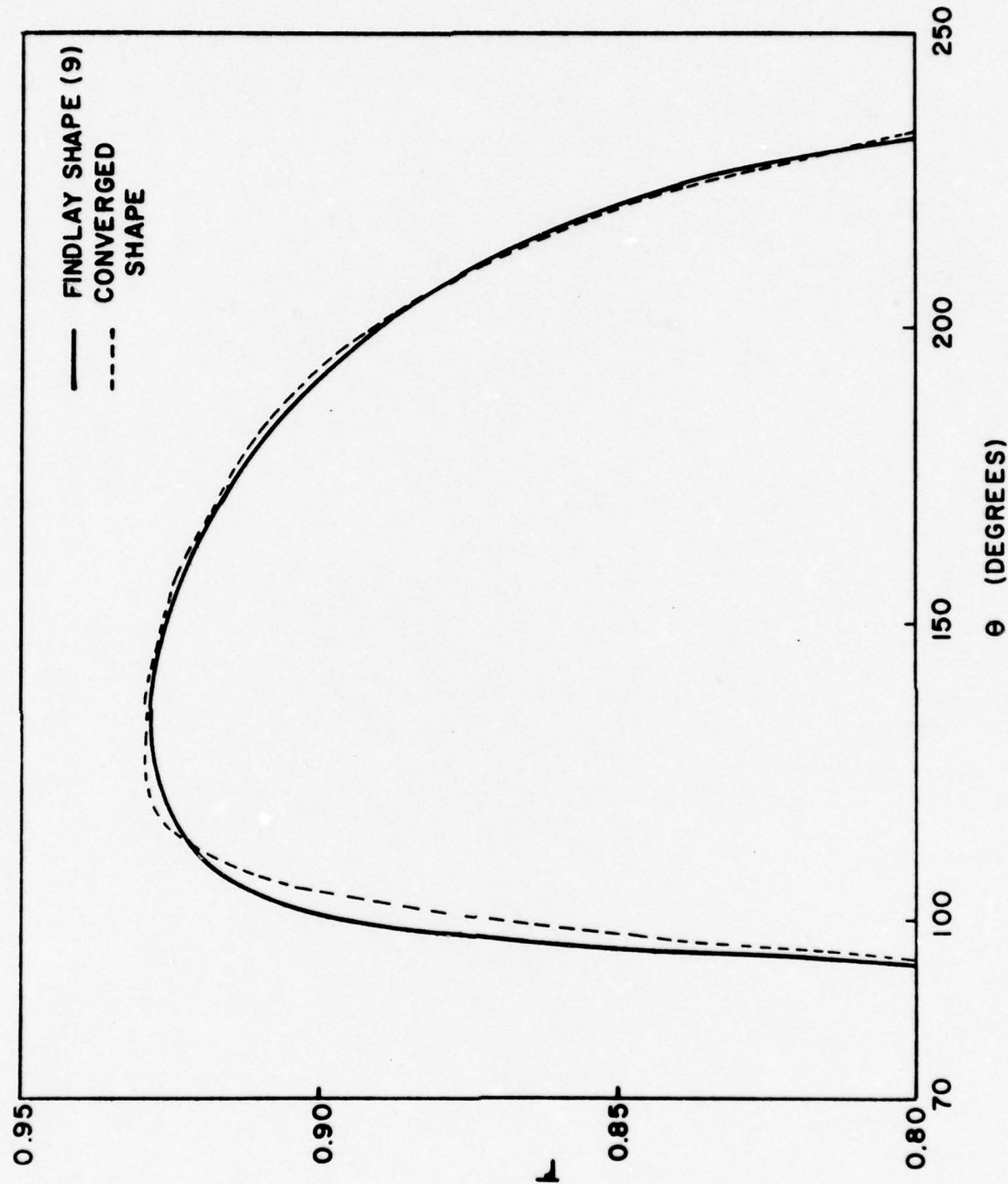


Figure 5-6. Comparison to Findlay Cavity Shape

## CHAPTER 6

### PRELIMINARY DESIGN OF AN EXPERIMENTAL TEST RIG

As a part of the present research program, some preliminary work was carried out on the design of an experimental test rig. This work was submitted as a proposal to the Department of the Navy, Naval Ship Engineering Center.

The primary purpose of the proposed test rig is to provide experimental results to verify some of the work herein. Thus, the test rig incorporates the moving wave principle discussed in Chapter 4 so that the continuous effects of waviness can be evaluated. A complete description of the test rig follows.

#### Proposed Test Rig Capabilities

Based on experience using Crane Packing Company test rigs and the types of testing desired, the basic test capabilities for the proposed test rig have been selected as follows:

- 1) 3-5/8" nominal seal shaft size. Somewhat larger and smaller seals can also be tested.
- 2) 4" nominal mean face diameter.
- 3) 500 - 4000 RPM variable speed drive. This gives a 9 - 70 ft/sec sliding speed range.
- 4) 0 - 600 psig continuous pressure capability.
- 5) 5 Hp drive motor.
- 6) Seawater capability. The entire system will be corrosion resistant.

Other features of the machine include:

- 1) Rotating seat (mating ring) - non-rotating and floating primary ring configuration.
- 2) Zero pressure moment design. This will eliminate problems associated with uncontrolled convergence and divergence due to pressure changes.

- 3) Overbalanced seal design. Because the seal is hydrodynamic, sealing could be lost due to full pressurization at the faces if the seal were balanced. The test rig can also be used for standard balanced seal designs.
- 4) Temperature control. The seal fluid temperature will be controlled using a cooling water system.

Systems will be provided to measure or control the following:

- 1) Seal friction torque
- 2) Sealed pressure
- 3) Sealed fluid temperature
- 4) Speed
- 5) Leakage

#### Unique Features

The test seal arrangement proposed has the capability of causing waviness of an arbitrary amount at the seal faces. This will be accomplished by distorting the seal primary ring as explained later. In addition, a mechanism is provided to rotate the waviness pattern relative to the carbon or primary ring face. In this way, the waviness pattern can be maintained without wearing away. This behavior has been described in detail in Chapter 4.

The arrangement described allows waviness to be controlled. The amount of waviness can be controlled by increasing or decreasing the distortion in the ring as described later. The shape of the waviness can also be controlled. This is done by using different waviness controlling profiles. The net amount of waviness at the faces can be calculated by subtracting the amount of waviness (flattening) caused by elastic deflection of the seal ring. Thus, waviness can be completely controlled.

Waviness has been lapped into seal faces previously. As far as is known, this has been done for a water seal in only one case [40]. This waviness was not controllable and would wear away with time due to the rubbing contact normally encountered in water seals. Face waviness has also been lapped into an oil seal [41]. As far as is known, controlled waviness as described above has never been used as a test parameter in any seal test. Hydrodynamic lubrication due to waviness has not been

studied in contacting water seals. Thus, the unique feature of the proposed test rig is that it will be possible to study the influence of waviness and hydrodynamic lubrication on friction, leakage, and wear.

#### Philosophy of Test Rig

The general philosophy behind the design of the proposed test rig is somewhat different than that used in many research test rigs [2, 10, 12, 13, 34]. Because of the difficulty encountered by previous researchers in measuring pressure and in controlling and/or measuring film thicknesses, and because of the need to make useful conclusions about basic seal design and to provide new directions for improved seal design, it was decided that the important seal performance parameters of friction, leakage, and wear should be studied as functions of controllable parameters such as waviness, radial taper (a controlled variable radial taper could be added to the proposed test setup in a manner similar to waviness), pressure, speed, and geometric face modifications.

In view of this decision, the test rig must be capable of simulating seals in actual application. Thus, pressures and speeds were selected to cover a wide range of application. Seal geometry and materials were selected to be similar to those in actual applications.

#### Research That Can be Conducted Using the Test Rig

The purposes for the proposed test rig are 1) to experimentally verify the hydrodynamic seal model described in Chapters 2, 3, and 5, 2) to conduct basic research on the effect of controllable waviness on friction, lubrication, and wear, and 3) to have available a test rig which can be easily adapted to study other aspects of mechanical face sealing.

More specifically, the following types of investigations using the proposed test rig are either planned or possible.

- 1) Using the controlled waviness feature, the hydrodynamic seal model developed under present research will be experimentally verified. There are several aspects of the present model that have never been experimentally verified. Primarily, the mixed lubrication model of Christensen [36] could be verified at least on the basis of overall performance. It will also be possible to obtain accurate values of certain empirical constants required

for the model. It will be possible to verify the effect of waviness magnitude on friction and leakage as predicted by the model.

2) The effect of waviness on seal leakage, friction, and wear will be determined experimentally. The effects of both the magnitude and the shape of the waviness curve on leakage and wear can be studied.

3) It will be possible to show to what extent waviness can be used to reduce the wear and friction and increase life in actual seal applications.

4) It will be possible to determine the effect of seal ring stiffness on waviness and its effects on seal behavior.

5) It will be possible to simulate a cavitation erosion situation. Basic information as to the conditions under which cavitation damage becomes significant could be examined. The relationships between gap size, speed, material, and erosion could be obtained.

6) The effects of other face features on seal performance could be evaluated. For example, Mayer [3] has shown that cutouts in the hard face reduce friction. Crane Packing Company has shown that cutouts in the soft face may also reduce friction. The exact mechanisms involved are not known. Such features could be tested and studied in a controlled environment using the proposed test rig.

7) Material test comparisons could be made. The parts for the proposed test rig are small, and rings from different materials can be fabricated economically so that many different tests under realistic seal operating conditions can be run.

#### Description of Test Rig

The proposed test rig is shown in Figure 6-1. The basic configuration was selected based on requirements outlined previously as well as on the following criteria.

1) The seal axis is to be horizontal to simulate many common seal installations.

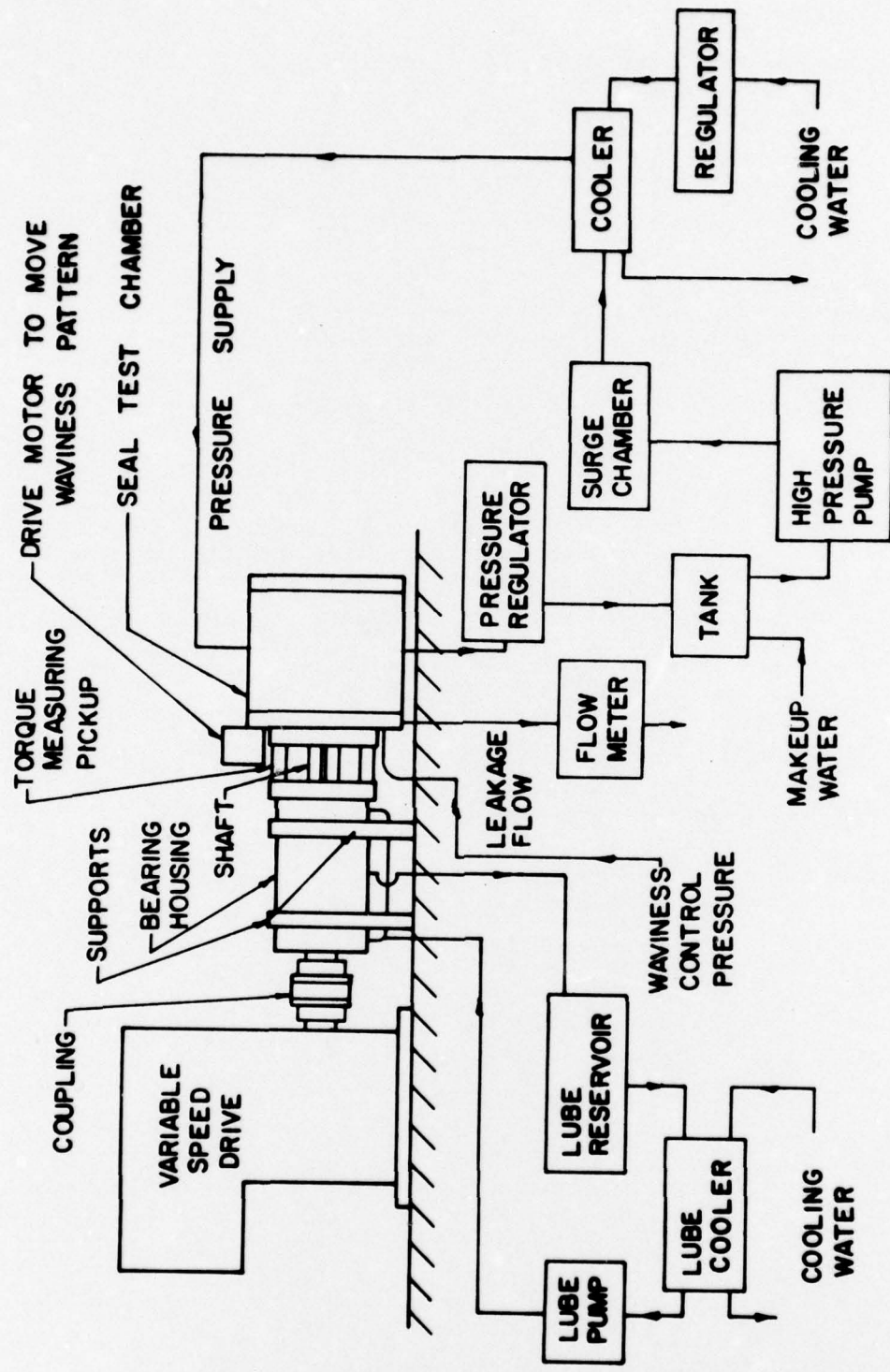


Figure 6-1. Controlled Waviness Mechanical Face Seal Test Rig

- 2) A single seal only is to be tested so that friction effects can be measured independent of a second seal and to simplify the design.
- 3) Friction torque at the seal faces only is to be measured accurately.

A belt type variable speed drive will be used to obtain a range of operating speeds. The seal mating ring is fastened to a rotating stainless shaft coupled to the variable speed drive by a shaft coupling. The shaft will be ground such that the right hand end is perpendicular to the bearing axis to minimize rotor wobble. The shaft is mounted in precision ABEC-7 bearings to minimize axial movement. These precautions will be taken to minimize the effects of wobble and axial motion on hydrodynamic lubrication.

Figure 6-1 also shows the auxiliary equipment. A lubrication system with a cooler is required. There is a large thrust load on the bearings due to the unbalanced pressure on the rotor. This necessitates large bearings and the cooling system. A controllable water pressure must be supplied to the seal test chamber. This is done using a small piston pump with a surge suppressor and reservoir. Cooling is provided by a heat exchanger using tap water. The piston pump also circulates the cooling water through the seal test chamber. A temperature regulator is included in the system.

The seal housing and internal components will be designed to resist a salt water or other corrosive environment. The sealed fluid cooling loop will also be designed for a corrosive fluid environment.

A controllable pressure must also be supplied to the waviness control cylinder so that the amount of waviness can be controlled independently of the seal test pressure. This pressure will be supplied by an air over water double cylinder arrangement (not shown). The waviness control water pressure will be regulated by an air pressure regulator on the air side of the double cylinder.

The torque transducer is shown just to the left of the test chamber. The configuration of this device is such that the large axial load due to the unbalanced pressure on the rotor will produce a uniform axial strain that will be cancelled whereas the torque will produce a strain signal due

to bending of the members. The torque transducer will provide an accurate measurement of the friction at the seal faces without including the friction effects of belts or bearings.

Figure 6-2 shows a section view of the seal test chamber. The test chamber inside dimensions are approximately 6" in diameter by 7" long. The vessel is designed for rapid assembly and disassembly. All sealing is accomplished using O-rings. After the housing has been disassembled and the rotating seat has been removed, the seal primary ring slips off of the waviness control cylinder.

The seal primary ring is designed such that additional waviness will not be introduced by drive forces. The drive lugs are positioned so that drive forces are in the plane of the centroid of the cross section of the seal. The primary ring is designed to have zero rotation due to pressure changes (so is the seat). This will eliminate problems associated with having an uncontrollable radial taper. There will, of course, be some convergence caused by axial temperature gradients, but this will be minimized by exposing the maximum possible surface area of the rings for heat transfer purposes.

The rotating seat is mounted on a rotor which has been designed to facilitate accurate grinding to minimize wobble of the rotor and seat.

The secondary O-ring seal of the primary ring is shown to the left end of the ring. The two O-ring seals toward the center of the primary ring are actually placed in wavy grooves as shown by Figure 6-3. The independent pressure supplied for the chamber formed by the wavy O-ring seals and the primary ring itself will produce a waviness at the face of the seal. The exact shape of the waviness at the face (sinusoidal or some other shape) is determined by the wavy pattern of the O-ring grooves in the waviness control cylinder. The magnitude of the waviness is dependent on the waviness control pressure. These relationships are derived from Reference [22]. Three high spots are planned initially. This number was chosen because three waves is the minimum number which provides a stable support arrangement. A larger number of waves is more difficult to control and manufacture for this small size seal.

The waviness pattern of the primary ring is moved relative to the primary ring by rotating the primary ring slowly on the waviness control

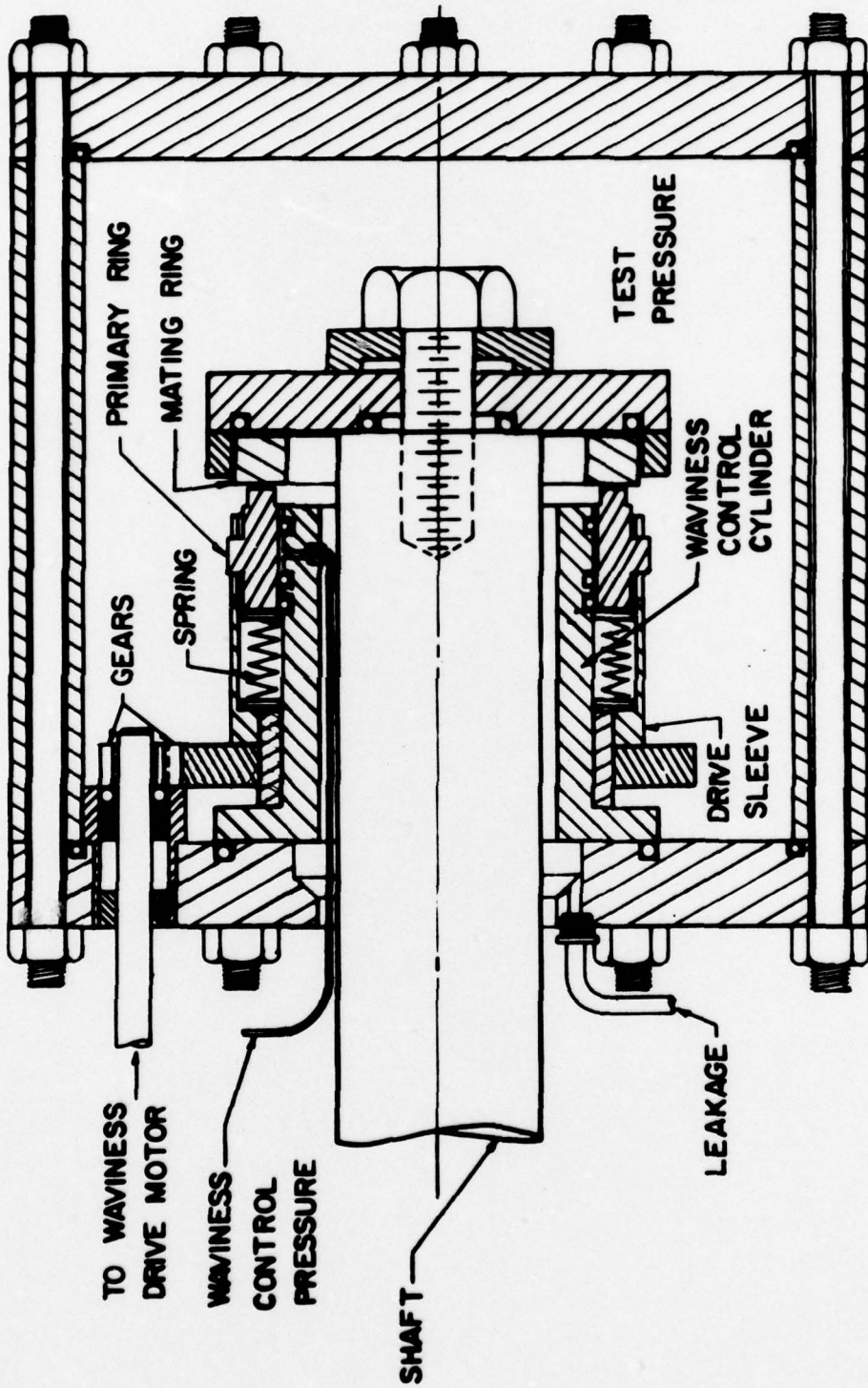


Figure 6-2. Test Chamber and Seal

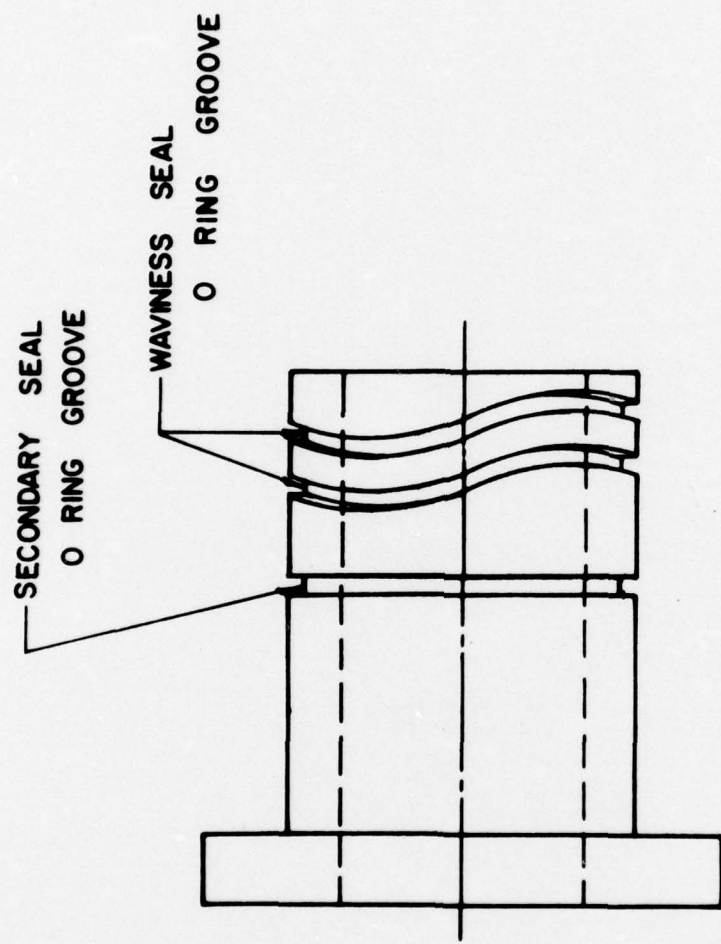


Figure 6-3. Waviness Control Cylinder

cylinder. The primary ring is driven (rotationally retained) by a drive sleeve with slots to accommodate the drive lugs on the ring. The drive sleeve is connected to a drive gear which is driven by a pinion whose shaft is extended through the seal housing and driven by a small low speed drive motor. Anticipated speeds are from one revolution per hour to one revolution every 10 to 20 hours.

This waviness arrangement causes the high spots on the seal face to continually move around the seal so that wear is uniformly distributed and so that the waviness profile is always maintained.

## CHAPTER 7

### CONCLUSIONS

Many conclusions have been made throughout this report. These conclusions are summarized and some of the implications are drawn here.

#### One Dimensional Equilibrium Model

Within the limitations of the validity of the model as discussed earlier, the following conclusions can be made concerning the effects of initial (unworn) waviness on behavior in a water seal of the type under study.

- 1) Waviness will cause some amount of hydrodynamic pressure and load support. In probably most cases, the load support will not be sufficient to cause complete liftoff. The balance of the load is supported by asperity contact. The amount can be determined for any particular seal by using the one dimensional model.
- 2) The effect of the hydrodynamic load support is to reduce both the wear rate and friction at the face. Thus any modification which causes the hydrodynamic load support to increase will reduce wear rate and friction at least initially (although leakage may be higher).
- 3) The maximum gap or  $h_{max} - 1$  is actually quite small for most cases examined. Although calculations show that static leakage across this gap would be small, hydrodynamic effects are expected to cause a much greater leakage. Thus it cannot be determined yet as to what extent hydrodynamic support can be used without causing excessive leakage.
- 4) Even though the results are based on an ideal waveform, it is expected that the results apply to face seals in general because there is always some initial waviness in a face seal [22] and there will be high regions and low regions although they will not be uniform in practice. However, the amount of waviness present may in many cases be too small for a given ring stiffness to cause a significant hydrodynamic effect.

This can be determined for any particular case. For the case under study, it appears to be marginal whether average initial waviness found in this seal would be large enough to cause a significant hydrodynamic load support. However, some of the extreme values found in practice could cause significant support, particularly if the surface roughness were lower than that used in the study.

- 5) There is an optimum amount of initial waviness that leads to a maximum hydrodynamic load support. As the harmonic number increases, the optimum initial waviness decreases and the percent load support increases.
- 6) Surface roughness is an extremely important parameter. A seal with a low surface roughness may have many times the hydrodynamic load support as a seal with a larger surface roughness. Thus, if an abrasive environment is not present, seal materials should be selected which give the least natural surface roughness.
- 7) Ring stiffness and initial waviness trade off with each other. That is, hydrodynamic load support can be obtained with a lower initial waviness if the ring is stiff than if not.
- 8) There appears to be an optimum face width which leads to a maximum load support. This is based on having a constant load per unit area on the face.
- 9) As the harmonic number increases, the amount of waviness required to cause  $h_{\max} > 1$  (initial liftoff condition) becomes less. This is caused by the relative increase in stiffness with increasing harmonic number.

#### One Dimensional Time Dependent Model

The time dependent model provides an indication of how hydrodynamic behavior acts beyond the initial equilibrium condition as the face shape is modified by the effects of wear.

- 1) In the studies made so far, the effect of time and wear is to reduce the % hydrodynamic load support for a seal running in the steady state condition. The implication is that for steady

state seals, the hydrodynamic effect would be of no practical consequence after a period of operation. This period may be from several to several hundred hours depending on various parameters.

- 2) Drive force caused friction feedback waviness does not appear to prolong the period of hydrodynamic load support.
- 3) Thermal expansion effects do not appear to prolong or modify the gradual decay of hydrodynamic load support. This is not to say that an unexpected behavior might not occur in extreme cases such as for a very high speed.
- 4) The effect of a time dependent load or pressure on the seal may cause the average % hydrodynamic load support to increase in some cases. In other cases the support decreases. These effects will require further study before any definite conclusions can be made.
- 5) A complete comparison of the theoretical results is not possible because experimental data are not available. However, the theoretical results have been qualitatively compared to those of Snapp and Sasdelli [40] where a given waviness was lapped into one of the seal rings. Results from the initial waviness equilibrium model show that some small amount of hydrodynamic load support would be caused by the waviness. However, the amount lapped in appears to be far from optimum. Good agreement is found between experimental and theoretical leakage at 50% test pressure. These results support the validity of the model, but a more thorough comparison will require the use of the two dimensional model.

#### Improved Seal Performance

- 1) It has been shown that if a wave is made to travel or move relative to the ring, the wave shape can be sustained over an indefinite period of time. This offers the possibility of designing a hydrodynamic contacting face seal. The seal would have a greatly reduced wear and friction.

- 2) There exist optimum profile shapes from the standpoint of load support. With such shapes and the use of the traveling wave, 70% or greater hydrodynamic load support can be sustained. This would reduce wear by a factor of three or more.

#### Two Dimensional Model

- 1) The basic two dimensional model has been verified by comparing with previous results [9]. More work remains to speed up convergence of the cavity boundary. Other more appropriate methods of solution for the two dimensional case are being evaluated. The program as written (which includes the asperity region) will serve as a check on any more approximate methods developed.

#### Experimental Test Rig

- 1) Some of the preliminary design considerations for a test rig have been made, and a proposal has been written. The moving waviness feature is to be included in the test rig. Wear, friction, and leakage are to be measured a function of various waviness parameters to experimentally verify the theory herein.

#### REFERENCES

1. Nau, B. S., "Hydrodynamic Lubrication in Face Seals," The British Hydromechanics Research Association Third International Conference on Fluid Sealing, Cambridge, England, April 1967, Paper E5.
2. Denny, D. F., "Some Measurements of Fluid Pressures Between Plane Parallel Thrust Surfaces with Special Reference to Radial-Face Seals," Wear, 4, 1961, pp. 64-83.
3. Mayer, E., Mechanical Seals, Iliffe Books Limited, London, American Elsevier, New York, 1973, 2nd Ed., 250 pages (Originally published in German in 1966).
4. Hamilton, D. B., Walowitz, J. A., and Allen, C. M., "A Theory of Lubrication by Microirregularities," Transactions of the ASME, Journal of Basic Engineering, March 1966, pp. 177-185.
5. Anno, J. N., Walowitz, J. A., and Allen, C. M., "Microasperity Lubrication," Transactions of the ASME, Journal of Lubrication Technology, April 1968, pp. 351-355.
6. Anno, J. N., Walowitz, J. A., and Allen, C. M. "Load Support and Leakage from Microasperity-Lubricated Face Seals," presented at the Fourth International Conference on Fluid Sealing Held in Conjunction with the 24th ASLE Annual Meeting in Philadelphia, May 5-9, 1969, FICFS Preprint Number 21.
7. Kojabashian, C., and Richardson, H. H., "A Micropad Model for the Hydrodynamic Performance of Carbon Face Seals," presented at the British Hydromechanics Research Association Third International Conference on Fluid Sealing, Cambridge, England, April 1967, Paper E4.
8. Findlay, J. A., Orsino, A. J., and Sneck, H. J., "Study of Dynamic and Static Seals for Liquid Rocket Engines--Final Report," for period April 1, 1967 to April 1, 1968, NASA Contract No. NAS 7-434, Phase II, prepared by General Electric Company, Research and Development Center, Schenectady, 1968, Accession Number N69-10749.
9. Findlay, J. A., "Cavitation in Mechanical Face Seals," Transactions of the ASME, Journal of Lubrication Technology, April 1968, pp. 356-364.
10. Findlay, J. A., "Measurements of Leakage in Mechanical Face Seals," presented at the Fourth International Conference on Fluid Sealing Held in Conjunction with the 24th ASLE Annual Meeting in Philadelphia, May 5-9, 1969, FICFS Preprint Number 19.
11. Nau, B. S., "Cavitation in Thin Films," The British Hydromechanics Research Association, November 1964, No. TN 832.

12. Nau, B. S., "Film Cavitation Observations in Face Seals," presented at the Fourth International Conference on Fluid Sealing Held in Conjunction with the 24th ASLE Annual Meeting in Philadelphia, May 5-9, 1969, FICFS Preprint Number 20.
13. Orcutt, F. K., "An Investigation of the Operation and Failure of Mechanical Face Seals," presented at the Fourth International Conference on Fluid Sealing Held in Conjunction with the 24th ASLE Annual Meeting in Philadelphia, May 5-9, 1969, FICFS Preprint Number 22.
14. Sneed, H. J., "The Effects of Geometry and Inertia on Face Seal Performance - Laminar Flow," Transactions of the ASME, Journal of Lubrication Technology, April 1968, pp. 333-341.
15. Sneed, H. J., "The Effects of Geometry and Inertia on Face Seal Performance - Turbulent Flow," Transactions of the ASME, Journal of Lubrication Technology, April 1968, pp. 342-350.
16. Sneed, H. J., "The Misaligned, Eccentric Face Seal," presented at the Fourth International Conference on Fluid Sealing Held in Conjunction with the 24th ASLE Annual Meeting in Philadelphia, May 5-9, 1969, FICFS Preprint Number 15A.
17. Sneed, H. J., "The Eccentric Face Seal with a Trangentially Varying Film Thickness," presented at the Fourth International Conference on Fluid Sealing Held in Conjunction with the 24th ASLE Annual Meeting in Philadelphia, May 5-9, 1969, FICFS Preprint Number 15B.
18. Sneed, H. J., "Reversed Flow in Face Seals," Transactions of the ASME, Journal of Lubrication Technology, July 1969, pp. 427-433.
19. Sneed, H. J., "Thermal Effects in Face Seals," Transactions of the ASME, Journal of Lubrication Technology, July 1969, pp. 434-437.
20. Stanghan-Batch, B. A., "Face Lubrication in Mechanical Face Seals," Instn Mech. Engrs., C59/71, pp. 54-59.
21. Lebeck, A. O., "Waviness Distortion and Wear in Mechanical Face Seals," Report No. ME-64(74)NSF-271-1, The University of New Mexico College of Engineering, Bureau of Engineering Research, Albuquerque, New Mexico, December 1974.
22. Lebeck, A. O., "Causes and Effects of Waviness in Mechanical Face Seals," Final Report, Technical Report ME-68(76)NSF-271-1, The University of New Mexico, College of Engineering, Bureau of Engineering Research, Albuquerque, New Mexico, January 1976.

23. Lebeck, A. O., "Mechanical Loading - A Primary Source of Waviness in Face Seals," ASLE Preprint 76-AM-63-2, Presented at the Annual Meeting of ASLE, Philadelphia, May 1976.
24. Cheng, H. S., and Snapp, R. B., "A Study of the Radial Film and Pressure Distribution of High Pressure Face Seals," presented at the British Hydromechanics Research Association Third International Conference on Fluid Sealing, Cambridge, England, April 1967, Paper No. E-3.
25. Davies, A. R., and O'Donoghue, J. P., "The Lubrication of High-Pressure Face Seals," presented at the Winter Annual Meeting and Energy Systems Exposition, New York, N. Y., November 27 - December 1, 1966, American Society of Mechanical Engineers, Paper No. 66-WA/LUB-7.
26. Hooke, C. J., and O'Donoghue, P. J., "Elastohydrodynamic Lubrication of High Pressure Face Seals," Journal of Mechanical Engineering Science, Vol. 10, No. 1, 1968, pp. 59-63.
27. Burton, R. A., Kilaparti, S. R., and Nerlikar, M., "Thermoelastic Instability in a Seal Like Configuration," Department of Mechanical Engineering, Northwestern University, Evanston, Illinois, for the Office of Naval Research Contact No. N00014-67-A-0356-0022, September 1973.
28. Burton, R. A., Kilaparti, S. R., and Nerlikar, V., "A Limiting Stationary Configuration with Partially Contacting Surfaces," Wear, 24 (1973), 199-206.
29. Dow, T. A., and Burton, R. A., "Thermoelastic Instability of Sliding Contact in the Absence of Wear," Wear, 19 (1972), 315-328.
30. Burton, R. A., "The Role of Insulating Surface Films in Frictionally Excited Thermoelastic Instabilities," Wear, 24 (1973), 189-198.
31. Lebeck, A. O., "Theory of Thermoelastic Instability of Rotating Rings in Sliding Contact with Wear," Journal of Lubrication Technology, ASME, April 1976, pp. 277-285.
32. Ludwig, L. P., "Face Seal Lubrication I - Proposed and Published Models", NASA Technical Note NASA TN D-8101, April 1976.
33. Ludwig, L. P., and Allen, Gordon P., "Face Seal Lubrication II - Theory of Response to Angular Misalignment" NASA Technical Note, NASA TN - D-8102, March 1976.

34. Orcutt, F. K., Bell, J. C., Glaeser, W. A., and Allen, C. M., "Summary Report on the Dynamic Behavior of High Speed Liquid-Lubricated Face Seals to the Rotary Shaft Seal Research Group," January 24, 1962, Battelle Memorial Institute, Columbus.
35. Christensen, H., "Some Aspects of the Functional Influence of Surface Roughness in Lubrication," Wear, 17 (1971), pp. 149-162.
36. Christensen, H., "A Theory of Mixed Lubrication," Proceedings of the Institution of Mechanical Engineers, Vol. 186, 41, 1972.
37. Thompson, R. A., and Bocchi, W., "A Model for Asperity Load Sharing in Lubricated Contacts," ASLE Transactions, Vol. 15, No. 1, January 1972, pp. 67-79.
38. Cameron, A. The Principles of Lubrication, Longmans, Green & Co., Ltd., London, 1966.
39. Robinowicz, Ernest, Friction and Wear of Materials, John Wiley & Sons, New York, 1965.
40. Snapp, R. B., and K. R. Sasdelli, "Performance Characteristics of a High Pressure Face Seal with Radially Converging Interface Shapes," Paper E4, 6th International Conference on Fluid Sealing, February 27 - March 2, 1973, Munich.
41. Stanghan-Batch, B., and Iny, E. H., "A Hydrodynamic Theory of Radial Face Seals," Journal of Mechanical Engineering Science, Vol. 15, No. 1, 1973.
42. Jakobsson, B., and Floberg, L., "The Finite Journal Bearing Corroding Vaporization," Report No. 3, from the Institute of Machine Elements, Chalmers University of Technology, Gothenburg, Sweden, 1957.
43. Ames, W. F., Numerical Methods for Partial Differential Equations, Barnes & Noble, Inc., New York, 1969.
44. Heller, S., and Shapiro, W., "A Numerical Solution for the Incompressible Hybrid Journal Bearing with Cavitation", Transactions of the ASME, Journal of Lubrication Technology, July 1969, pp. 508-515.